Annual greenhouse gas budget for a bog ecosystem undergoing restoration by rewetting

by

Sung-Ching Lee

B.Sc., National Taiwan University, 2013

A THESIS SUBMITTED IN PARTIAL FULFILLMENT OF

THE REQUIREMENTS FOR THE DEGREE OF

MASTER OF SCIENCE

in

THE FACULTY OF GRADUATE AND POSTDOCTORAL STUDIES

(Geography)

THE UNIVERSITY OF BRITISH COLUMBIA

(Vancouver)

August 2016

Abstract

Many peatlands have been drained and harvested for peat mining, which turned those landscapes into carbon (C) emitters. Rewetting of disturbed peatlands facilitates their ecological recovery, and may help them revert to carbon dioxide (CO_2) sinks. However, it may also cause substantial emissions of the powerful greenhouse gas (GHG) methane (CH_4). Our knowledge on year-round measurements of CO_2 and CH_4 fluxes in restored peatlands is currently very limited. This study quantifies C exchanges in a disturbed and rewetted area located in the Burns Bog Ecological Conservancy Area (BBECA) in Delta, BC, Canada. The BBECA is recognized as the largest raised bog ecosystem on North America's West Coast. It was substantially reduced in size and degraded by peat mining and agriculture. Since 2005, the bog has been declared a conservancy area, and restoration efforts focus on rewetting disturbed ecosystems to recover *Sphagnum* and suppress fires.

Year-round (16th June 2015 to 15th June 2016) turbulent fluxes of CO_2 and CH_4 were measured from a tower platform in an area rewetted in 2007 using the eddy-covariance (EC) technique. The annual CO_2 budget was -179 g CO_2-C m^{-2} $year^{-1}$and the annual CH_4 budget was 16 g CH_4-C m^{-2} $year^{-1}$. Gross ecosystem productivity (GEP) exceeded ecosystem respiration (R_e) during summer months (June-August), causing a net CO_2 uptake. In summer, high CH_4 emissions were measured. In winter (December-February), substantially lower CH_4 emissions and roughly equal magnitudes of GEP and R_e made the bog C neutral. Oxygen limitation due to the high water table caused by ditch blocking suppressed R_e. With low temperatures in winter, CH_4 emission was more suppressed than R_e. The key environmental factors controlling the seasonality of these exchanges in the study area were downwelling photosynthetically active radiation and 5-cm soil temperature.

Annual net GHG flux from CO_2 and CH_4 during the study period totaled to -23.48 g CO_2e m^{-2} $year^{-1}$ and 1242.04 g CO_2e m^{-2} $year^{-1}$ by using 100-year and 20-year global warming potential (GWP) values, respectively. Consequently, the ecosystem was almost CO_2e neutral annually on a 100-year time horizon but was a significant CO_2e source on a 20-year time horizon.

Preface

The code to compute the turbulent source area used this thesis (section 3.2.1) has been programmed by my supervisor Andreas Christen (Christen et al. 2011, available on Github). The database and data processing, as well as the approach to gap fill fluxes used in this thesis has been coded in part by my supervisor Andreas Christen. Data from the stations "Delta - Burns Bog" and "Vancouver International Airport" has been provided by Environment Canada and data from "Vancouver-Sunset" was provided by UBC Geography. Data on water table depth from dip wells has been provided by Sarah Howie, Municipality of Delta.

Table of Contents

List of Tables

List of Figures

List of Symbols and Acronyms

Symbols/Acronyms	Units	Definition
BBECA		Burns Bog Ecological Conservancy Area
BC		British Columbia
C		carbon
CO_2		carbon dioxide
CO_2e		carbon dioxide equivalent
CH_4		methane
C_v		convexity
EC		eddy-covariance
EC-1		the first eddy-covariance system (see section 2.2.3)
EC-2		the second eddy-covariance system (see section 2.2.3)
F_c	μmol m^{-2} s^{-1}	CO_2 flux density
GEP	g C m^{-2} $time^{-1}$ or μmol m^{-2} s^{-1}	gross ecosystem photosynthesis
GHG		greenhouse gas
GWP		global warming potential
H	W m^{-2} or GJ m^{-2} $year^{-1}$	sensible heat flux density
IRGA		infrared gas analyzer
K	W m^{-2}	downwelling or upwelling shortwave radiation

Symbols/Acronyms	Units	Definition
L	W m^{-2}	downwelling or upwelling longwave radiation
MQY	mol C mol^{-1} photons	maximum quantum yield
NEE	g C m^{-2} $time^{-1}$ or μmol m^{-2} s^{-1}	net ecosystem exchange
N_2O		nitrous oxide
P	mm	precipitation
PAR	μmol m^{-2} s^{-1}	photosynthetically active radiation
P_M	μmol m^{-2} s^{-1}	maximum photosynthetic rate
PPFD	μmol m^{-2} s^{-1}	photosynthetic photon flux density
Pr	Pa	air pressure
Q^*	W m^{-2}	net all-wave radiation
R_e	g C m^{-2} $time^{-1}$ or μmol m^{-2} s^{-1}	ecosystem respiration
RH	%	relative humidity
r_1, r_2, r_3	μmol m^{-2} s^{-1} or ℃	empirical parameters
T_a	℃	air temperature
T_s	℃	soil temperature
T_w	℃	water temperature
WTH	cm	water table height
m_a	g	molecular mass of air
m_{CH_4}	g	molecular mass of CH_4
m_{CO_2}	g	molecular mass of CO_2
m_v	g	molecular mass of water vapour
u	m s^{-1}	horizontal wind speed

Symbols/Acronyms	Units	Definition
u_*	m s^{-1}	friction velocity
v	m s^{-1}	lateral wind speed
w	m s^{-1}	vertical wind speed
z_0	m	roughness length
z	m	height of EC system
θ_w	m^3 m^{-3}	soil volumetric water content
ρ_a	mol dry air m^{-3}	dry air density
ρ_c	mol CO_2 m^{-3}	CO_2 density
ρ_m	mol CH_4 m^{-3}	CH_4 density

Acknowledgements

I was most fortunate to be supervised by Professor Andreas Christen. His genius and hard-work always motivated me to do more and learn more. His fast and helpful feedback continuously supported my progress. I would like to specially thank him for sharing his programming and his creative visualisation skills with me. I could not have imaged to have a better supervisor and I am looking forward to our partnership in my PhD.

Professors Andy Black and Mark Johnson, two extremely enthusiastic and knowledgeable committee members, were always there to offer insightful comments, encouragement and enormous resources. It is difficult to find any other committee more capable and more enjoyable to learn from and work with than the one I had.

This work, the construction and maintenance of the EC tower and the challenging power and communications infrastructure would not have been built and maintained without Zoran Nesic and Rick Ketler. I am indebted to them for their extensive technical support to solve all the "no small tasks". I will miss all the fun and misery we had in the lab and field.

I would like to express my sincerest appreciation to Markus Merkens, Joe Soluri, Sarah Howie, and Conor Reynolds. In my past, I did not have any experience about friendly and smart people from the government organization. They completely surprised and proved I was wrong. It was definitely a wonderful collaboration.

I express my gratitude to the UBC Department of Geography's staff, in particular Sandy Lapsky, Stefanie Ickert, Julie Ranada, Mimi Yu, Jeanne Yang, Vincent Kujala, Suzanne Lawrence, and Alex Pysklywec. All the friendly faces, fun chat and assistance made my graduate school life great.

I thank all my field partners, in particular Yimei Li, Jane Wang, Brenda D'Acunha, Johannes Exler, Pascal Armborst, Haven Jerreat-Poole, Ernest Wu, Thea Rodgers, Devin Gamble, Zhou Wang, Anson Yam, and Zarah Zheng. This study area is a challenging location to do research, but it became so fun to go with all of you!

Last, I thank all the researchers and friends I made here and those good friends I made in Taiwan. They have been exceptionally supportive and helpful.

This research was funded by several research contracts between Metro Vancouver and UBC (Christen / Moore). Selected equipment was supported by the Canada Foundation for Innovation (Grant # 33600, Christen) and NSERC RTI (Christen). Financial support through scholarships and training were provided by UBC Faculty of Graduate and Postdoctoral Studies and UBC Geography.

Dedication

I dedicate this thesis to my dear family and to my girlfriend for their incredible support, patience and love.

Chapter 1: Introduction

The global carbon (C) cycle regulates the Earth's climate by controlling the concentration of long-lived greenhouse gases (GHG) (Revelle and Suess, 1957). Of particular concern are increasing concentrations of carbon dioxide (CO_2) and methane (CH_4) in the atmosphere (IPCC, 2013). Wetland ecosystems play a disproportionately large role in the global C cycle compared to the surface area they occupy. Wetlands cover only 6%–7% of the Earth's surface (Lehner and Döll, 2004), but they act as a major sink for the long-term storage of C by sequestering CO_2 from the atmosphere. C storage in wetlands has been estimated to be up to 450 Gt C or approximately 20% of the total C storage in the terrestrial biosphere (Gorham, 1991; Maltby and Immirzi, 1993). However, wetlands emit significant quantities of the powerful GHG, CH_4, due to anaerobic microbial decomposition (Aurela et al., 2001; Rinne et al., 2007). CH_4 emissions from wetlands are responsible for 60% of all global CH_4 emissions (Cao et al., 1998).

1.1 Previous studies on C exchanges in peatlands

1.1.1 Biogeochemical processes

Peatlands are wetlands with an accumulated peat layer formed from C rich dead plant material under water saturated conditions. Peatlands are the most widespread of all wetland types in the world, representing 50 to 70% of global wetlands (Mundava, 2011). Their dynamics have played an important role in the global C cycle during the Holocene period (Gorham, 1991; Yu, 2011), and it has been shown that including peatlands in the modelling and analysis of the global C cycle to mitigate the changes in other C reservoirs is highly relevant (Brovkin et al., 2002; Kleinen et al., 2010; Menviel and Joos, 2012). Understanding the mechanisms controlling C exchange, both above- and below-ground in peatlands at small spatial scales is particularly

important for predicting future trajectories of the terrestrial C cycle and inform land management strategies of the terrestrial C cycle.

CO_2 and CH_4 are the major two long-lived GHGs that dominate the land-atmosphere fluxes of C. CH_4 is the third most important long-lived GHG. Its concentration in the atmosphere is currently 1.89 μmol mol^{-1}, which is lower than that of CO_2 (400 μmol mol^{-1} in 2015, National Oceanic and Atmospheric Administration). However, considering the atmospheric lifetime of CH_4 and its radiative properties, a Global Warming Potential (GWP) was calculated that is 28 times higher than for CO_2 (emission of 1 g of CH_4 is equivalent to 28 g of CO_2) (IPCC, 2014). GWP provides a simple method to determine the ratio of warming of the atmosphere caused by various GHGs to that by the same mass of CO_2, taking into account the specified time horizon (Lashof and Ahuja, 1990). Both CH_4 and CO_2 exchange between peatlands and the atmosphere are the major components of the peatland C budget (Figure1.1) (Rinne et al., 2007).

Ecosystems assimilate most of their C in form of CO_2 from the atmosphere. Using absorbed solar energy in the range of 0.4 to 0.7 μm (called photosynthetic active radiation, PAR), cells in plant leaves combine CO_2 and water to form carbohydrates and oxygen in the process of photosynthesis. Plants break down the sugar to obtain the energy they need for maintenance and growth (autotrophic respiration). Animals and consume plants, and break down the plant carbohydrates to get energy. Bacteria and other microorganisms decompose root exudates and dead plant material, e.g. litter (heterotrophic respiration). In addition, fire consumes plants. In each case, oxygen combines with carbohydrates to release water, CO_2, and energy (oxidation).

CH_4 emissions in peatlands are the result of biogeochemical processes, which are governed by physical, chemical and biological factors (Le Mer and Roger, 2001). Unlike in most other terrestrial ecosystems where the microbial decomposition is aerobic; CH_4 is produced by

microbial decomposition in anaerobic conditions. Wetlands are usually flooded with a water table near the surface for at least part of the year, which makes wetlands an ideal anaerobic, or oxygen poor, environments for fermentation. Fermentation is a process used by certain kinds of microorganisms to break down essential nutrients. Between the water table and the peat surface, CH_4 is consumed (i.e., oxidized) by methanotrophic bacteria evolving in aerobic conditions (Segers, 1998). CH_4 production is controlled partly by biological factors, such as substrate and nutrient availability (Clement et al., 1995), and partly by environmental factors, such as water table depth and peat temperature, whose role has been widely documented (Mikkelä et al., 1995). Methane gas is liberated from peat via three main pathways:

1. Diffusion: It refers to the movement of CH_4 up through soil and bodies of water to reach the atmosphere. Diffusion of CH_4 is slower in the saturated peat layers below the water table and becomes faster in the unsaturated layer above the water table (Levy et al., 2012).
2. Ebullition: It is a process that releases CH_4 into the atmosphere in the form of gas bubbles (Vasander and Kettunen, 2006).
3. The plant vascular system: The xylem tissue of vascular plants transports water containing dissolved CH_4 from the roots to the leaves, leading to the observation that methane is released during transpiration (Fechner-Levy and Hemond, 1996; Shannon and White, 1994).

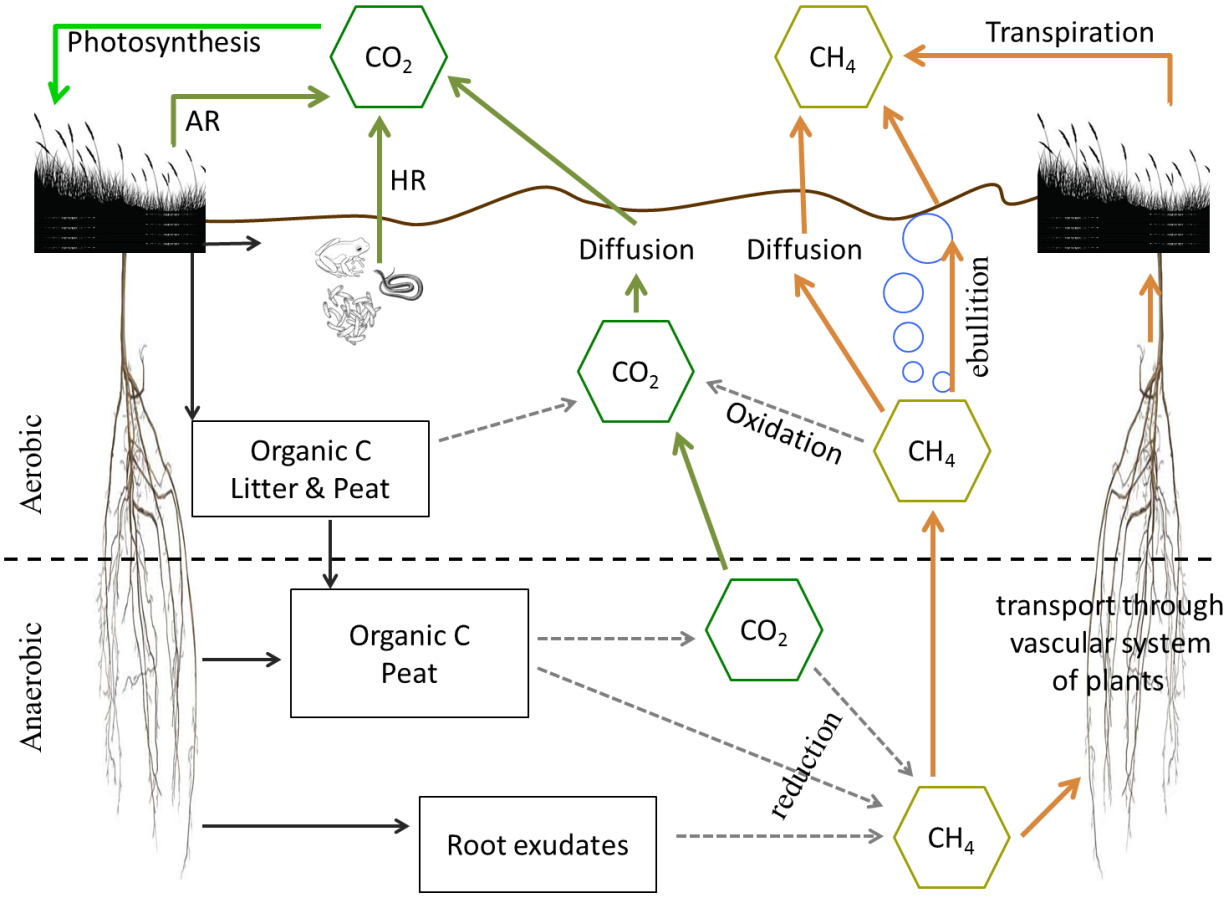

Figure 1.1 The C cycle in peatland ecosystems and the associated biogeochemical processes. AR means autotrophic respiration, and HR means heterotrophic respiration. Modified from Lloyd et al., 2013.

1.1.2 Annual C exchange between peatlands and the atmosphere

The annual exchange of CO_2 or CH_4 between peatlands and the atmosphere has been estimated by several studies, although most of the studies in the literature report exchange of one of the two gases at a time. Whole-year measurements of CO_2 and CH_4 fluxes for peatlands has been reported for one site. Tables 1.1 and 1.2 list values of the annual ecosystem-atmosphere exchange, separately of CO_2 and CH_4 in bog ecosystems.

According to the results summarized in Table 1.1 and 1.2, we can say that generally a peatland is a C sink by considering CO_2 fluxes only. But after adding net CH_4 emission, it may

turn the ecosystem from sink to source. The C balance obtained using both CO_2 and CH_4 exchange in peatland ecosystems shows significant variation between different study sites in different climates in the literature.

Table 1.1 Comparison of annual CO_2 ecosystem-atmosphere exchange (NEE = R_e - GEP) measured in undisturbed temperate peatlands from the literature. Sorted by the magnitude of NEE.

Ecosystem	Site	CO_2 flux (NEE) (g C m^{-2} yr^{-1})[1]	Study
Bog	Ontario, Canada	-621	Neumann et al. (1994)
Bog	Western Siberia	-597	Schulze et al. (1999)
Ombrotr. bog	Southern Finland	-266	Pihlatie et al. (2010)
Ombrotr. bog	Ontario, Canada	-248	Lafleur et al. (2001)
Bog	Minnesota, USA	-146	Shurpali et al. (1995)
Low sedge pine fen	Salmisuo, Finland	-98	Alm et al. (1997)
Ombrotr. bog	Quebec, Canada	-76	Roehm and Roulet (2003)
Moderately rich fen	Alberta, Canada	-71	Syed et al. (2006)
Ombrotr. bog	Ontario, Canada	-60	St-Hilaire et al. (2010)
Ombrotr. bog	Ontario, Canada	-25	Roehm and Roulet (2003)
Eccentric bog	Southern Sweden	-21	Lund et al. (2007)
Fen	Saskatchewa, Canada	-1	Suyker et al. (1997)
Ombrotr. bog	Quebec, Canada	+251	Strack and Zuback (2013)
Bog	Minnesota, USA	+329	Shurpali et al. (1995)

[1] Positive values indicate loss from ecosystem, and negative values indicate uptake by ecosystem.

Table 1.2 Comparison of annual CH_4 ecosystem-atmosphere exchange measured in undisturbed temperate peatlands from the literature. Sorted by decreasing magnitude of CH_4 fluxes.

Ecosystem	Site	CH_4 flux ($g\ CH_4\text{-}C\ m^{-2}\ yr^{-1}$)	Study
Mineral poor fen	New Hampshire, USA	113	Treat et al. (2007)
Poor fen	Minnesota, USA	66	Dise (1993)
Ombrotr. bog	Quebec, Canada	65	Moore and Roulet (1995)
Fen	Minnesota, USA	49	Chasar et al. (2000)
Boreal bog	Manitoba, Canada	48	Bellisario et al. (1999)
Boreal bog	Quebec, Canada	47	Liblik et al. (1997)
Ombrotr. bog	Minnesota, USA	43	Dise (1993)
Minerotrophic fen	Germany	42	Augustin et al. (1998)
Ombrotr. bog	Alberta, Canada	24	Turetsky et al. (2002)
Ombrotr. bog	Michigan, USA	13	Shannon and White (1994)
Ombrotr. bog	Quebec, Canada	7	Strack and Zuback (2013)

[1]Positive values indicate loss from ecosystem

1.1.3 Seasonal changes and controls on C exchange

Over the growing season, some peatlands are estimated to be net C sources (Lafleur et al., 1997; Nieveen et al., 1998; Schreader et al., 1998) but some of them can be net C sinks (Aurela et al., 2001; Oechel et al., 1997; Suyker et al., 1997). Other studies have showed that a peatland was a C sink in the growing season of one year and a net source in the next year (Griffis et al., 2000; Joiner et al., 1999; Shurpali et al., 1995). In addition to determining the C budget, quantifying the ecosystem response to seasonal variations of environmental factors is an important issue. Only a few studies have addressed how the C cycle in peatlands reacts to seasonality in different latitude ecosystems.

In high-latitude peatlands, daytime CO_2 uptake occurs during growing season only. Ideally, as soon as snow cover starts to disappear in spring and early summer, the vegetation in high latitude peatland ecosystems can begin photosynthesizing. Low sun angles and short day lengths partly account for the lower CO_2 sequestration during winter and spring (Lafleur et al., 2001; Metzger et al., 2015). However, in high-latitude peatlands, the emergence of photosynthesizing plant tissue is delayed, so there is a lag in the initial CO_2 uptake. Water table depth is another important driver, which greatly alters the magnitude of CO_2 uptake in high-latitude peatlands (Moore et al., 2006). Daytime uptake of CO_2 usually occurs during all months of the year in mid- and low-latitude peatlands (Glenn et al., 2006; Lafleur et al., 2001). In general, inter-annual differences in low- and mid-latitude peatlands are likely related to the phenology of the vascular plant cover and the environmental conditions that influence phenology.

CH_4 emission is a function of its rate of production, transport and oxidation. Most studies of CH_4 release were conducted during the growing season. However, it is also altered by seasonally varying environmental conditions, especially water table depth and soil temperature (T_s). An increase in CH_4 flux may be caused by a release of pore water CH_4 with the rapid drop in the water table (Moore and Dalva, 1993). Few studies conducted in peatlands have provided information on the seasonality of the CH_4 emission. Furthermore, these studies have employed chambers that can only represent a small fraction of the area that is often highly heterogeneous (Chojnicki et al., 2010; Czobel et al., 2005).

Not only vertical fluxes (land-atmosphere) but also lateral fluxes have been shown to be relevant (Alkhatib et al., 2007; Baum et al., 2007; Müller et al., 2015). The C exchange between land and water varies with catchment properties and the hydrogeologic setting. The area of peatland contributing to organic C export is mainly controlled by water table depth. For example,

if the water table is low, the area contributing to organic C export can be reduced. Rapid runoff occurs over the peatland surface during late-winter and spring melt. Land-aquatic fluxes will increase in magnitude with peat depth (Fraser et al., 2001).

CO_2 and CH_4 fluxes in peatlands are known to vary considerably between different study sites (Bubier et al., 1998; Frolking et al., 1998; Lindroth et al., 2011; Moore, 2002). Various controlling factors for this variation at different spatial scales have been suggested. At the ecosystem scale, C exchange is controlled by vegetation composition, water level, soil structure and pH (Limpens et al., 2008). At the regional scale, subsurface and surface hydrology and topography affect C export to other adjacent ecosystems and the atmosphere. A large number of drivers are related to some aspect of hydrology, which illustrates the scale-dependency of the main drivers, making full integration across scales difficult. Therefore, how the C balance of peatlands will respond to disturbances requires a process-level understanding of C cycles through individual wetlands, and mapping of the spatial distribution of relevant ecosystems characteristics. More research is needed to better capture the dynamics of impacts of environmental factors on fluctuations of C fluxes in peatlands under variable climatic regimes.

1.2 Knowledge gaps in current studies

1.2.1 Restoration of disturbed wetlands

Many peatlands were disturbed by the extraction of peat for horticultural use and especially to catalyze the formation of fire bombs during World War II (Cowen, 2015). During harvesting, the surface vegetation was removed, and then wetlands were drained by a network of ditches (Price and Waddington, 2000; Waddington and Roulet, 2000). When they were no longer economical, many harvested peatlands were abandoned with artificially low water tables due to the drainage ditches. This environmental condition limits the abandoned peatlands ability to return to their pristine state. It resulted in increased oxidation in peat soils, which became a strong source of CO_2 (Langeveld et al., 1997; Tapio-Biström et al., 2012). Additionally, degraded peat is easier to burn, which can produce significant CO_2 emissions (Gaveau et al., 2014; Page et al., 2002; van der Werf et al., 2004). These consequences could be worse if nothing is done after the peat extraction. Therefore, and for reasons of conservation ecology (unique habitat), many developed and disturbed peatlands are currently under restoration. Ecological restoration is the process of assisting the recovery of a degraded peatland ecosystem. Management strategies can involve simply raising the water table by blocking peat drains to restore and improve disturbed peatland habitats (Evans et al., 2005). Other peatland restoration processes can be initiated by reseeding or planting bare surfaces, spreading straw, and applying phosphorus fertilizer (Petrone et al., 2004). All plans aim to reverse peatland degradation and restore peatlands to a functioning ecosystem being able to establish the moss and vascular plants (Quinty and Rochefort, 2003).

1.2.2 The effects of restoration on CO_2 and CH_4 fluxes

Restoration efforts can have an immediate impact on the C exchange between the peatland surface and the atmosphere.

The water table depth and the amount of vegetation are the most important factors affecting land-atmosphere C exchange. Rewetting has strong direct and indirect effects on CO_2 and CH_4 fluxes. Raising the water level has been found to suppress the CO_2 flux from the soil and result in an increase in net CO_2 uptake by the plants (Komulainen et al., 1999). CH_4 emission from rewetted sections in a bog in Finland, were three times higher than the release from the disturbed and dry area (Tuittila et al., 2000). Another study found similar rates of CH_4 production in disturbed and restored wetlands in southern United States (Schipper and Reddy, 1994).

Re-vegetation of degraded peat leads to faster peat reestablished formation that can have significant effects on C exchange. The increased above- and below-ground biomass of plants and litter enhanced organic matter oxidation which raised CO_2 emissions (Finér and Laine, 1998; Minkkinen and Laine, 1998). Re-establishing the peat formation also initially increased CH_4 emission, but the C exchange did not reach the level of seasonal emissions from pristine peatland (Crill et al., 1992; Dise et al., 1993; Shannon and White, 1994).

Very few studies provide long-term measurements to determine how restored peatlands function. It remains unclear when, or even if, restored peatland ecosystems could show a similar magnitude of C fluxes as in pristine (undisturbed) peatland ecosystems. Furthermore, most investigation focusing on GHG exchange of restored peatlands only measured CO_2 and CH_4 fluxes during the growing season. Few studies are year-round, but for several reasons, only chamber measurements were used in most cases. Thus, there are only few published studies of

complete annual C balances of restored peatlands (Table 1.3) and three studies measured both GHGs simultaneously using EC.

Table 1.3 Comparison of annual CO_2 and CH_4 ecosystem-atmosphere exchanges measured in disturbed temperate peatlands from the literature. Sorted by magnitude of CO_2 or CH_4 fluxes.

Disturbed but not restored

Disturbed year	Site	CO_2 flux ($g\ C\ m^{-2}\ yr^{-1}$)*	Study
1980	Central Estonia	268	Järveoja et al. (2016)
1960	Eastern Estonia	285	Salm et al. (2012)
1950	Western Finland	306	Maljanen et al. (2013)
1972	Quebec, Canada	516	Strack and Zuback (2013)
Disturbed year	Site	CH_4 flux ($g\ CH_4\text{-}C\ m^{-2}\ yr^{-1}$)	Study
1950	Western Finland	-0.02	Maljanen et al. (2013)
1960	Eastern Estonia	0.01	Salm et al. (2012)
1980	Central Estonia	0.14	Järveoja et al. (2016)
1972	Quebec, Canada	0.66	Strack and Zuback (2013)

Disturbed and restored

Years after restoration	Site	CO_2 flux ($g\ C\ m^{-2}\ yr^{-1}$)	Study
5	California, USA	-804	Anderson et al. (2016)[1]
18	California, USA	-397	Knox et al. (2015)[1]
5	California, USA	-368	Knox et al. (2015)[1]
13	California, USA	-21	Anderson et al. (2016)[1]
4	Central Estonia	103	Järveoja et al. (2016)
4	Central Estonia	111	Järveoja et al. (2016)
14	Indiana, US	138	Richards and Craft (2015)
13	Quebec, Canada	142	Strack and Zuback (2013)
Years after restoration	Site	CH_4 flux ($g\ CH_4\text{-}C\ m^{-2}\ yr^{-1}$)	Study
4	Central Estonia	0.1	Järveoja et al. (2016)
4	Central Estonia	0.2	Järveoja et al. (2016)
15	Quebec, Canada	1	Strack and Zuback (2013)
9	Western Denmark	11	Herbst et al. (2011)[1]
18	California, USA	39	Knox et al. (2015)[1]
6	California, USA	53	Knox et al. (2015)[1]
13	California, USA	56	Anderson et al. (2016)[1]

* Positive values indicate loss from ecosystem, and negative values indicate uptake by ecosystem.
[1] Based on EC, all other studies are based on year-round chamber measurements.

1.3 Current study

1.3.1 Knowledge gaps and policy context

Burns Bog in Delta, BC, on Canada's Pacific Coast, is part of a remnant peatland ecosystem which is recognized as the largest raised bog ecosystem on North America's west coast. Started in 1900s, it was significantly disturbed as a result of it being used for housing, peat mining and agriculture (MetroVancouver, 2007). The Burns Bog Ecological Conservancy Area (BBECA, Figure 2.1) was established in 2005 to maintain the largest remaining undisturbed area and restore disturbed locations to a raised bog. A recent study by The University of British Columbia (UBC) measured summertime CO_2 and CH_4 exchanges using chamber systems in the rewetted sector of the BBECA in 2014 and found substantial emissions of CH_4 (Christen et al., 2014). Based on this study, it was concluded that CO_2 and CH_4 fluxes should be measured continuously year round to determine the magnitude of annual emissions. This M.Sc. thesis aimed to quantify the land-atmosphere exchanges of CO_2 and CH_4 for a full annual cycle and to identify which environmental factors control the CO_2 and CH_4 fluxes in in this ecosystem. The results of this investigation will help to increase our knowledge on CO_2 and CH_4 fluxes from disturbed bogs in general, and specifically inform the future restoration management by Metro Vancouver for the BBECA. Many areas have not yet been rewetted, and it is important to know how we can reduce unnecessary emissions, e.g. by controlling water table and timing of the rewetting in future restoration efforts in the BBECA.

1.3.2 Research objectives

This research proposal aims to complete the goals mention in the previous section through a field-based observational study in this representative peatland ecosystem. The three main objectives are to:

- Quantify seasonal and annual CO_2 and CH_4 fluxes by means of continuous EC measurements in a disturbed ecosystem that is representative of areas subject to recent restoration efforts (ditch blocking) in the BBECA.
- Quantify whether the study ecosystem is net source or sink of GHG at different time scale by considering GWPs.
- Identify the key environmental controls and their effects on CO_2 and CH_4 fluxes.

Chapter 2: Methods

2.1 Study site

2.1.1 Burns Bog Ecological Conservancy Area

The current study was conducted in the BBECA in Delta, BC, on Canada's Pacific Coast (Figure 2.1). The BBECA is the largest raised peat bog on the west coast of the Americas and one of the largest bogs within a heavily urbanized area in Canada (see Chapter 1). The BBECA is classified as a raised or domed peat bog (Hebda et al. 2000); in its development, this type of bog forms a shallow dome of peat (Wheeler and Shaw 1995). It contains an internal mound of water that is acidic and nutrient-poor, a two-layered peat deposit. Thickness of the peat in centre of the BBECA is 5.4 m and the thickness decreases to 0.5 m at the boundary; the total volume of the peat at the BBECA has also been estimated to be 108.8 hm^3 (Biggs, 1976).

The climate in the BBECA is near Mediterranean type with warm and dry summers with mostly cloudless skies. Winters are cool and wet, but generally above freezing. At least 65% of the precipitation falls in the winter and annual snowfall is less than 40 cm. Based on the 30-year average data (1981-2010) from Vancouver International Airport, Environment Canada, the mean annual temperature was 10.4 ℃ and 1189.0 mm of precipitation fell. Relative humidity (RH) remains mostly above 60% throughout the year, often reaching 80-90% especially in the winter (Oke and Hay, 1998).

Burns Bog originally covered between 4,000 and 4,900 ha and it had been used by First Nation for thousands of years as a source of food and clothing. The bog started to be disturbed after Dominic Burns and his brother purchased the bog in 1906. Initially, the bog was used for agriculture and animal husbandry. Small scale of peat mining took place in 1930 with the harvested peat being used for weapons production, as fertilizers and as a fuel (Burns, 1977). Peat

mining expanded with time; 70% of Burns Bog was affected by peat extraction by the end of the 1940s (Cowen, 2015). The hydrology and ecology of the rest of the bog were also disrupted by development of transportation and a drainage network.

The importance of this unique ecosystem started to be formally recognized in 1999. After lengthy negotiations, the government of Canada, the province of British Columbia, the Greater Vancouver Regional District (GVRD) and the Corporation of Delta purchased 2,042 ha of Burns Bog and claimed it as a conservancy area. The BBECA currently contains 70% of disturbed wetland ecosystems. The remaining 30% of its total area are a close-to undisturbed raised peat bog. In 2007, a 100-year management plan was developed to restore the disturbed sections (Metro Vancouver, 2007). The main goal of the restoration at the BBECA is to allow bog plants to grow. This was achieved by controlling the water table using a ditch-blocking program to retain rain water. Ditches have been blocked with peat dams, wood dams, steel weirs, and also with dams built by beavers (Metro Vancouver, 2007).

2.1.2 Study site

The study site is a rewetted area located in the centre of the BBECA (122°59’05.87"W, 49°07’47.20”N, WGS-84) with dimensions of 400 m by 250 m surrounded by a windbreak to the west and an abandoned (now blocked) drainage ditch to the north (Figure 2.2). The study area was harvested between 1957 and 1963 using the Atkins-Durbrow Hydropeat method to remove the peat (Heathwaite and Göttlich, 1993). This method cuts down trees in preparation then blasts the peat surface with pressurized water to dislodge peat from exposed tree roots. The study site has been rewetted by dams built with plywood and using wooden stakes as bracing in 2007 (Howie et al., 2009) (Figure 2.3). This site is noticeably wetter than many other recently rewetted

ecosystem types in the BBECA with the water table remaining very near the surface for most of the year (Christen et al., 2016). The site has been selected for this study by Metro Vancouver staff and the Scientific Advisory Panel to the BBECA as being representative of recently rewetted ecosystems in the BBECA. This site is in the ecosystem type classified as a White beak-rush-Sphagnum (RS) ecosystem, which covers 14% of the BBECA (Madrone Consultants Ltd., 1999).

The plant communities in the study ecosystem are dominated by *Sphagnum* and *Rhynchospora alba*. The average height of the vegetation during the growing season is about 0.3 m (Madrone Consultants Ltd., 1999). Plants are separated by shallow open water pools, some of them populated by algae developing (Figure 2.4). Birch trees are dispersed and appear to be growing on the remnants of baulks but none of them was taller 2 m. *Sphagnum* covers over 25% of the surface inside the study area (Hebda et al., 2000). The area of the open water ponds was estimated to beabout 20% of the surface in summer by aerial photo.

Water table height (WTH) fluctuates between 20 cm above ground and 20 cm below ground over the year. In all years since rewetting (2007), water table positions are lowest in late summer and early fall and high all winter and spring (Figure 2.5). They start to decrease steadily between June and September. In September and October, the water table rises due to the increase in precipitation and the reduced evapotranspiration as a consequence of senescence. The highest (January 17th 2016) and lowest (July 30th 2015) WTH among all 9 years since the rewetting were found in the current study year.

The depth of peat at the study site is 5.83 m. A silty clay layer is located below the peat layer. The properties of peat were classified by peat core sampling according to the Von Post Humification Scale. From the surface to 1.6-m depth, the peat is not yet decomposed (H1). The

soil was negligibly decomposed (H2) from 1.6- to 2.1-m depth. It started to have slightly decomposed peat (H3, H4) from the 2.1-m depth to the 3.1-m depth. Moderately decomposed (H5) took place from 4.6-m to 5-m depth. The bottom part of the core was highly decomposed (Chestnutt, 2015).

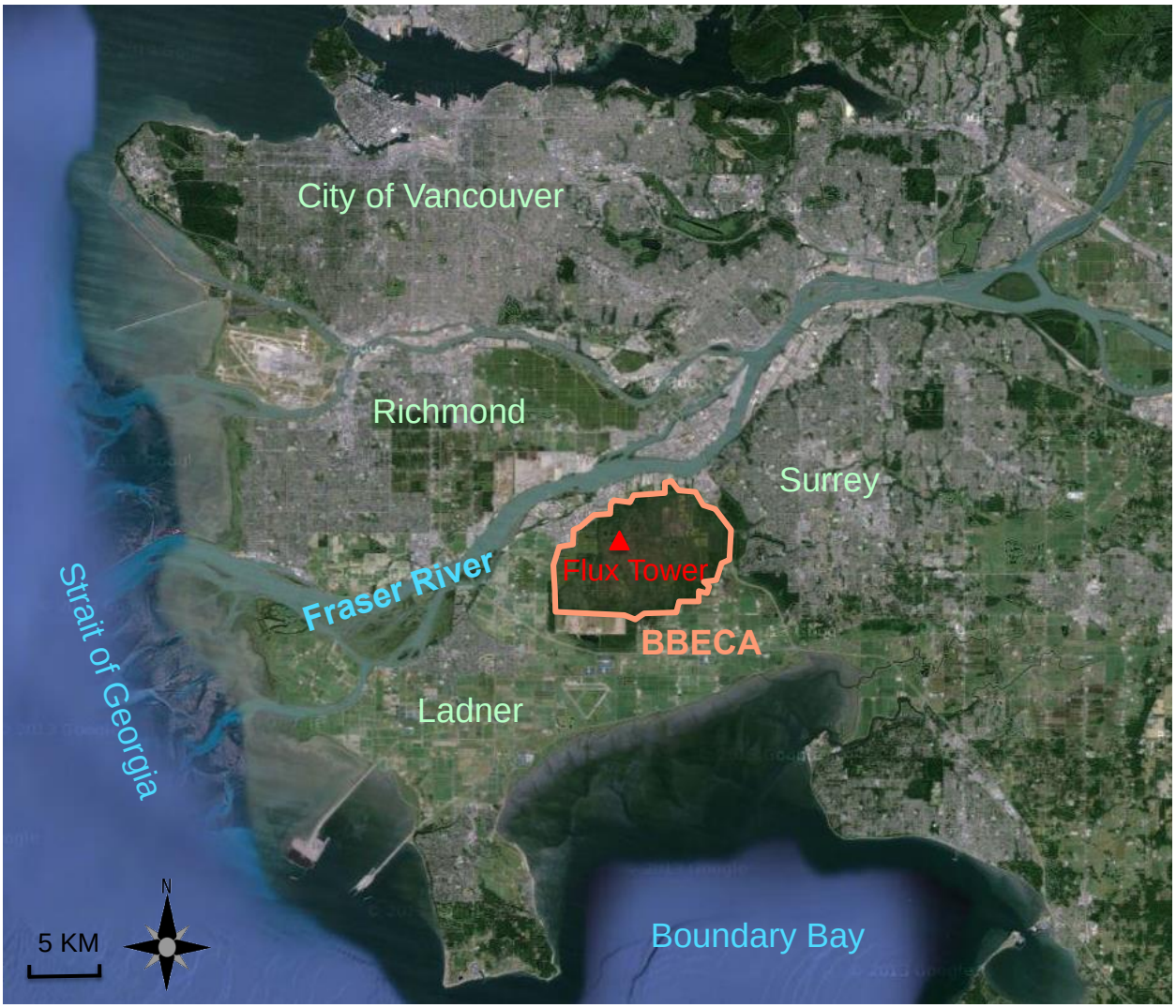

Figure 2.1 Location of the flux tower at the BBECA in Delta, BC. Background aerial photo: Google Earth.

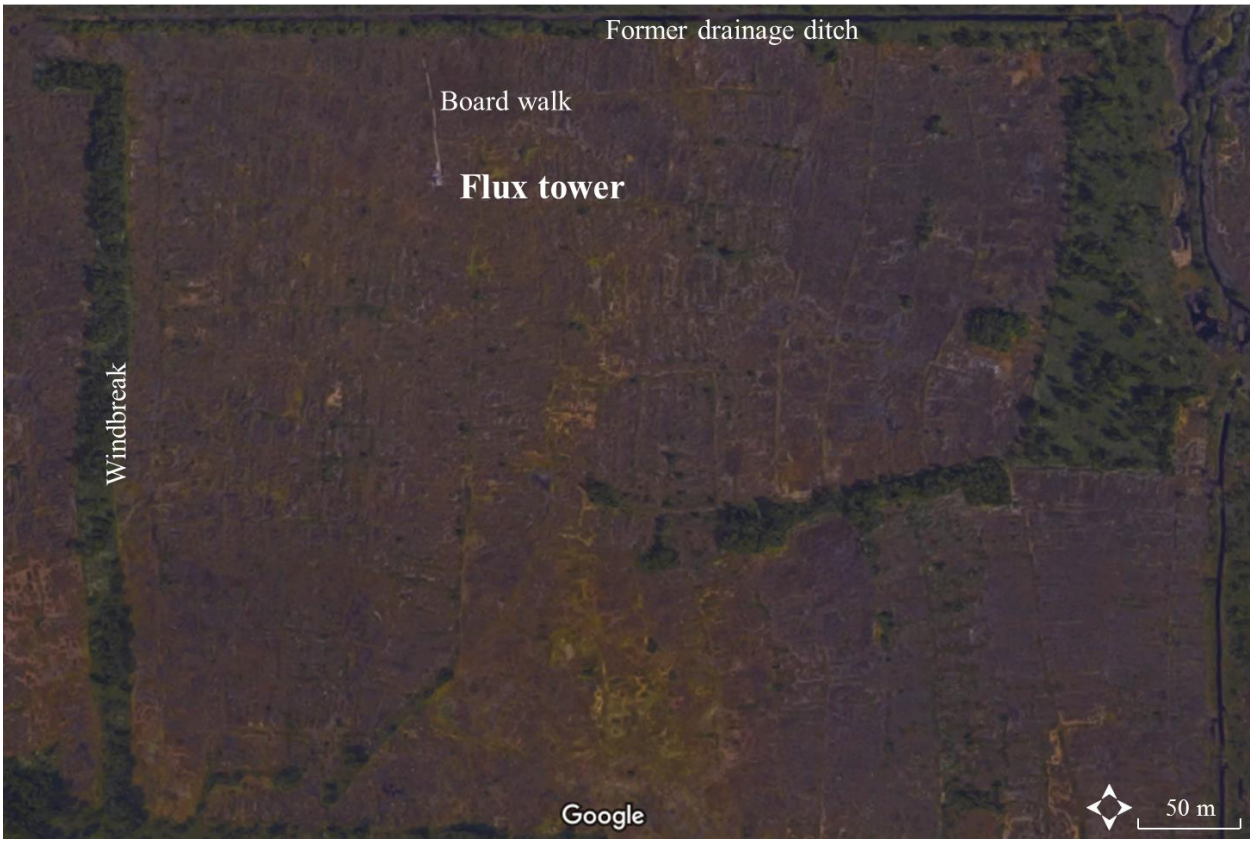

Figure 2.2 Study block of the flux tower and the access by boardwalk. This photo was centred at 122°59’03"W, 49°07’42”N (WGS-84). Background aerial photo: Google Maps.

Figure 2.3 The dam built for blocking water to rewet the disturbed surfaces (photo taken by Andreas Christen on April 8th 2016).

Figure 2.4 Aerial photograph of the flux tower seen from the NW. To the left is the boardwalk (photo taken by Metro Vancouver by helicopter in July 2014).

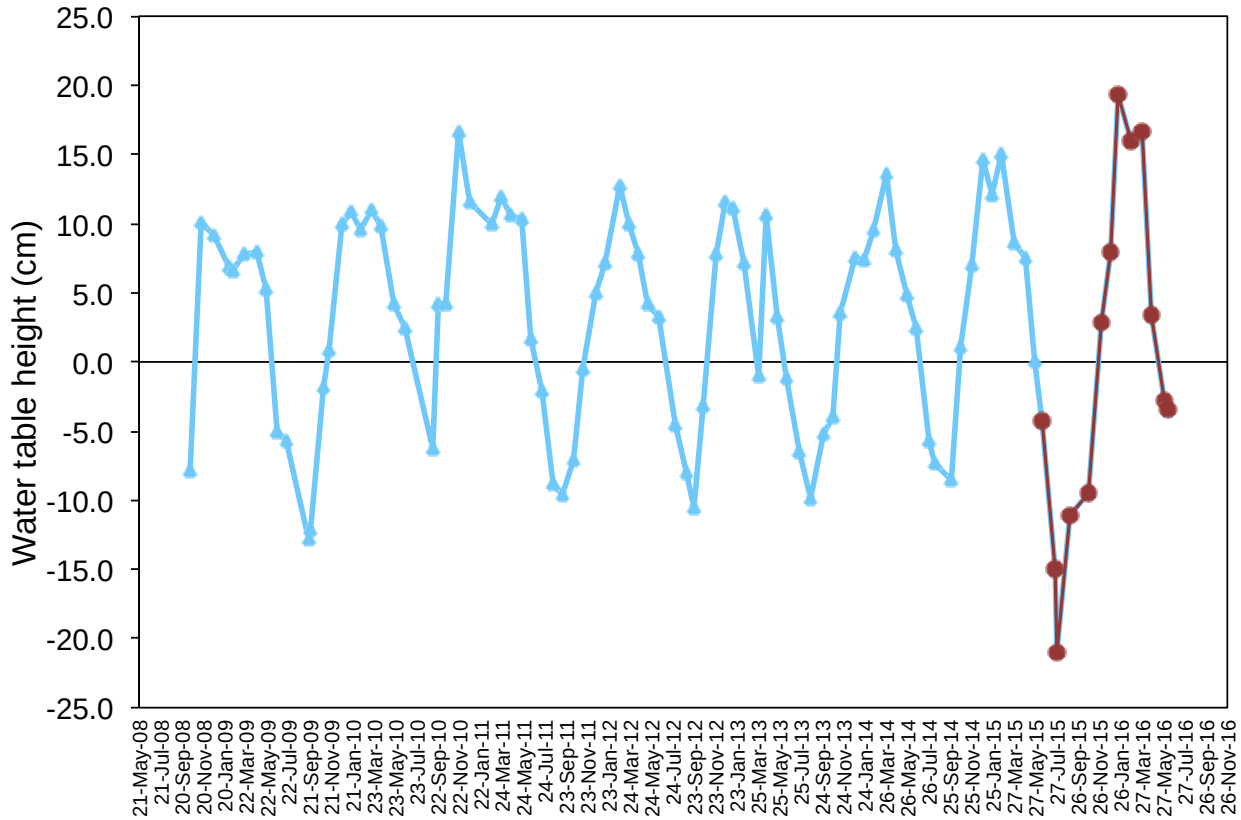

Figure 2.5 The fluctuations of water table position recorded by the Municipality of Delta from October 12th 2008 to June 11th 2016 from the Delta 08-55 site (400 m away from the tower, but in the same rewetted area). The measurements during the study year are shown in red.

2.2 Instrumentation

2.2.1 Tower platform

In June 2014, a flux tower has been established in the homogeneous plot at the study site (Figure 2.2), initially to provide continuous eddy covariance (EC) measurements of the energy balance and evapotranspiration and standard climate variables (wind, temperature, humidity, radiation). The 4-m-tall flux tower is located on a floating platform, 150 m to the east of a windbreak, and 100 m to the south of the drainage ditch (Figure 2.2 for exact location). For the

current study, the tower was also used to mount instrumentation to measure additional environmental variables and GHG fluxes by means of EC.

2.2.2 Climate measurements

All four radiation components (shortwave (K) / longwave (L) incoming (↓) and outgoing (↑)) were measured since July 9th 2014 by a four-component net radiometer (CNR1, Kipp and Zonen, Delft, Holland) on top of the tower. On June 9th 2015, two quantum sensors (LI-190, LI-COR Inc., Lincoln, NE, USA) were installed at the top of tower to measure incoming and outgoing photosynthetically active radiation (PAR). Precipitation is measured with an unheated tipping bucket rain gauge (TR-525M, Texas Electronics, Dallas, TX, USA, since June 2014) at 1 m height, which is 10 m north of the tower. Air temperature (T_a) and relative humidity (RH, HMP-35 A, Vaisala, Finland, since June 2014) are measured at heights of 2.0 m and 0.3 m, and soil thermocouples (home-made type T (copper-constantan) thermocouples, since June 2014) are recording soil/water temperatures at depths of 0.05, 0.10 and 0.50 m. A soil volumetric water content (θ_w) sensor (CS616, Campbell Scientific (CSI), Logan, UT, USA, since June 2014) is inserted vertically to measure integrated θ_w from the surface to a depth of 0.30 m. A pressure transducer (CS400, CSI) was installed on July 28th 2015 at the observation wells at west of the tower to continuously measure WTH. Also on July 28th 2015, two redox sensors (Single-Junction ORP Electrode, Cole-Parmer) and two thermocouples were installed at the 0.10-m and 0.30-m depths to record oxidation reduction potential and water temperatures. These sensors are 1.5-m away from the tower at the southwest side. At the time of writing of this thesis (July 2016), all measurements are ongoing (Figure 2.6).

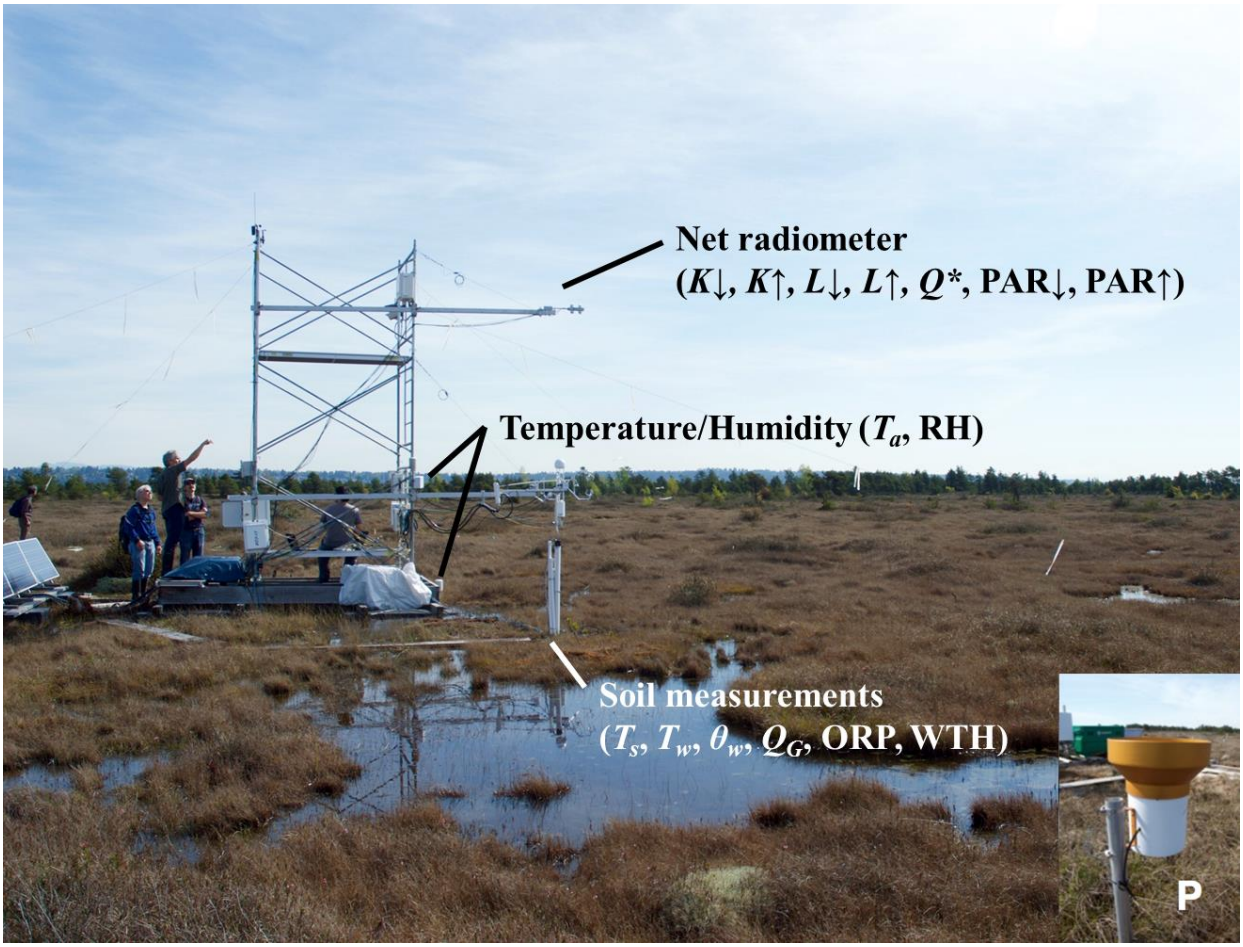

Figure 2.6 Flux tower with instruments that measured climate variables indicated (photo taken by HaPe Schmid on April 8th 2016).

2.2.3 Eddy-covariance measurements

A first eddy-covariance system (EC-1) was operated at a height of 1.8 m (facing south) between July 9th 2014 and June 16th 2016. The EC-1 system consisted of an ultrasonic anemometer-thermometer (CSAT-3, Campbell Scientific Inc. (CSI)) and an open-path CO_2/H_2O infrared gas analyzer (IRGA, LI-7500, LI-COR Inc.). The ultrasonic anemometer-thermometer measures three-dimensional wind (u, v, w, in m s^{-1}) and sonic temperature (T_s, in ℃) at 60 Hz and outputs data at 10 Hz. The IRGA measures water vapor density (ρ_v) and CO_2 density (ρ_c) at

10 Hz. The 10-Hz data from both instruments are sampled on a data logger (CR1000, CSI) and all data are stored on a CompactFlash Module (NL115, CSI).

A second EC system (EC-2) was added on June 10th 2015 and at the time of writing of this thesis is still running. The EC-2 system is also located at a height of 1.8 m, 1.8 m to the west of EC-1 (Figure 2.7), and faces south. EC-2 consists of an ultrasonic anemometer-thermometer (CSAT-3, CSI) and two IRGAs. One IRGA measures H_2O/CO_2 (enclosed-path analyzer, LI-7200, LI-COR Inc.) and the other one measures CH_4 (open-path analyzer, LI-7700, LI-COR Inc.). All embedded software for LI-7200 (version 8.0.0) and LI-7700 (version 1.0.23) were updated to the latest version offered by LI-COR during the study period. The ultrasonic anemometer-thermometer measures three-dimensional wind (u, v, w, in m s^{-1}) and sonic temperature (T_s, in ℃) at 60 Hz and outputs data at 20 Hz. The IRGA measures water vapor density (ρ_v), CO_2 density (ρ_c), and CH_4 density (ρ_m) at 20 Hz. Therefore, EC-2 measures the same varaibles as EC-1 (u, v, w, ρ_v, ρ_c redundancy) but additionally measures ρ_m. Data from EC-2 are collected by an analyzer interface unit (LI-7550, LI-COR Inc.) and processed on-site by a SMARTFlux system (Synchronization, Management And Real Time Flux system, LI-COR Inc.). The SMARTFlux system consists of a hardware component that is integrated into the LI-7550, and features a built-in GPS receiver, and a compact processor that is based on the established EddyPro flux processing software (LI-COR Inc.). It can process fluxes of sensible heat (H), latent heat (LE) or H_2O vapour (i.e., evapotranspiration), CO_2, and CH_4 fluxes at the site in real time.

The path separation between LI-7500 and CSAT3 is 5 cm in EC-1. The northward-separation of LI-7200 is 20 cm. The northward-separation of LI-7700 is 40 cm and eastward-separation of LI-7700 is 20 cm. A roughness length (z_0) of 0.055 m was used as a constant for

study period (see Appendix A for calculation). In this thesis, data from June 16th 2015 to June 15th 2016 are used unless otherwise stated, and this time period is referred to as "study year".

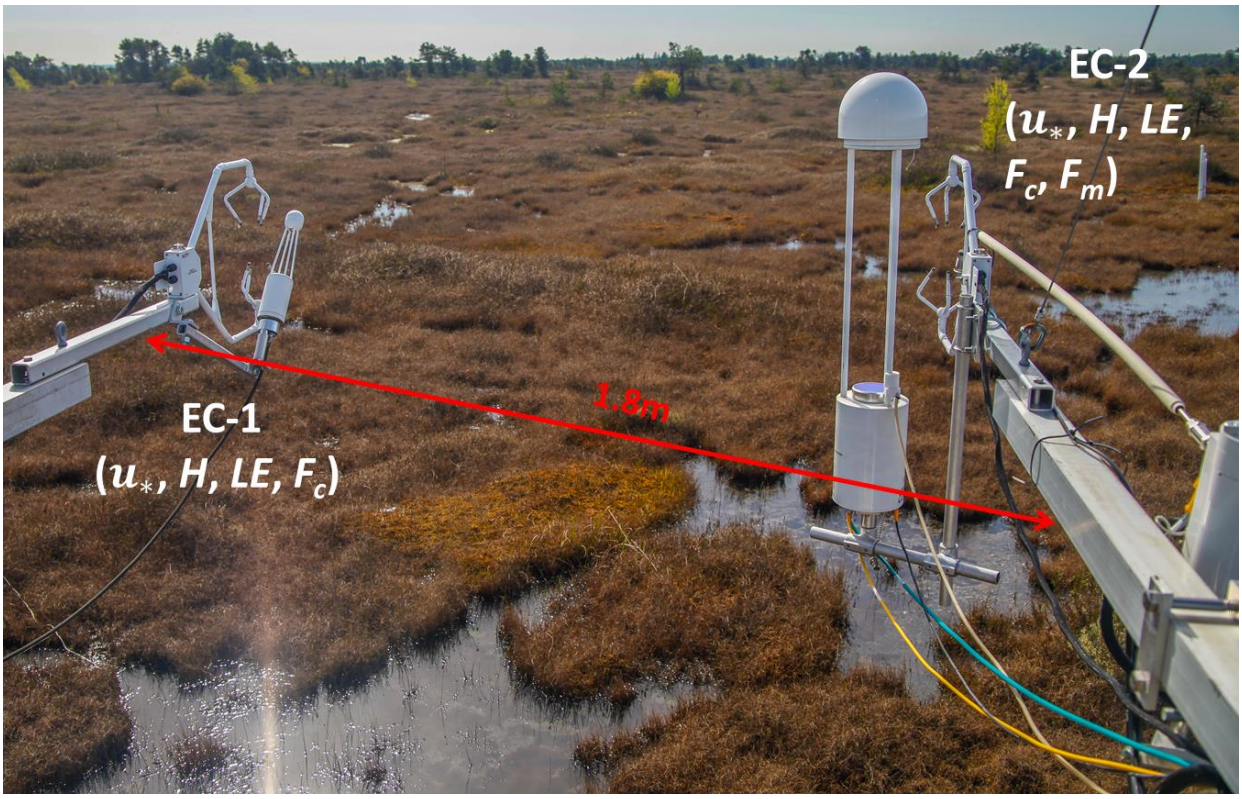

Figure 2.7 EC-1 and EC-2 systems on the tower facing south (photo taken by Andreas Christen on April 8th 2016).

2.2.4 Power and communication system

Each EC system was powered by 8 x 110 Ah AGM (Absorbent Glass Mat) batteries that were charged by 4 x 110-W solar panels. The low-frequency data from the data logger was transferred to the University of British Columbia (UBC) every four hours by cellular modem (Huawei B890 4G cellular modem). Processed summary files from SMARTFlux were automatically downloaded daily at 7 am. The automatic data transfer (Figure 2.8) allowed the performance of the system to be monitored and the measurements to be displayed in real time on

the internet. The high-frequency data of the EC-1 system were stored on industrial CF cards then processed manually. The EC-2 system stored high-frequency data on USB sticks. Both were manually swapped every two weeks, and a backup created on DVDs at UBC.

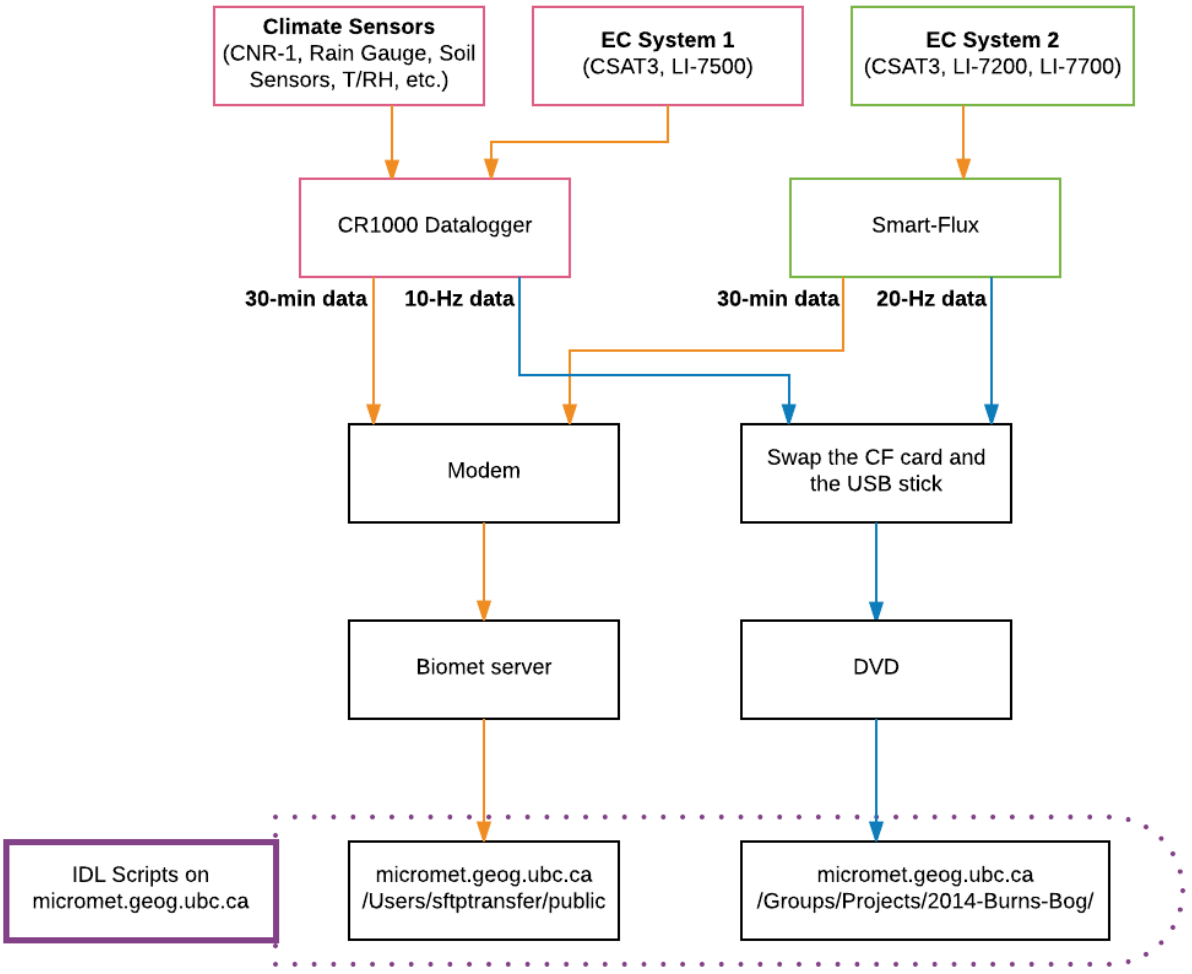

Figure 2.8 Data transfer and processing scheme for EC-1 and EC-2.

2.2.5 IRGA calibration and maintenance

Prior to installation, all three IRGAs were calibrated in the laboratory and the internal chemical scrubbers were all renewed. IRGAs measuring CO_2 were calibrated by using pure N_2 (zero gas) and two tanks of different CO_2 mixing ratios (span). Water vapour concentrations were calibrated using a dew point generator (LI-610, LI-COR Inc.). The CH_4 IRGA was calibrated using a two-stage calibration process with N_2 for zero and CH_4 in air at a known mixing ratio. The IRGA in the EC-1 system was calibrated in May 2014 and IRGAs in the EC-2 system were calibrated in June 2015. Gas tanks for zero (N_2) and span (CO_2 in air and CH_4 in N_2) were available at the tower and were used regularly to recalibrate sensors on-site (Figure 2.9). IRGAs in EC-2 were calibrated every two weeks in the first three months after the system was installed. Based on the stable performance in this period, it was decided to calibrate them once every 90 days afterwards, to minimize any disturbance.

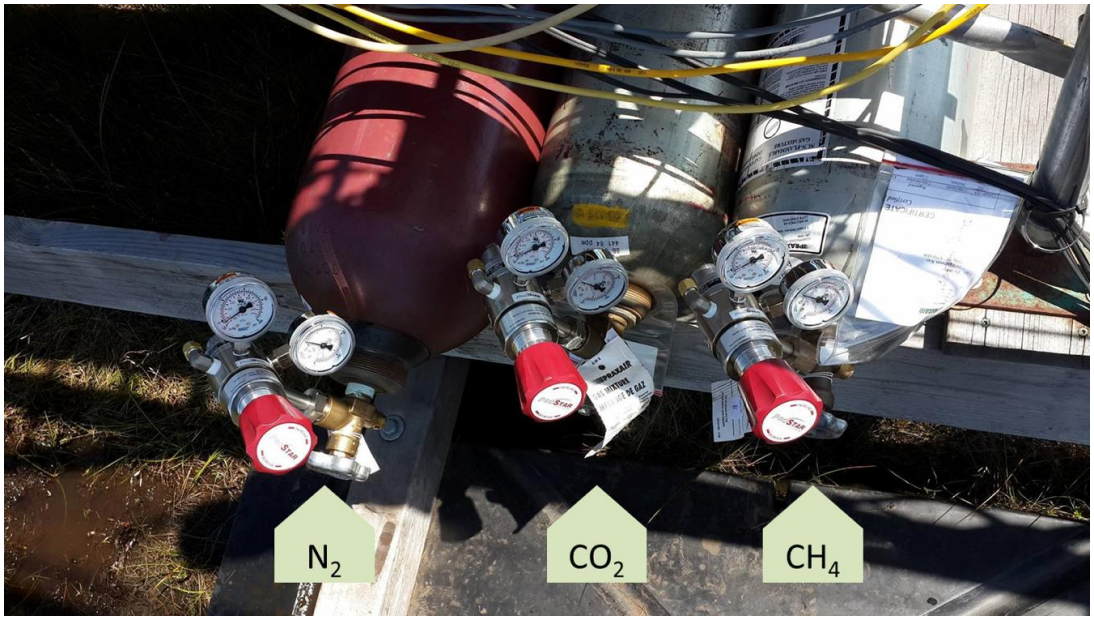

Figure 2.9 The field calibration gas tanks for the EC-2 system at base of the tower (photo taken by Sung-Ching Lee on June 11th 2015).

It is critical to keep the mirrors on LI-7700 clean. A user-specified time slot (at 23:00 PST for this study) and a signal strength threshold (below 55% for this study) were set up for automatic cleaning for lower mirror. However, it was found that this strategy did not maintain the signal strength and as was not able to clean the upper mirror. Therefore, we used microfiber cloth to manually clean both mirrors every ~15 days. With the combination of daily automatic and bi-weekly manual cleaning, the signal strength of LI-7700 was strong enough most of the time (Figure 2.10).

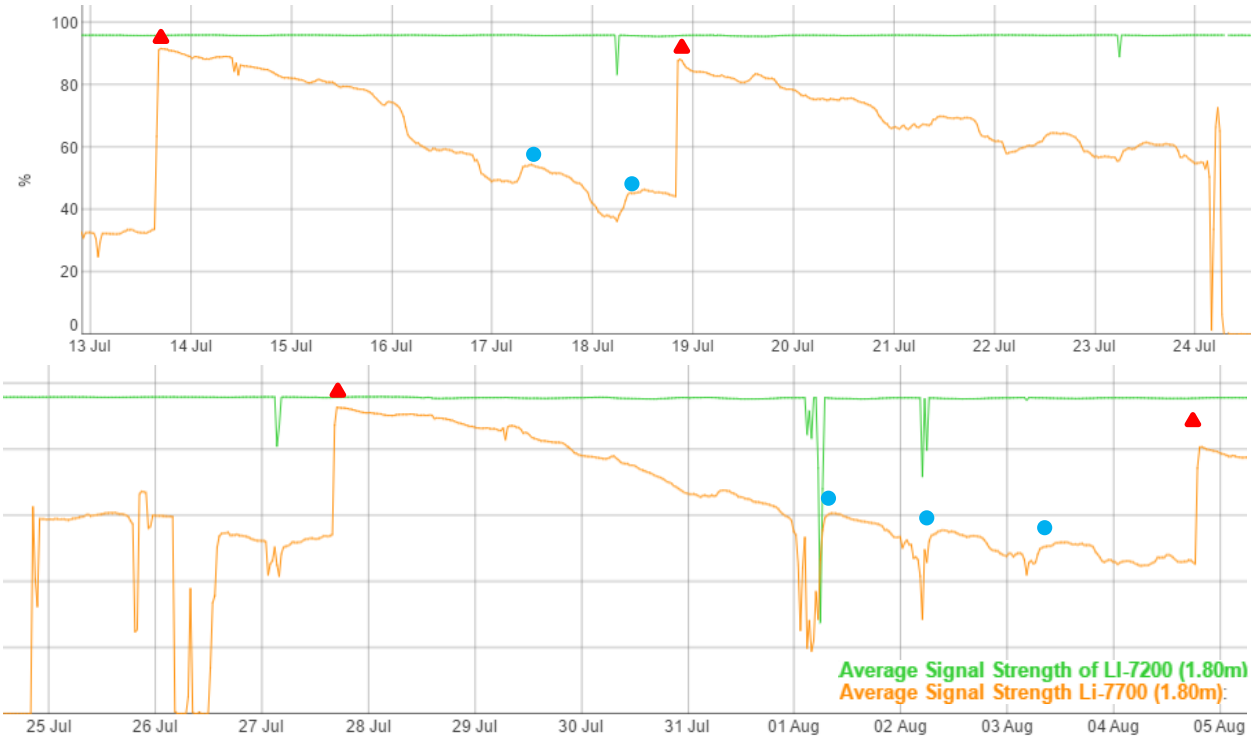

Figure 2.10 The signal strength of LI-7700 in summer 2015. The red triangle indicates when the manual cleaning was performed. The blue circle indicates when the automatic cleaning was triggered.

2.3 Data processing

2.3.1 Calibration and correction of climate measurements

Each CNR1 is provided with the sensor serial number and calibration factors by the manufacturer. The calibration factors were checked based on the procedures described in internal report written by Eugénie Paul-Limoges in 2010 (Paul-Limoges, E., 2010). The coefficients are 113.73 W m^{-2} mV^{-1} and 113.74 W m^{-2} mV^{-1} for shortwave and longwave radiation, respectively. Six uncalibrated quantum sensors (PAR sensors) were compared to the Biomet Standard quantum sensors (LI-190, LI-COR Inc.) to determine the best two for this study in May 2015. See Appendix B for details.

Temperature could cause error in measured θ_w (CS616). The magnitude of the temperature sensitivity changes with θ_w. The following equation was used to correct the CS616 output (Rhoades et al., 1989):

$$\theta_{\text{corrected}} = \theta_{\text{raw}} + (20 - T_s) * (0.526 - 0.052 * \theta_{\text{raw}} + 0.00136 * {\theta_{\text{raw}}}^2) \quad (1)$$

where θ_{raw} is the measured soil volumetric water content, and $\theta_{\text{corrected}}$ is the post-processed soil volumetric water content to exclude the errors. The pressure transducer to measure WTH was calibrated by plastic cylinder from 0 cm to 30 cm of water in the lab. The conversion from the laboratory test was initially used in September 2015 then modified on site on December 10th 2015. Thus, the WTH measurements before the new calibration were corrected as follows:

$$WTH_{\text{corrected}} = \left(\frac{\text{Multiplier}_{\text{new}}}{\text{Multiplier}_{\text{old}}} * (WTH_{\text{uncorrected}} + 100 - \text{Offset}_{\text{old}})\right) + \text{Offset}_{\text{new}} \quad (2)$$

2.3.2 Eddy covariance flux calculation

All variables required to calculate fluxes were filtered in EC-1 (based on Crawford et al, 2009) and in EC-2 (based on EddyPro Express mode). After the preliminary process, the raw molar fluxes of CO_2 and CH_4 were calculated by vertical wind and molar densities, using Reynold's rules of averaging (Reynolds, 1895):

$$F_c = \overline{w\rho_c} = \overline{w'\rho_c{}'} + \overline{w}\,\overline{\rho_c} \tag{3}$$

$$F_m = \overline{w\rho_m} = \overline{w'\rho_m{}'} + \overline{w}\,\overline{\rho_m} \tag{4}$$

F_c and F_m are the CO_2 and CH_4 molar fluxes, respectively. The first term on the right hand side in Eq. (3) and Eq. (4) include the fluctuations of vertical velocity (w'), CO_2 molar density ($\rho_c{}'$), and CH_4 molar density ($\rho_m{}'$). The second term is the product of the mean vertical wind velocity ($\overline{w}$), mean CO_2 molar density ($\overline{\rho_c}$), and mean CH_4 molar density ($\overline{\rho_m}$). The magnitude of $\overline{w}$ is too small to be measured using anemometry and so is evaluated indirectly as shown by Webb et al (1980). They showed it is sensitive to variations in air temperature (T_a) and water vapour molar density (ρ_v) and derived the following "Webb-Pearman-Leuning (WPL)" equations for calculating the vertical fluxes of trace gases (in this case CO_2 and CH_4):

$$F_c = \overline{w'\rho_c{}'} + \frac{\overline{\rho_c}}{\overline{\rho_a}}\overline{w'\rho_v{}'} + \frac{\overline{\rho}}{\overline{\rho_a}}\frac{\overline{\rho_c}}{\overline{T}}\overline{w'T'} \tag{5}$$

$$F_m = \overline{w'\rho_m{}'} + \frac{\overline{\rho_m}}{\overline{\rho_a}}\overline{w'\rho_v{}'} + \frac{\overline{\rho}}{\overline{\rho_a}}\frac{\overline{\rho_m}}{\overline{T}}\overline{w'T'} \tag{6}$$

Other variables in Eq. (5) and Eq. (6) are the air molar density (ρ) and dry air molar density (ρ_a). Further computations carried out using the EddyPro software (LI-COR Inc.). Wind data from EC-2 has been corrected in the post-processing to account for a floating channel in the communications cable (see details of the correction in Appendix C).

The measured CH_4 density is not only affected by T_a and ρ_v, but also by spectroscopic effects from changes in temperature, pressure, and water vapor (Rothman et al., 2009). To include the spectroscopic correction in Equation 6, a modified equation can be written as follows:

$$F_m = \bar{\chi}\left\{\overline{w'\rho_m{}'} + \frac{m_a}{m_v}\frac{\overline{\rho_m}}{\overline{\rho_a}}\overline{w'\rho_v{}'}[A] + \left(1 + \frac{\overline{\rho_v} m_a}{\overline{\rho_a} m_v}\right)\frac{\overline{\rho_m}}{\bar{T}}\overline{w'T_a{}'}[B]\right\} \quad (7)$$

$$[A] = \left[1 + (1 - \overline{x_v})\alpha_v \overline{Pr}\frac{\chi_{Pt}}{\bar{\chi}}\right] \quad (8)$$

$$[B] = \left[1 + (1 - \overline{x_v})\bar{T}\frac{\chi_T}{\bar{\chi}}\right] \quad (9)$$

where the gray rectangles show multipliers in Equation 7. χ is the dimensionless correction factor which is a function of temperature and equivalent pressure (Burch et al., 1962), α_v is the gas broadening coefficient for water vapor, x_v is the partial water pressure, *Pt* is the water vapour pressure and *Pr* is the total air pressure. This correction was applied to CH_4 fluxes only. An overview of flux calculations are shown in Table 2.1.

Table 2.1 Procedures of flux calculation in EC-1 and EC-2.

	EC-1	EC-2
Instrumentation	CSAT-3 Ultrasonic Anemometer (60 Hz → 10 Hz) LI-7500 (Open path, 10 Hz) Height is 1.8 m	CSAT-3 Ultrasonic Anemometer (60 Hz → 20 Hz) LI -7200 (Enclosed-path, 20 Hz) LI -7700 (Open-path, 20 Hz) Height is 1.8 m
Filters	· Block averaging · Double rotation · Spike removal · Absolute limits · Skewness and kurtosis	· Block averaging · Double rotation · Covariance maximization · Spike removal · Amplitude resolution · Drop-outs · Absolute limits · Skewness and kurtosis
Flux calculations	· Sonic temperature correction for humidity in *H* (Schotanus et al. 1983) · Compensations for density fluctuations in *LE* and CO_2 fluxes (Webb et al., 1980) · Sensor separation in *H*, *LE* and CO_2 fluxes (Moore 1986)	· Angle of attack corrections · Sonic temperature correction for humidity in *H* (van Dijk et al. 2004) · Compensations for density fluctuations in *LE*, CO_2 and CH_4 fluxes (Webb et al., 1980) · Spectral correction in *LE* and CO_2 fluxes (Moncrieff et al. 1997) · Spectroscopic corrections CH_4 fluxes (McDermitt et al., 2010).
Quality control	Diagnostic value u_* filter Wind directions from 330° to 30° were discarded to exclude the influence from the tower itself	CarboEurope IP project Wind directions from 330° to 30° were discarded to exclude the influence from the tower itself

2.4 Gap filling algorithms

For annual and continuous climate and flux measurements, missing data is unavoidable due to challenging weather and possibly power outages during low-light situations (solar panels).

2.4.1 Gap filling of climate data

Small gaps (<180 minutes) of missing climate were filled by linear interpolation. Larger gaps in T_a, precipitation and RH were filled by data from the station "Delta - Burns Bog", Environment Canada, located in the BBECA 1.3 km to the west of the current study site. Missing data in WTH were filled by interpolating manual measurements from the municipality of Delta at the site closest to the tower. Large gaps in the rest of the climate data were infilled with data from "Vancouver-Sunset" (FLUXNET ID "Ca-VSu", 13 km to the NW of the current site) by means of linear regression. PAR was not measured at Sunset Tower, thus gap filling of PAR irradiance data was done by converting shortwave irradiance using factor determined by the relationship between measured PAR irradiance and shortwave irradiance ($K_{\downarrow}$, in W m^{-2}) at the study tower:

$$\text{PAR} = 1.7943\ (\mu\text{mol J}^{-1})\ K_{\downarrow} \quad (10)$$

Reflected PAR was filled by determining a typical PAR reflecting coefficient from available data in the given month, then PAR reflectance could be converted by the filled PAR irradiance based on the coefficient (α, $\text{PAR}_{\uparrow} = \alpha\text{PAR}_{\downarrow}$).

The WTH sensor was installed later than the beginning of the study year. WTH in the period before installation and the gaps in WTH were filled by the manual measurements from the

Delta observation site “Delta 08-55” interpolated using a spline interpolation between measurement times. Below gap filling techniques employed for climate and flux data are presented.

2.4.2 Gap filling of flux data

Quality control procedures were applied to the data through different strategies in EC-1 and EC-2, respectively. Data from the EC-1 system was processed at UBC using in-house software following the procedures documented in Crawford et al. (2013). Data from EC-2 was processed on-site by SMARTFlux (version 1.4.0) using ‘express mode’ and later through re-processing in advanced mode using Eddy Pro (version 6.1.0). For EC-2 quality flags are calculated based on the quality flagging policy of the CarboEurope IP project (Foken et al., 2004). “0” means high quality fluxes, “1” means fluxes were only used for budget and controls analysis, “2” fluxes were discarded from the final dataset.

Small gaps (<60 minutes) of missing CO_2 and CH_4 fluxes were filled by linear interpolation. Longer gaps are filled using empirical relationships between CO_2 / CH_4 fluxes and environmental variables. Two-year of measurements of CO_2 fluxes were used for modelling R_e and GEP.

Since there were two EC systems running with redundant fluxes of CO_2, the sensitivity of different combinations of data (EC-1 vs. EC-2 or using an average of both) have been explored (Appendix D). For the data presented in the current thesis, data from EC-1 were used for CO_2 fluxes, *H*, *LE* and EC-2 was for fluxes of CH_4 fluxes only, as justified in Appendix C and D.

2.4.2.1 Gap filling of CO_2 flux data

For gaps longer than 2 hours in CO_2 fluxes, the CO_2 flux was modelled as net ecosystem exchange (NEE), which is the difference between ecosystem respiration (R_e) and gross ecosystem photosynthesis (GEP):

$$\mathrm{NEE} = R_e - \mathrm{GEP} \tag{11}$$

where a negative NEE represents a net-sink and a positive NEE represents a net source of CO_2 from the surface. Nocturnal NEE is equal R_e as there is no photosynthesis (GEP) at night.
R_e is modelled based on soil temperature at the 5-cm depth ($T_{s,5cm}$) using a logistic fit (Barr et al., 2002; Kljun et al., 2006; Krishnan et al., 2008):

$$R_e = \frac{1}{r_1 r_2^{T_{s,5cm}} + r_3} \tag{12}$$

The empirical parameters r_1, r_2, and r_3 were determined separately for each day, using a moving window of 120 days (60 days into past and 60 days into future) based on all measured nighttime data when friction velocity was higher than 0.08 m s^{-1}. Appendix D.2 determines the effect of using different window sizes (60, 90, 120 and full year) on the annual modelled and gap-filled R_e and justifies why a moving window size of 120 days was used. The sensitivity of window size on gap filled R_e was small (between 221 and 229 g C m^{-2} $year^{-1}$ for R_e, see Appendix D.2).

GEP is modelled using the photosynthetic light-response curves (Ö gren and Evans, 1993) based on photosynthetic photon flux density (PPFD in µmol m^{-2} s^{-1}):

$$\mathrm{GEP} = \frac{MQY \cdot \mathrm{PPFD} + P_M - ((MQY \cdot \mathrm{PPFD} + P_M)^2 - 4 \cdot C_v \cdot MQY \cdot \mathrm{PPFD} \cdot P_M)^{0.5}}{4 \cdot C_v} \quad (13)$$

Maximum photosynthetic rate at light saturation (P_M) and maximum quantum yield (MQY) were fitted parameters based on measured daytime NEE by subtracting daytime R_e (using Equation 12). Convexity (C_v), an empirical parameter to describe curvature, was fixed at 0.7. The time-varying parameters MQY and P_M were fitted separately for each day, using a moving window of 90 days (45 days into past and 45 days into future) using all data when friction velocity was higher than 0.08 m s^{-1}. The sensitivity of window size on gap filled GEP was small (385 and 415 g C m^{-2} $year^{-1}$, see Appendix D.2).

This gap filling approach was also compared against an independent online tool provided by the Department of Biogeochemical Integration at the Max Planck Institute for Biogeochemistry in Jena, Germany. Differences between the online tool and the current approach on annual NEE are small (less than 20 g C m^{-2} yr^{-1}) and comparisons are summarized in Appendix D.3.

2.4.2.2 Gap filling of CH_4 flux data

CH_4 fluxes with quality flags 0 and 1 were plotted against all related variables including WTH, θ_w, oxidation reduction potential, T_a, and $T_{s,5cm}$. The main control was $T_{s,5cm}$ and used to build a model to fill the gaps in CH_4 fluxes (for a selection and discussion of the relationship, see Section 3.4.3):

$$F_m = ae^{bT_{s,5cm}} \quad (14)$$

where F_m is CH_4 fluxes, $T_{s,5cm}$ is soil temperature at 5 cm depth, and *a* and *b* are empirical parameters.

2.5 Calculating CO_2e by GWP

The effect of CO_2 and CH_4 was compared considering the GWP for both gases by converting the molar fluxes to CO_2 equivalent mass fluxes as follows:

$$CO_2\text{e (g)} = m_{CO_2}F_{CO_2} + GWP_{CH_4}m_{CH_4}F_{CH_4} \quad (15)$$

where CO_2e (g) is CO_2 equivalent mass fluxes of CO_2 and CH_4, respectively. The unit of CO_2e is g CO_2e m^{-2} s^{-1}. GWP_{CH_4} is the mass-based GWP (g g^{-1}). In this study, 100-year and 20-year GWPs were used following IPCC's fifth assessment report (IPCC, 2014). The 100-year GWP of CH_4 is 28, and 20-year GWP of CH_4 is 84, respectively (IPCC, 2014). F_{CO_2} and F_{CH_4} are the study-period averaged molar fluxes expressed as mmol m^{-2} day^{-1} for both gases, and m_{CO_2} and m_{CH_4} are their molar mass (in g $mmol^{-1}$). N_2O fluxes have been neglected in this study, because previous chamber-based measurements during the growing season found no significant emissions or uptake of N_2O in several plots in the BBECA (Christen et al., 2016).

Chapter 3: Results and Discussion

3.1 Weather during the study year

3.1.1 Temperatures

Table 3.1 shows the T_a and T_s, measured at the flux tower in each month of the study year from June 2015 to June 2016.

The site experienced an annual average T_a (2 m height) of 11.3 ℃ from June 16th 2015 to June 15th 2016. Mean monthly T_a ranged between 4.4 (Jan 2016) and 19.3 ℃ (Jul 2015). The minimum T_a was -7.5℃ (on December 31st 2015 08:15 PST) and the maximum T_a was 35.0℃ (on August 8th 2015 14:50 PST). The annual average T_s at 5-cm depth and 50 cm depth are 11.7 ℃ and 11.3 ℃. Although the annual average values of both T_s were similar to T_a, the amplitudes were smaller in $T_{s,50cm}$ than T_a, as expected. Mean monthly $T_{s,5cm}$ ranged from 4.8 ℃ (Jan 2016) to 19.6 ℃ (Jul 2015), which followed T_a closely. The rate of warming on monthly scale for $T_{s,5cm}$ was same as T_a, but the rate of cooling for $T_{s,5cm}$ was lower than T_a. Mean monthly $T_{s,10cm}$ ranged from 6.4 ℃ (Jan 2016) to 16.1 ℃ (Jul 2015), the amplitude was smaller (9.7 K) than $T_{s,5cm}$ and T_a (12.8 K). The rate of warming and cooling on monthly scale for $T_{s,10cm}$ were both lower than $T_{s,5cm}$ and T_a.

Climate normals over 30 years do not exist for Burns Bog (the Environment Canada climate station "Delta Burns Bog" has operated since 2010 only). Therefore, T_a and P measured 16 km to the NW at Vancouver International Airport (YVR) are used as climate normals. The mean temperature at YVR during the study year was 10.6 ℃ compared to 10.4 ℃ from the climate normals for 1981-2010 (Table 3.2). Almost all months during the study period were warmer than the 30-year average (Figure 3.1). June 2015 departed most from the climate normals, it was the most unusual month with the highest temperature.

Table 3.1 Monthly precipitation, temperature and shortwave irradiance measured at the flux tower during the study period.

Month	Air temperature *2m* (T_a, ℃)	Soil temperature –5 cm ($T_{s,5cm}$, ℃)	Soil temperature –50 cm ($T_{s,5cm}$, ℃)	Precipitation *1m* (P, mm month^{-1})
Jun-15	18.1	18.3	14.9	10.7
Jul-15	19.3	19.6	16.1	22.7
Aug-15	18.2	19.2	17.0	55.6
Sep-15	13.2	15.6	15.8	18.8
Oct-15	11.4	12.6	13.6	116.9
Nov-15	4.6	6.7	10.2	146.8
Dec-15	4.9	5.5	7.6	204.6
Jan-16	4.4	4.8	6.4	149.9
Feb-16	7.1	7.7	7.6	136.8
Mar-16	8.8	10.0	9.0	133.3
Apr-16	12.4	14.5	11.6	18.2
May-16	14.6	16.2	13.4	31.4
Jun-16	16.1	18.6	14.9	42.7
Jun 16th 2015 - Jun 15th 2016	**11.3**	**11.7**	**11.3**	**1061.7 mm yr^{-1}**

Table 3.2 Monthly precipitation and temperature measured during the study year and over 30 years at Vancouver International Airport (Data: Environment Canada).

Month	Study year Air temperature (℃)	30-year Air temperature (℃)	Study year Precipitation (mm month^{-1})	30-year Precipitation (mm month^{-1})
Jun-15	17.9	15.7	11.0	53.8
Jul-15	19.3	18	20.8	35.6
Aug-15	18.4	18	67.9	36.7
Sep-15	14.1	14.9	41.8	50.9
Oct-15	11.8	10.3	112.8	120.8
Nov-15	5.0	6.3	170.8	188.9
Dec-15	5.2	3.6	230.2	161.9
Jan-16	4.7	4.1	167.2	168.4
Feb-16	7.1	4.9	130.4	104.6
Mar-16	8.3	6.9	161.6	113.9
Apr-16	11.8	9.4	24.2	88.5
May-16	14.3	12.8	51.6	65.0
Jun-16	16.1	15.7	34.6	53.8
Jun 16th 2015 - Jun 15th 2016	**10.6**	**10.1**	**1205.0 mm yr^{-1}**	**1189.0 mm yr^{-1}**

Figure 3.1 Comparison between the monthly precipitation and temperature measured during the study year and the 30-year climate normals at Vancouver International Airport (Data: Environment Canada).

3.1.2 Precipitation

The study site received a total precipitation of 1061.7 mm from June 16th 2015 to June 15th 2016 (Table 3.1). June 2015 was the driest month with only 10.7 mm at the site. The wettest month was December 2015 (204.6 mm). Snowfall was less than 5 cm, and there was no snow cover during the study year. However, based on the behaviour of $T_{s,5cm}$, the surface was frozen up to ten days at the flux tower in January 2016. The thickness of ice reached up to 10 cm.

During the study year the total precipitation at YVR was 1205.0 mm compared to the 30-yr normal of 1189.0 mm (Table 3.2). The largest difference in monthly total precipitation was observed in December 2015, when YVR received 230.2 mm (which is 68.3 mm more than its climate normal of 161.9 mm for December at YVR).

3.1.3 Radiation

The site received a total net all-wave radiation of 2.58 GJ m^{-2} year^{-1} (Table 3.3). The highest shortwave irradiance happened in June 2015 (791.4 MJ m^{-2} month^{-1}), the highest longwave irradiance was in August 2015 (946.9 MJ m^{-2} month^{-1}), and the highest upward longwave radiation was in July 2015 (1127.5 MJ m^{-2} month^{-1}). There was no negative monthly net all-wave radiation during the study year in each of the months. Albedo was lowest in April 2016 (10.5%) and highest in in November 2015 (17.2%), it may be caused by the frozen surface, shorter vegetation and lower sun angle. Annual total of PAR irradiance was 7868 mol m^{-2} year^{-1} and PAR reflectance was 499 mol m^{-2} year^{-1} (Table 3.4). The PAR reflection coefficient changed with time. It was lowest in June 2015 and 2016 (5.5%) and was highest in December 2015 (9.2%), which was related to the lack of green vegetation (mostly inactive sedges).

Table 3.3 Monthly shortwave irradiance ($\boldsymbol{K}_{\downarrow}$), shortwave reflectance ($\boldsymbol{K}_{\uparrow}$), longwave irradiance ($\boldsymbol{L}_{\downarrow}$), upward longwave radiation ($\boldsymbol{L}_{\uparrow}$), net all-wave radiation (Q^*), and albedo measured at the flux tower during the study period.

Radiation						
Month	$K_{\downarrow}$	$K_{\uparrow}$	$L_{\downarrow}$	$L_{\uparrow}$	Q^*	Albedo (%)
	MJ m^{-2} $month^{-1}$					
Jun-15	791.4	99.0	877.7	1078.3	491.7	12.5
Jul-15	735.1	99.4	938.2	1127.5	446.4	13.5
Aug-15	577.3	77.5	946.9	1104.8	341.9	13.4
Sep-15*	418.4	55.6	870.6	995.7	237.8	13.3
Oct-15	206.0	27.0	915.5	992.1	102.5	13.1
Nov-15	124.0	21.4	788.1	863.7	26.9	17.2
Dec-15	66.3	11.1	843.6	894.0	4.8	16.7
Jan-16	87.5	14.1	845.6	889.4	29.7	16.1
Feb-16	152.6	18.3	799.8	867.6	66.4	12.0
Mar-16	300.7	32.1	850.3	956.1	162.7	10.7
Apr-16	523.8	55.3	831.2	989.6	310.1	10.5
May-16	626.0	72.5	891.5	1056.3	388.8	11.6
Jun-16	657.6	78.8	891.5	1047.9	422.4	12.0
Jun 16th 2015 - Jun 15th 2016	GJ m^{-2} $year^{-1}$					**13.3**
	4.54	**0.57**	**10.84**	**11.80**	**2.58**	

* 3 days of the data in this month were filled by the procedure mentioned in Section 2.4.1. All other months have uninterrupted data.

Table 3.4 Monthly PAR irradiance (**$PAR_{\downarrow}$**), PAR reflectance (**$PAR_{\uparrow}$**), and PAR reflection coefficient measured at the flux tower during the study period.

PAR			
	$PAR_{\downarrow}$	$PAR_{\uparrow}$	PAR reflection coefficient (%)
	mol m^{-2} $month^{-1}$		
Jun-15*	1420.0	78.1	5.5
Jul-15	1322.3	79.9	6.0
Aug-15	1038.9	65.4	6.3
Sep-15*	750.7	48.8	6.5
Oct-15	368.3	24.2	6.6
Nov-15	202.3	17.4	8.6
Dec-15	107.5	9.9	9.2
Jan-16	148.1	12.0	8.1
Feb-16	266.7	17.7	6.6
Mar-16	527.7	32.7	6.2
Apr-16	723.1	56.3	6.1
May-16	1112.4	62.7	5.6
Jun-16*	1179.9	64.9	5.5
Jun 16th 2015 - Jun 15th 2016	mol m^{-2} $year^{-1}$		**6.7**
	7868	**499**	

* Part of the data in these months were filled by the procedure mentioned in section 2.4.1. All other months have uninterrupted data.

3.1.4 Wind

Figure 3.2 shows the wind rose at the flux tower for the study period. During day, winds at this site are influenced by a sea-land breeze circulation, a see breeze came from Boundary Bay (S) and Strait of Georgia (W) (Oke and Hay 1998). Therefore, wind mainly came from the south over the daytime, i.e. from Boundary Bay (Figure 3.2), which is the same direction both EC systems heading toward to (i.e. undisturbed). This direction was responsible for around 40% of all cases. The wind velocity can reach up to 7 m s^{-1}. Sometimes, the daytime wind blew from the

west, i.e. from the Strait of Georgia (primarily between 17:00 and 19:00 PST). The wind direction on average turned to east during the nighttime (Figure 3.3),), related to the land breeze and mountain wind down the Fraser Valley, and generally at night, the winds became weaker.

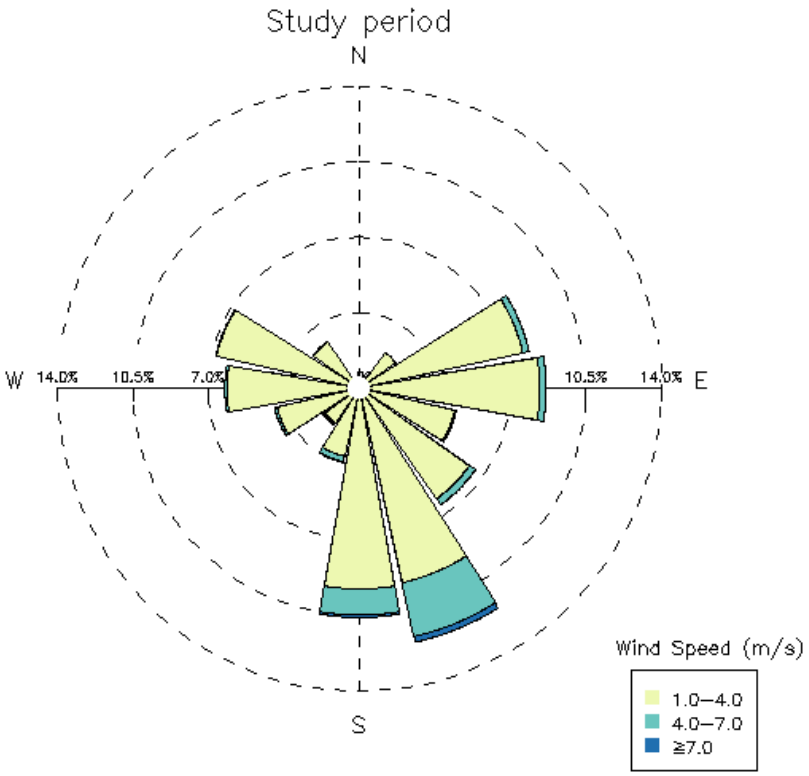

Figure 3.2 Wind rose shows the cumulative frequency in which wind speeds increase from the centre to the outside over the study period.

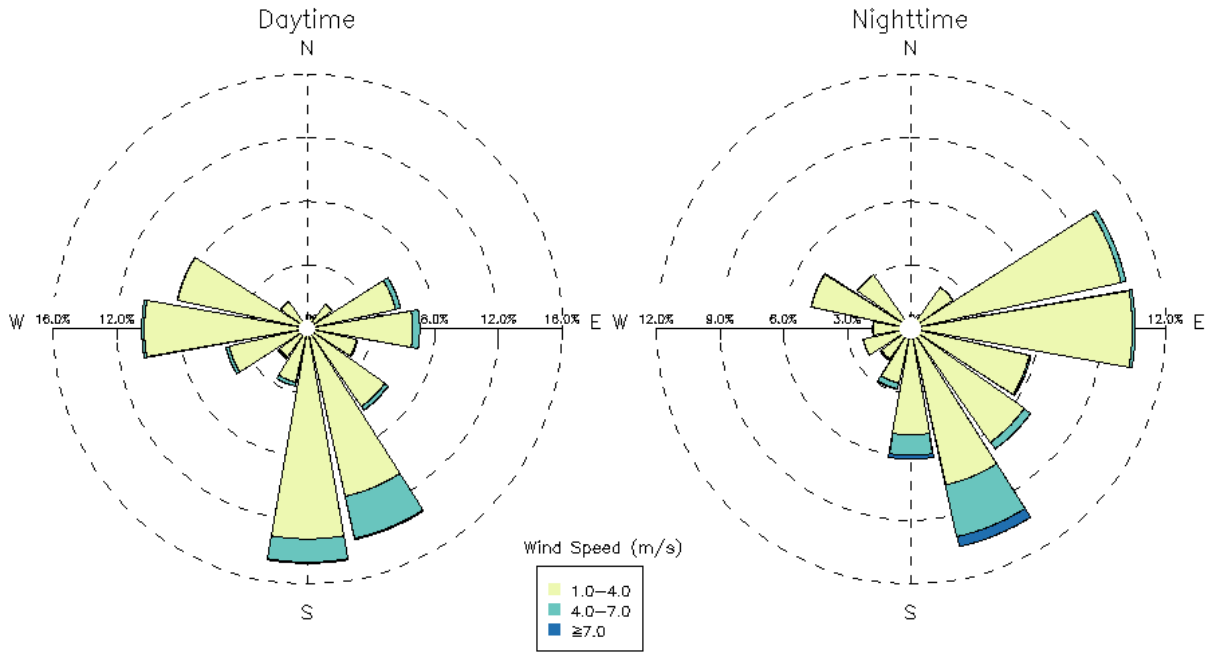

Figure 3.3 Wind rose shows the cumulative frequency in which wind speeds increase from the centre to the outside in day (when PAR was higher than 5 μmol m^{-2} s^{-1}) and night (when PAR was less than 5 μmol m^{-2} s^{-1}), respectively.

3.2 Surface conditions

3.2.1 Turbulent flux footprints

Cumulative turbulent source area was calculated using the analytical turbulent source area (turbulent footprint) model of (Kormann and Meixner, 2001) following the procedure outlined in Christen et al., 2011[1]. Figure 3.4 shows the cumulative footprint for each of the four seasons for the EC-1 overlaid on the satellite image of the site. The 80% contour line (enclosing 80% of the cumulative probability for a unit source) was entirely inside the plot in spring and summer. It reached beyond the ditches at the north side. Figures 3.5 shows the footprints for

[1] Source code is available under https://github.com/achristen/Gridded-Turbulent-Source-Area

daytime and nighttime, respectively. Unstable conditions during daytime allowed for a more constrained footprint surrounding the tower in a heart shape. The 80% contour line (enclosing 80% of the cumulative probability for a unit source) was again entirely inside the plot, and hence considered homogeneous. The stable conditions at night led to a much larger footprint, lots of fluxes came from north west of the flux tower beyond ditches. This would not cause problems, because data associated with winds from that direction were discarded due to the disturbance from the tower itself.

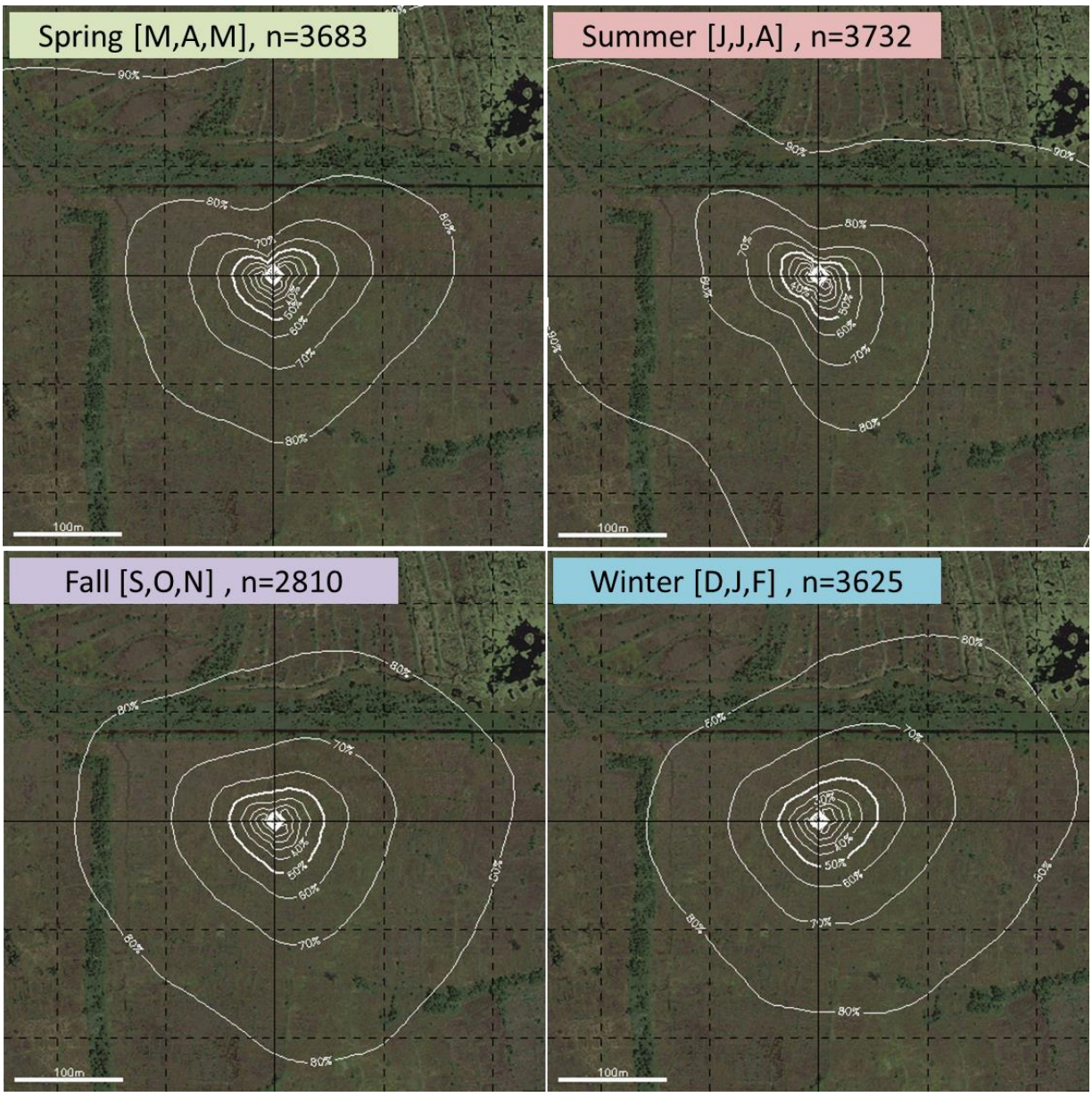

Figure 3.4 Cumulative flux footprint contours during the study period for each of seasons. The background area was centered at the flux tower, and the area is 500 m x 500 m. The contour lines are in steps of 10% from 10 to 90% of the cumulative probability. The upper left bars in each sub plot explain which months were included and list the number of available half-hourly data (*n*).

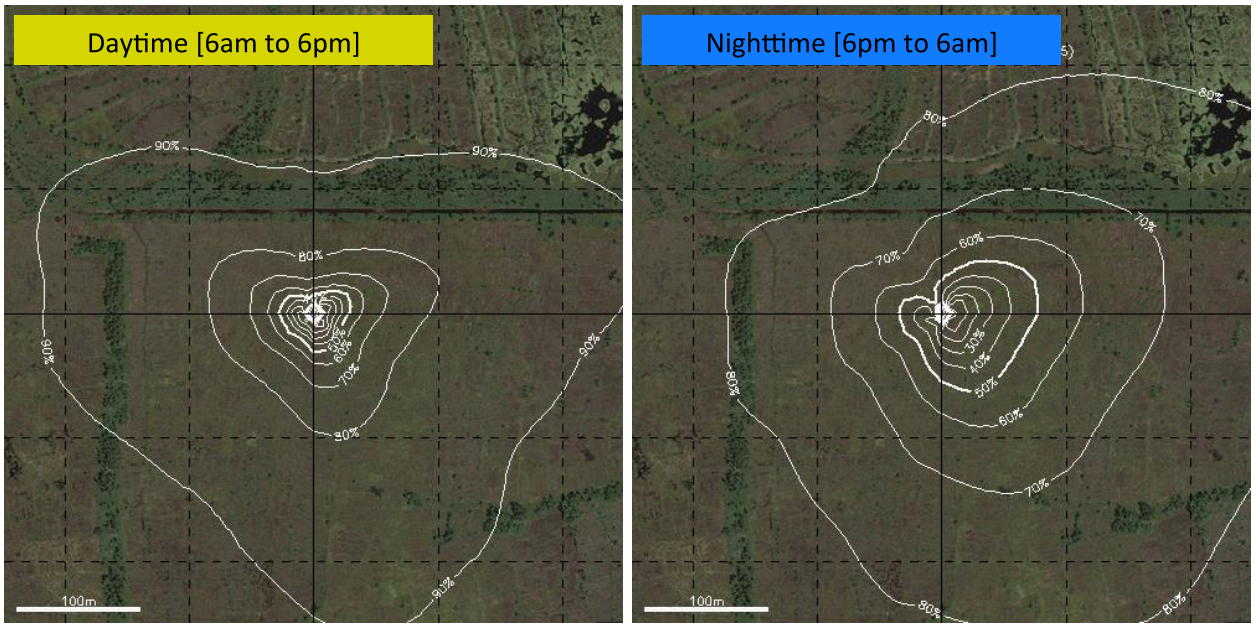

Figure 3.5 Daytime and nighttime flux footprint contours during the study period. The background area was centered at the flux tower, and the area is 500 m x 500 m. The contour lines are in steps of 10% from 10 to 90% of the cumulative probability.

3.2.2 Vegetation cover

Vegetation cover experienced a change over the study year (Table 3.5). Based on regular surveys and photos, mosses and sedges started to grow in spring and grasses grew up to 0.3 m in summer. In summer, vegetation covered almost all surface, including ponds (some with algae), the surface became less patchy compared to other seasons. Standing water ponds showed up in fall and winter, and the study area became flooded. In fall and winter, mosses and sedges were less green but continued to be active near the surface.

Table 3.5 Documentation of vegetation cover around the flux tower (photos taken by Sung-Ching Lee).

Season	Photos view towards SW from the tower	Photos view towards NE from the tower
Spring (Apr. 26th 2015)		
Summer (Jun. 27th 2015)		
Fall (Nov. 06th 2015)		
Winter (Feb. 11th 2016)	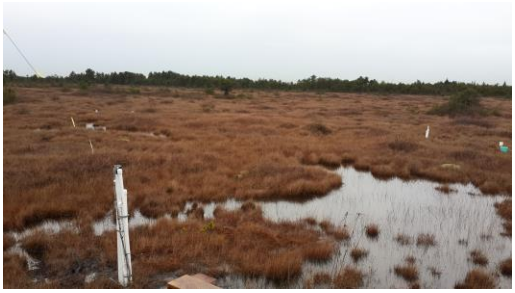	

3.2.3 Water table and soil moisture

Winter was the wettest season and WTH was above the bare soil (reference surface) (Table 3.6). The highest water table position was 7.74 cm above the reference surface in December 2015. In the dry season, the water table position dropped to 26.48 cm beneath bog surface in August 2015. The WTH decreased in spring, and dry hummocks could be seen from April to September. After receiving the fall precipitation, the water table started to rise above the surface. The study site was flooded in winter during the study year.

Table 3.6 Monthly water table height at the study site during the study period.

Month	Water table height (cm)
Jun-15	-7.79
Jul-15	-19.48
Aug-15	-26.48
Sep-15	-21.22
Oct-15	-12.49
Nov-15	1.27
Dec-15	7.74
Jan-16	6.48
Feb-16	6.55
Mar-16	7.51
Apr-16	4.33
May-16	-0.61
Jun-16	-6.21

3.3 CO_2 exchange at the BBECA

3.3.1 Data availability

The EC-1 system was running for almost the entire study year (86.3%, Table 3.7), most of the missing data were caused by high frequency loss in sampling, except two events. First one was the tower shut down from September 18th to 21st 2015, and second one was the broken CF card dropping all data from May 25th to June 9th 2016. There were more gaps in measurements of LI-7500 due to lack of power (solar panel), especially in winter. More fluxes were discarded in winter (around 15%) than in summer (around 7%) due to the unfavorable weather, i.e. rain. The u_* filter and wind direction filter generally eliminated 30% to 50% of the valid data.

Table 3.7 Data availabilities of CSAT-3, LI-7500, valid data (filtered by signal strength), and the filtered data for each of months in the study year.

Month	Up-time of CSAT-3 in EC-1 (based on acoustic temperature)	Up-time of LI-7500 in EC-1 (based on CO_2 density)	Valid CO_2 fluxes measured	Valid CO_2 fluxes after u_* and wind direction filter applied
Jan	94.6%	59.9%	43.5%	24.0%
Feb	95.5%	74.9%	59.8%	39.6%
Mar	98.1%	84.9%	70.1%	53.6%
Apr	98.8%	90.6%	84.3%	59.7%
May	77.2%	73.3%	66.8%	50.8%
Jun*	59.2%	58.0%	51.7%	38.4%
Jul	95.6%	90.1%	82.7%	65.0%
Aug	94.4%	91.4%	82.1%	59.3%
Sep	82.1%	77.4%	69.1%	44.2%
Oct	92.5%	70.5%	29.4%	17.4%
Nov	91.1%	53.8%	44.0%	17.4%
Dec	96.5%	37.9%	26.6%	21.5%
Study year	**86.3%**	**69.3%**	**59.1%**	**40.9%**

* Jun 1 – 15 is from 2016, Jun 16 to 30 is from 2015.

3.3.2 Monthly and annual NEE, R_e and GEP

Overall, the study area was a CO_2 sink in spring (-1.10 g C m^{-2} day^{-1}) and in summer (-0.82 g C m^{-2} day^{-1}). Net CO_2 fluxes were near zero in fall (+0.03 g C m^{-2} day^{-1}) and winter (-0.07 g C m^{-2} day^{-1}). Over the entire year, the annual CO_2-C budget (i.e., NEE) was -179 g C m^{-2} yr^{-1}. Almost in each month of the calendar year, the site was consistently a weak sink for CO_2 except October, November and December (Figure 3.6). Net fluxes of CO_2 (NEE) ranged from +1.77 (November 2015) to -56.20 g C m^{-2} $month^{-1}$ (May 2016). In Figure 3.7, the cumulative GEP, R_e and NEE are presented as a composite year, starting in January (June 16th – December are from 2015, January – June 15th are from 2016). The annual R_e and GEP during the study year was 236 and 415 g C m^{-2} yr^{-1}, respectively. The curves are closely linked to the plant phenology and temperature. Based on GEP we can divide the study period into three segments, 'winter' (Oct-Mar), 'early growing season' (Apr – Jun), and 'late growing season (Jul – Sep). The rising temperature triggered growth in the early growing season (GEP = 59.73 g C m^{-2} $month^{-1}$), while the later growing season had limited growth (GEP = 25.08 g C m^{-2} $month^{-1}$) (Table 3.8). Despite a large amplitude in monthly GEP, R_e showed less variability over the year. Based on two figures, the highest increasing rate of NEE and the highest magnitude of NEE both happened in May, the early growing season. This was caused by R_e being delayed compared to GEP, resulting in the greatest imbalance between respiratory and assimilatory fluxes. Such a situation was also reported from temperate deciduous and boreal coniferous forests (Falge et al., 2002).

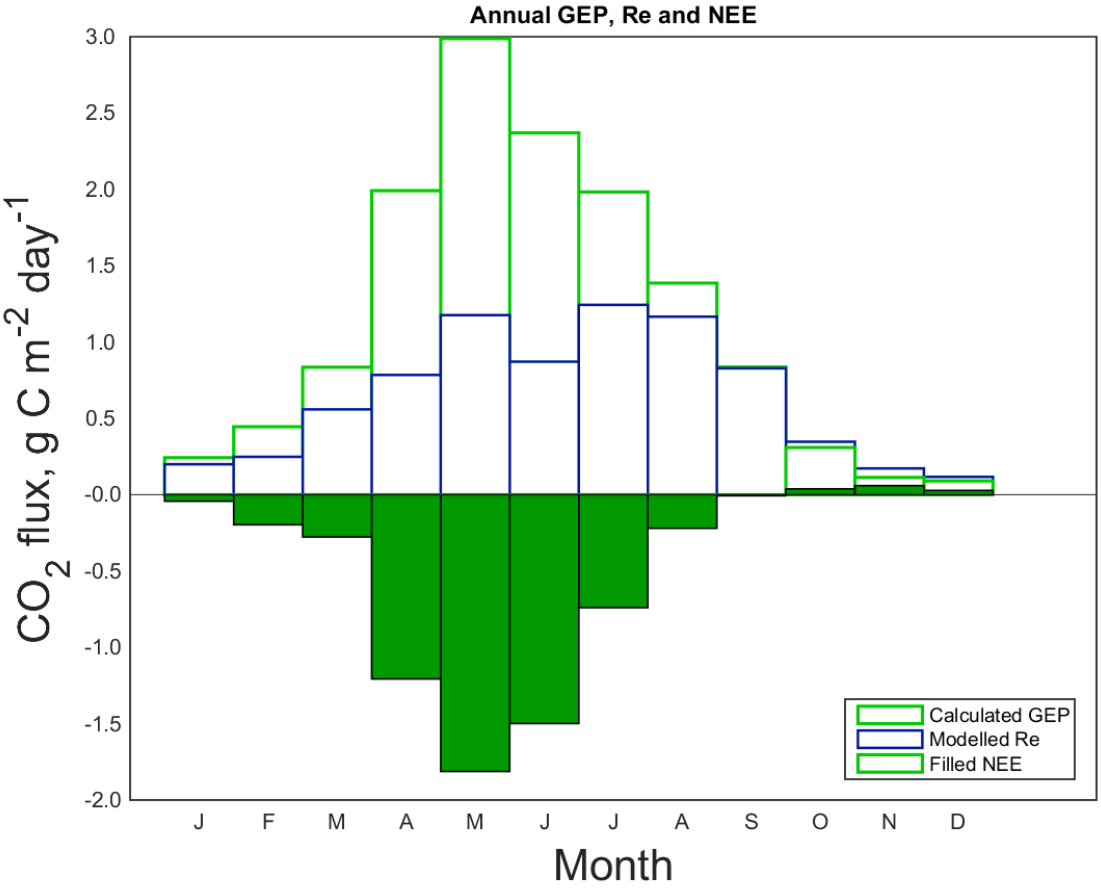

Figure 3.6 Monthly EC-measured NEE, and the gaps were filled by modelled R_e using Equation 12, and calculated GEP using daytime NEE measurements and modelled R_e.

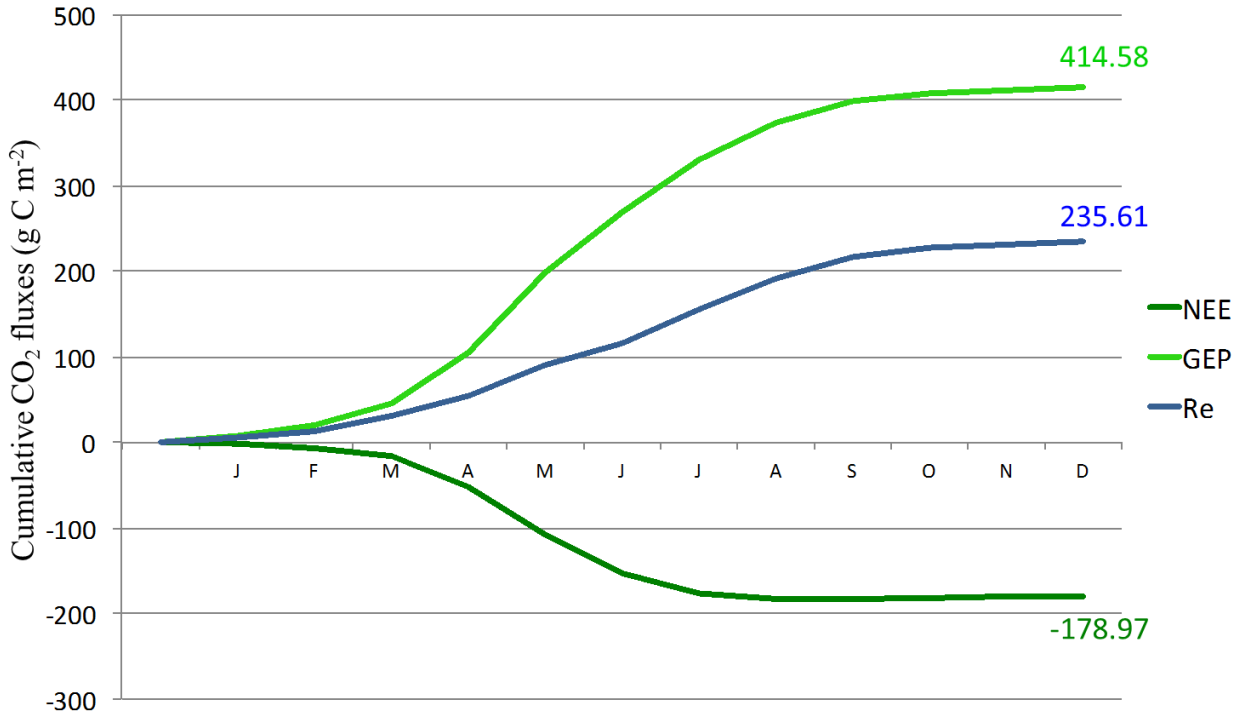

Figure 3.7 Cumulative NEE, R_e and, GEP at a monthly resolution from June 2016 to May 2016.

Table 3.8 Monthly NEE, R_e and, GEP during the study year.

Month	R_e (g C m^{-2} $month^{-1}$)	GEP (g C m^{-2} $month^{-1}$)	NEE (g C m^{-2} $month^{-1}$)
Jan	6.17	7.50	-1.33
Feb	6.94	12.46	-5.52
Mar	17.33	25.89	-8.59
Apr	23.52	59.73	-36.21
May	36.46	92.63	-56.20
Jun*	26.13	71.10	-44.97
Jul	38.53	61.47	-22.94
Aug	36.15	42.97	-6.82
Sep	24.84	25.08	-0.21
Oct	10.76	9.58	1.18
Nov	5.16	3.39	1.77
Dec	3.63	2.79	0.87
Study year	g C m^{-2} $year^{-1}$		
	235.61	**414.58**	**-178.97**

*Jun 1 – 15 is from 2016, Jun 16 – 30 is from 2015.

3.3.3 Ecosystem respiration

Figure 3.8 shows the relationship between nighttime R_e and $T_{s,5cm}$ using the data for the entire study period (i.e. full year). Negative R_e values were caused by measurement uncertainties. R_e increased with increasing $T_{s,5cm}$ as expected. The increase followed the logistic shape more than the exponential shape. Before the $T_{s,5cm}$ reached 15 ℃, R_e did not change substantially and remains rather small compared to other temperature region. After this threshold, R_e increased dramatically to above 1.00 μmol m^{-2} s^{-1}, but leveled after 19 ℃. R_e reacted differently in different months (Figure 3.9). In winter (DJ), the fitted curves were close to zero. From FM to AM, the fitted curves started to become closer to logistic shape. In JJ, $T_{s,5cm}$ remained above 15 ℃. This resulted in the fitted curve being a flat line at the magnitude of 1 μmol m^{-2} s^{-1}. The study area had the highest R_e in these two months. In fall, R_e curves were closer to an exponential relationship. It was due in part to the leave out (Shurpali et al., 2008). The newly dead plants on the soil surface made R_e in fall had higher value compared to spring and winter at the same $T_{s,5cm}$. Another factor could be the WTH. In fall, water table was not high enough to suppress the R_e as it did in winter (Juszczak et al., 2013). The differences could be up to 0.4 μmol m^{-2} s^{-1}.

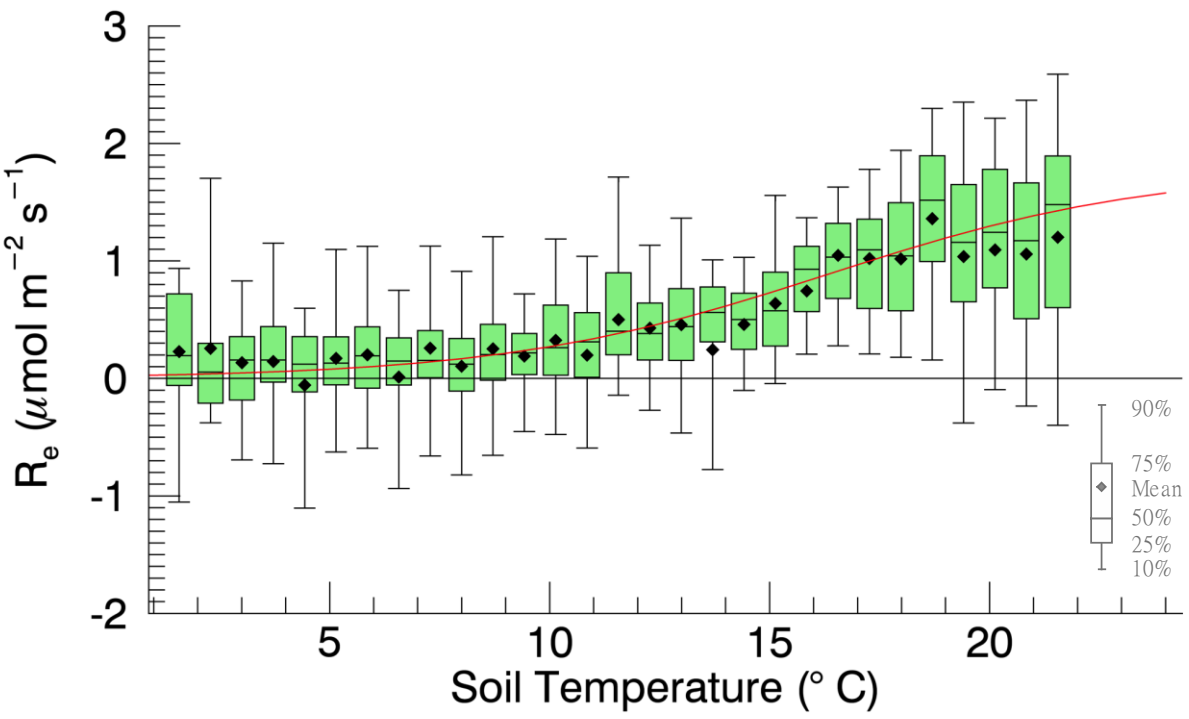

Figure 3.8 Relationship between R_e (nighttime 30-minute CO_2 flux measurements) and $T_{s,5cm}$ during the entire study period. The u_* threshold was 0.08 m s^{-1}. The fitted curve is the logistic relationship in Equation (12). $T_{s,5cm}$ was binned for 32 classes from minimum of $T_{s,5cm}$ to maximum of $T_{s,5cm}$.

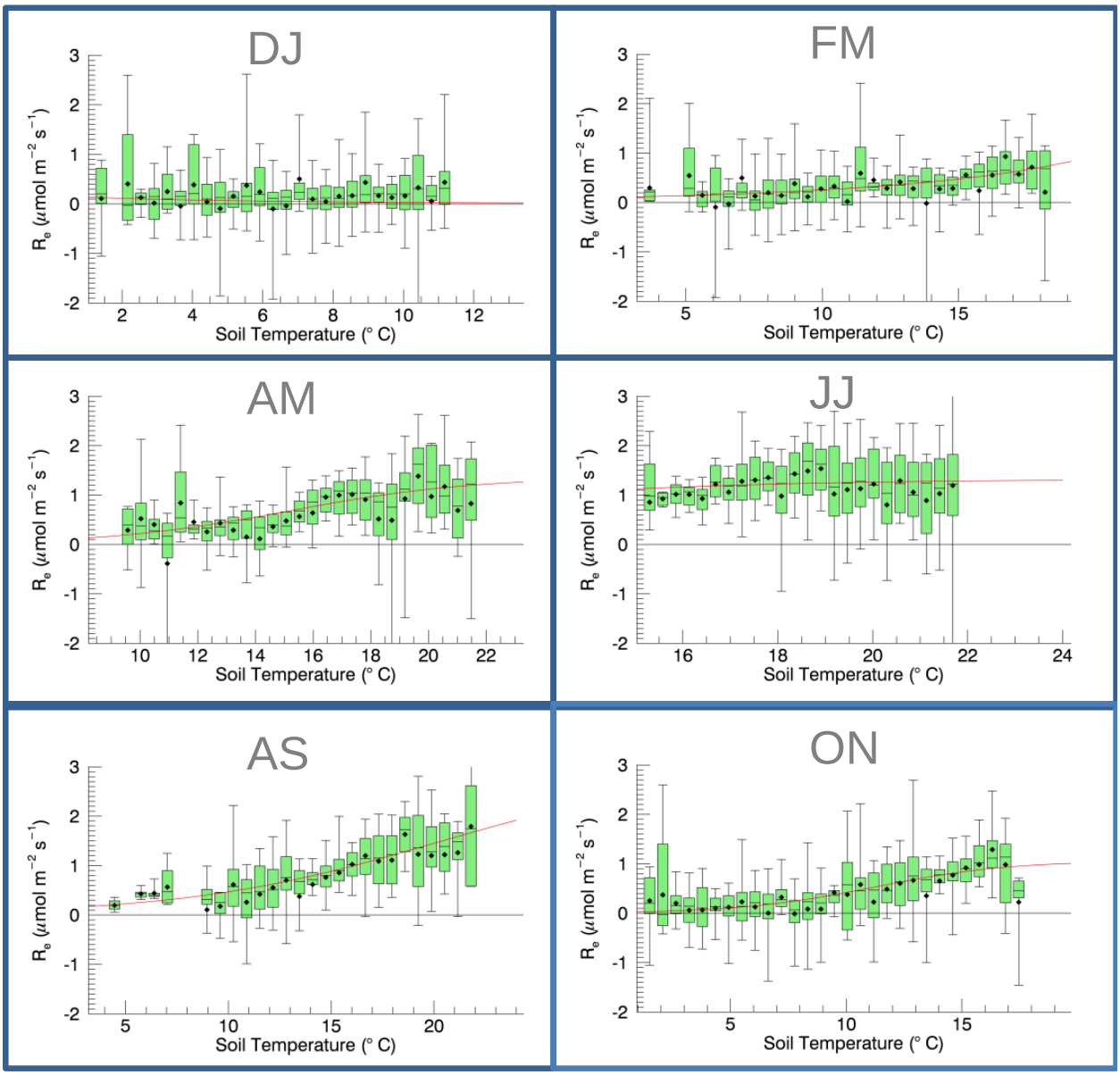

Figure 3.9 R_e curves on first day of every two months by using window size of 120 days. R_e was binned for 32 classes from minimum of $T_{s,5cm}$ to maximum of $T_{s,5cm}$ in each period. Note: Although y-axis is fixed, the x-axis is variable.

3.3.4 Gross ecosystem photosynthesis

Figure 3.10 shows half-hourly GEP as a function of PPFD. Due to different phenology and the typical solar altitude angle among different months, light response curves were calculated for each month. GEP reached a maximum in May 2016 with 92.63 g C m^{-2} $month^{-1}$, and a minimum of 2.79 g C m^{-2} $month^{-1}$ in December 2015. GEP at light saturation reached roughly 5.09 μmol m^{-2} s^{-1} in summer, and remained below 2.49 μmol m^{-2} s^{-1} in winter (Table 3.9), due to reduced leaf area and lower temperatures. GEP also exhibited significant inter-annual variability as R_e. But the rate of change in GEP was greater than R_e. The light response curve in February-March (FM) had the same shape as the annual one (Figure 3.11). Other than the phenological reason, this might be highly connected to the warmer winter we had in 2015. The temperature anomaly can have important consequences of increases in early season ecosystem uptake (Randerson et al., 1999). GEP also dropped faster than R_e did after summer. The magnitude of R_e already got close to GEP in the late August to make the study area become CO_2 neutral.

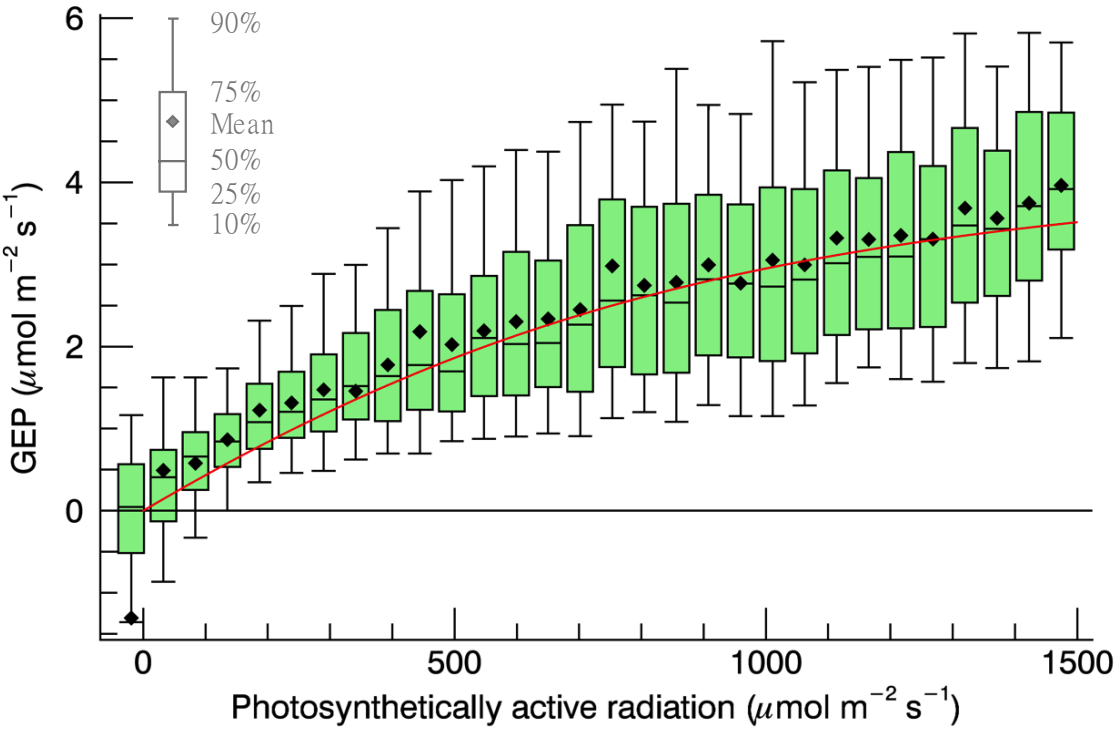

Figure 3.10 Annual light response curve determined from the daytime 30-minute NEE measurements and Equation 12, i.e., GEP = R_e + -NEE. The curves are the best fit of the equation (13). PPFD was binned for 30 classes from 0 to 1500 μmol m^{-2} s^{-1}. Annual *MQY* was 4.00 mmol C mol^{-1} photons, P_M was 4.68 umol m^{-2} s^{-1}, and C_v was 0.7 (fixed).

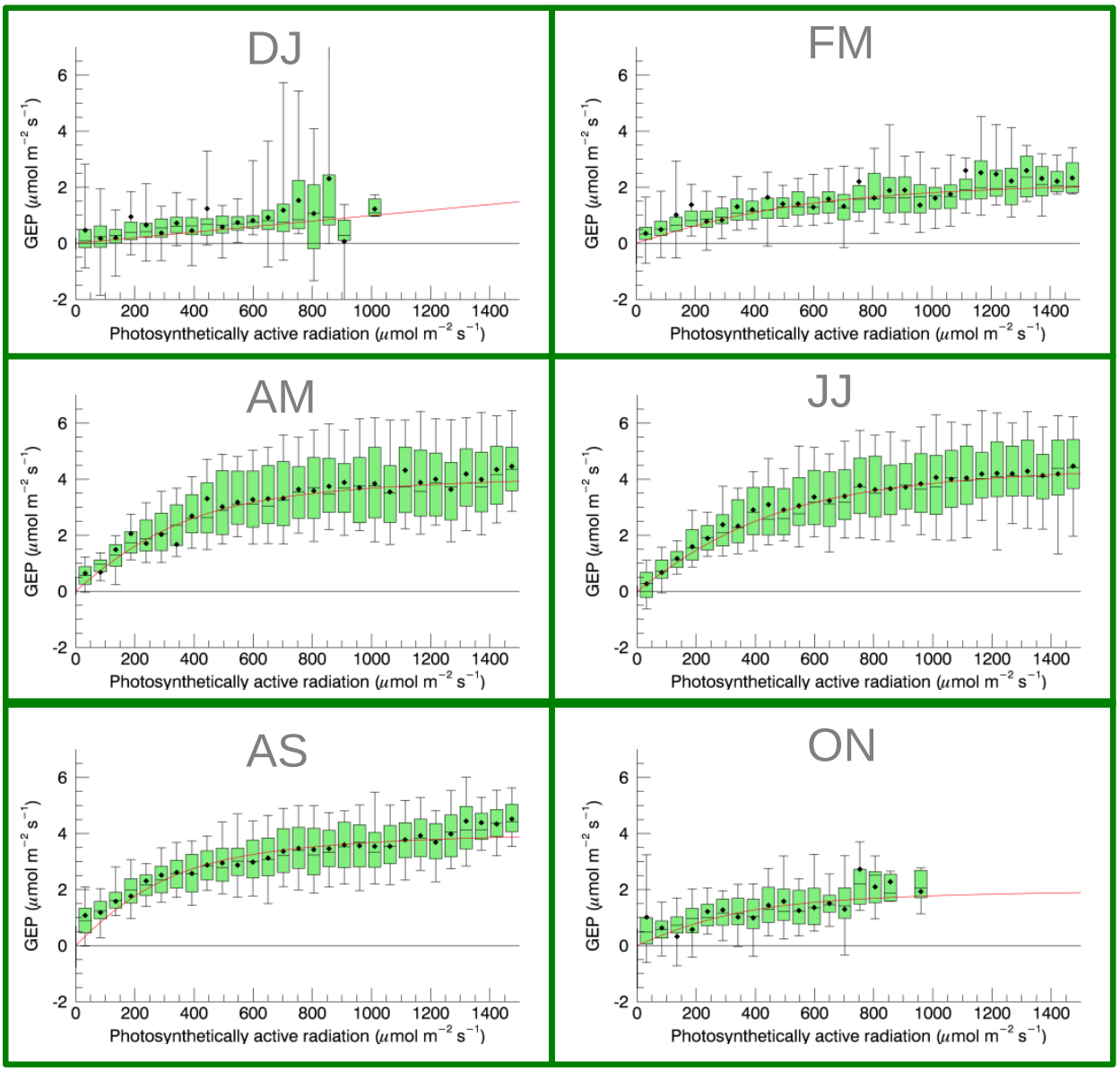

Figure 3.11 Light response curves on first day of every two months by using window size of 90 days. PPFD was binned for 30 classes from 0 to 1500 μmol m^{-2} s^{-1}

Table 3.9 *MQY* and P_M in each of six time periods.

Time	***MQY* (mol C mol-1 photons)**	**P_M (umol m^{-2} s^{-1})**
DJ	1.70	2.49
FM	4.33	3.71
AM	10.37	5.09
JJ	7.68	4.35
AS	14.68	3.48
ON	2.19	3.09

3.3.5 Diurnal variability of CO_2 fluxes

The ensemble diurnal courses of the filled NEE, modelled R_e, and calculated GEP by the EC-1 system are shown in Figure 3.12 from June 16th 2015 to June 15th 2016. The diurnal course of NEE is caused by photosynthesis (daytime) and respiration (day and night). R_e remained relatively constant over a day compared to GEP, which followed available light levels during day. The magnitude the daily maximum of GEP changed a lot through the study period, the highest values happened between May and July (-3.5 μmol m^{-2} s^{-1} at noon) (Figure 3.13). R_e at night was less changing, and on average was most of the time ≤ 1 μmol m^{-2} s^{-1} over the study year, and only some values exceeded in August. The time lag between the highest GEP (mid-May) and the highest R_e (August) is also observed in Figure 3.13.

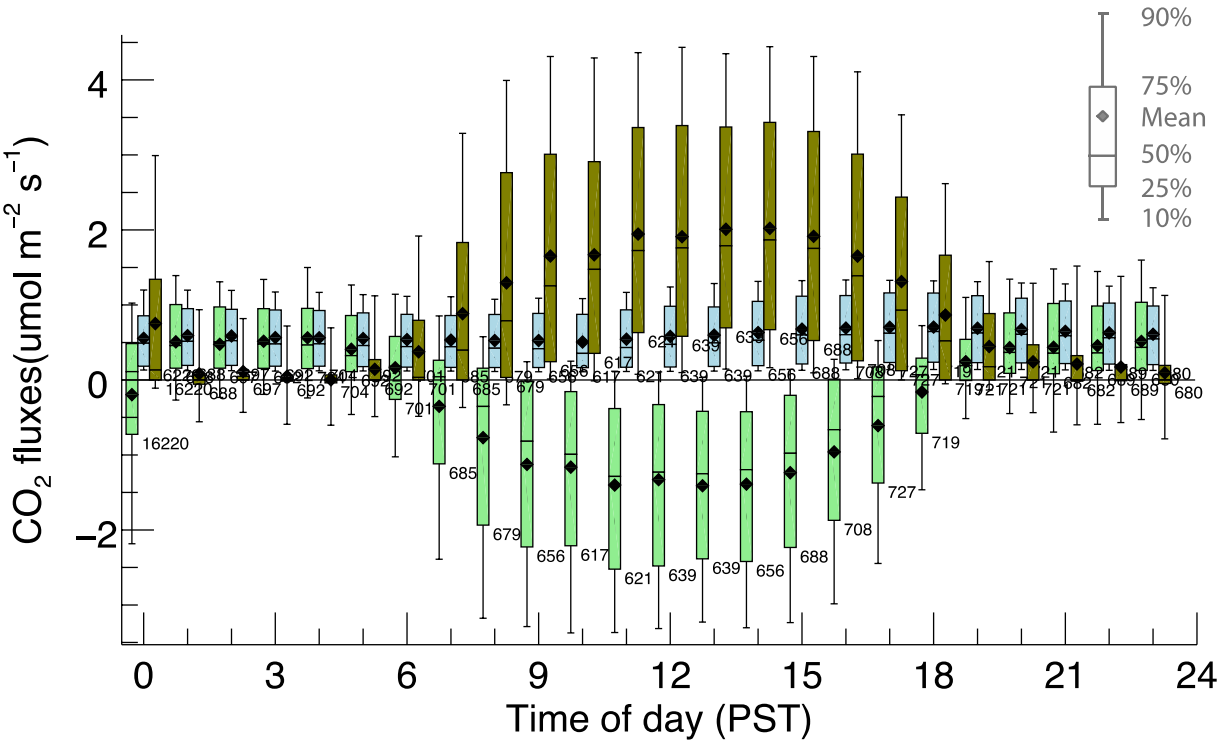

Figure 3.12 Diurnal course of filled NEE (net CO_2 fluxes, light green), modelled R_e (light blue), and calculated GEP (olive) from the EC-1 system during the entire study period.

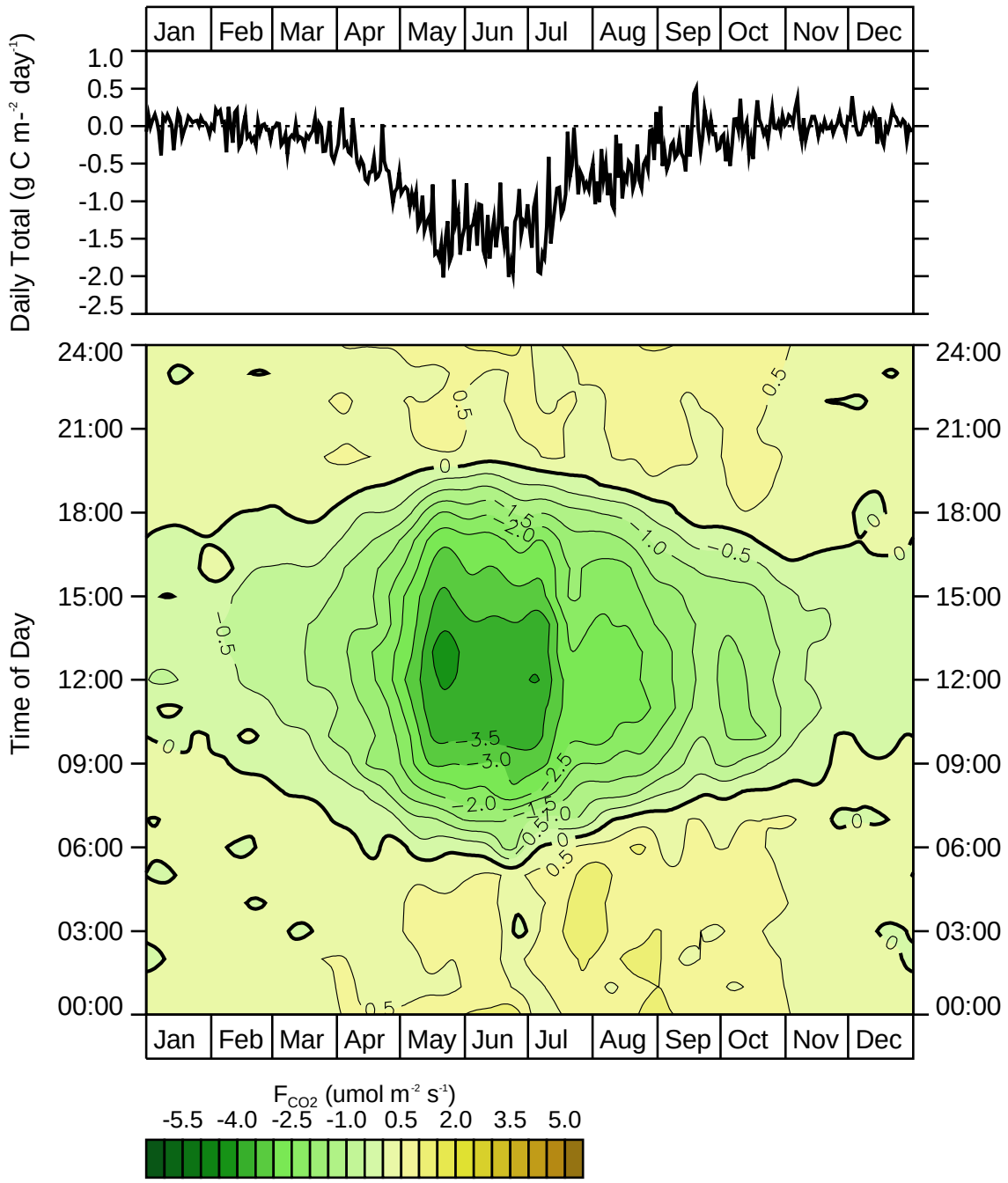

Figure 3.13 Isopleths of gap-filled NEE (net CO_2 fluxes) from the EC-1 system plotted as a composite in year. The graph uses a Gaussian filter of σ = 45 days (which conserves total NEE) to smooth horizontal variations.

3.3.6 Other controls on R_e

Figure 3.14 explores other possible controls on R_e, in addition to $T_{s,5cm}$ (those controls include T_a, WTH, and θ_w). The role of those controls is demonstrated using measured nighttime NEE as R_e. T_a did have some impact on R_e, but this effect stopped after the temperature reached 16℃ (Figure 3.14a). Unlike T_a, $T_{s,5cm}$ still controlled CO_2 fluxes most dominantly when it was warmer than 16℃ (Figure 3.8). The reason is the activity of soil microbes contributing to R_e, is depending on soil, not T_a (Davidson et al., 2002; Edwards, 1975; Lloyd and Taylor, 1994). In most ecosystems, the activity of soil microbes is also governed by moisture status, having little activity when the surface is dry, and more activity after rain pulses (Davidson et al., 2002; Edwards, 1975). Interestingly, however, like other wetlands, R_e was small when the water table was above the surface (Figure 3.14b) because this situation suppressed aerobic decomposition of peat (Rochefort et al., 2002; Weltzin et al., 2000). When the water table was below surface, R_e jumped to near 1 μmol m^{-2} s^{-1} and became stable no matter how low the water table position was. This relationship was also found in many other peatlands (Bridgham et al., 2006; Ellis et al., 2009; Strack et al., 2006). There is no obvious relationship between θ_w (integrated from 0-30 cm depth) and R_e (Figure 3.14c). R_e slightly decreased from 1.0 to 0.6 μmol m^{-2} s^{-1} when θ_w increased from 84% to 88%. Other than this range, θ_w has no more impact on R_e.

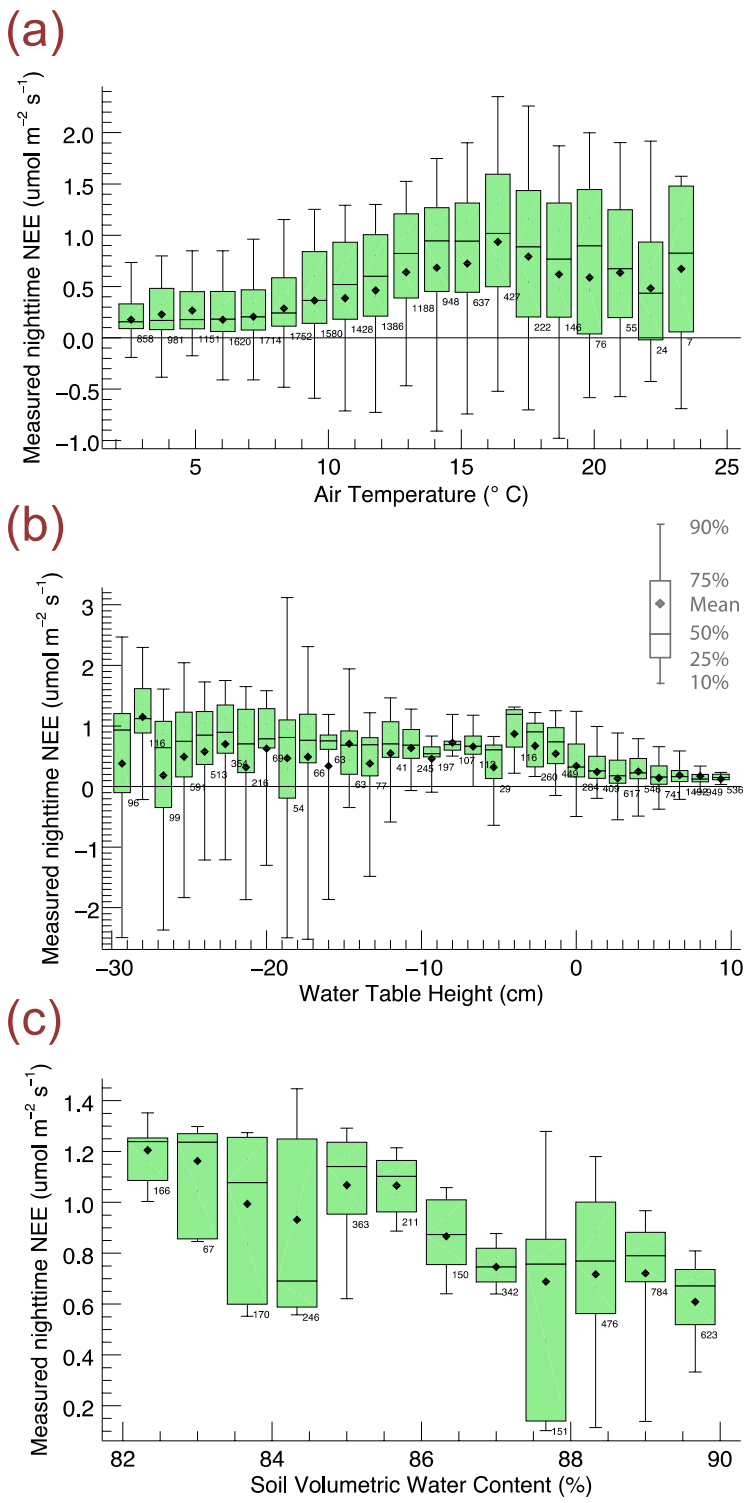

Figure 3.14 The relationships between environmental factors other than $T_{s,5cm}$ and and CO_2 fluxes at nighttime (used to study R_e). The relation of nighttime CO_2 flux and $T_{s,5cm}$ is shown in Figure 3.8.

3.3.7 Other controls on GEP

Figure 3.15 explores all possible controls on GEP other than PAR such as T_a, WTH, and θ_w. To exclude the primary driver, PAR, here only data when PAR was between 300 and 500 μmol m^{-2} s^{-1} were used. The light-independent photosynthesis occurring in the stroma depends on T_a (Calvin, 1962). This reaction is catalyzed by enzymes. Between 0 and 10 ℃, the enzyme activity was low and hence photosynthesis was low (Figure 3.15a). The optimal temperature level for photosynthetic enzymes is from 10 to 20 ℃. The rapid increase in GEP in this range was found at the study site from 10 to 15 ℃. When T_a is higher than 15 ℃, enzymes activity was low again in the study ecosystem. WTH and θ_w did not have any influence on GEP. The lower GEP when water table was above the surface and θ_w was above 88% was not caused by the suppression mentioned in the previous section (Figure 3.15b and 3.15c). It was caused by the phenology. The wet environment happened in the winter, at the same time, the plants species were all inactive. The low GEP was found due to this reason.

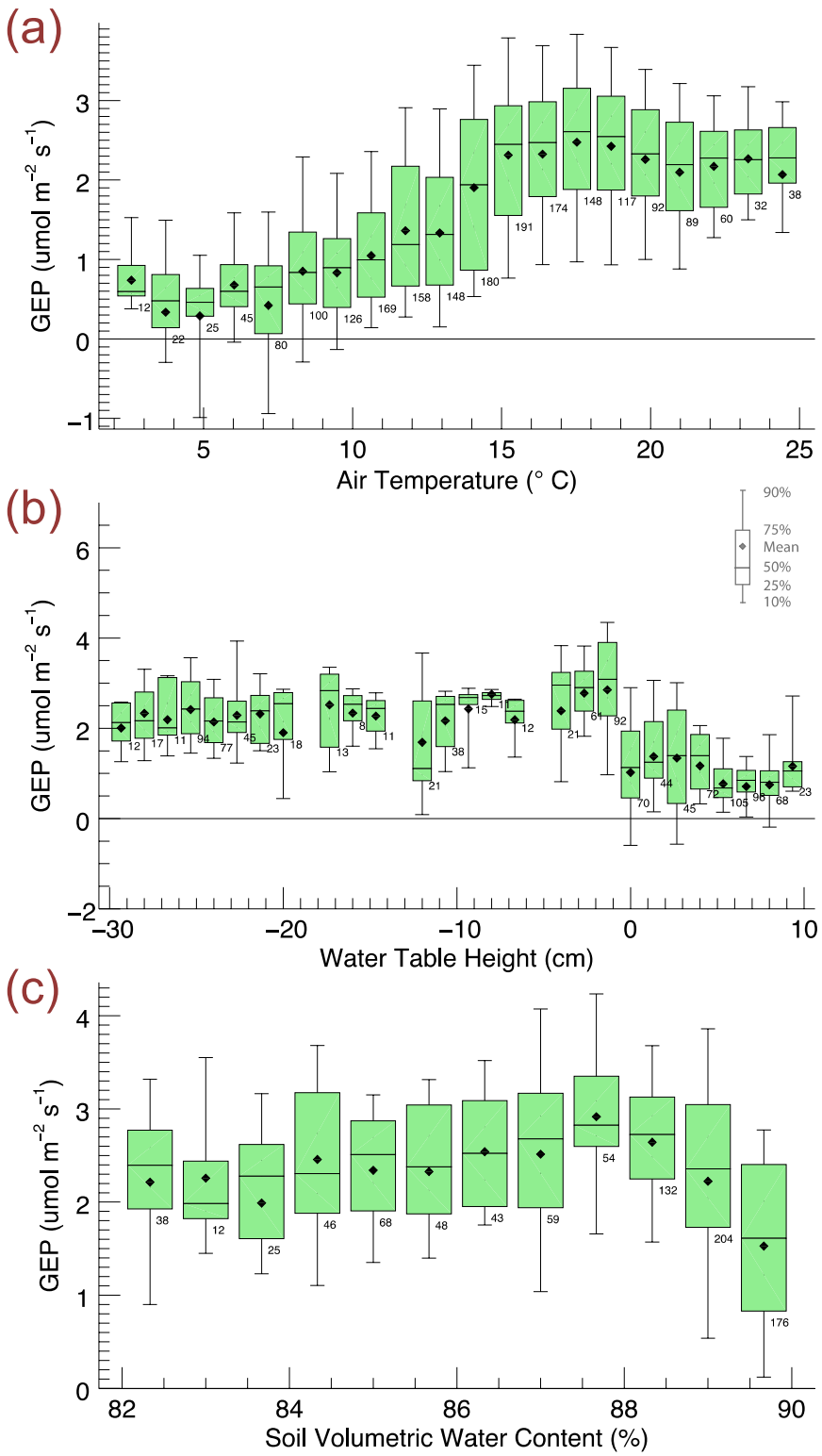

Figure 3.15 The relationships between GEP (PAR is between 300 and 500 μmol m^{-2} s^{-1}) and other environmetal factors. The relation of GEP and PAR is shown in Figure 3.10.

3.3.8 Comparison to CO_2 fluxes from the previous year

Measured CO_2 flux data from this site were also available for the year preceeding the study year. It is of interest whether the unusually low water table in summer 2015 and the wet winter were causing abnormal NEE in the study year. Therefore, in this section, the current study year is compared against measurements from the previous year.

The period from July 10th 2014 to July 9th 2015 was used to estimate annual NEE, R_e and GEP using a slightly different methodology (presented as poster in CMOS 2015 conference, Lee et al., 2015). In order to make the comparison reliable, the CO_2 flux data during the previous year were now re-processed using the exactly same methodology as for the study year for partioning NEE (Section 2.4.2.1). Annual NEE, R_e and, GEP for the previous year (date range) is -181.38, 235.62, and 416.75 g C m^{-2} year^{-1} during the previous year, respectively (Table 3.10). The magnitudes of three fluxes during the two years were similar. On a monthly basis, the most significant difference was July and August. GEP in July 2014 (77.89 g C m^{-2} month^{-1}) and August 2014 (57.26 g C m^{-2} month^{-1}) could still maintain at the same level as May 2014 (68.63 g C m^{-2} month^{-1}) and June 2014 (87.72 g C m^{-2} month^{-1}). However, GEP in July 2015 (61.47 g C m^{-2} month^{-1}) and August 2015 (42.97 g C m^{-2} month^{-1}) dropped rapidly. This might have been caused by the extreme low water table position that was observed in late summer 2015. The WTH was only – 5.8 cm in July 2014 but it went down to – 21 cm in July 2015 (Figure 2.5). The dry conditions must have suppressed the growth (and hence photosynthesis) of plants lowering the GEP in July and August during the study year. Although aerobic conditions may have promoted R_e in late summer 2014, autotrophic respiration ceased due to lower GEP. Therefore, the seasonality of R_e remained more similar in both years.

Table 3.10 Monthly NEE, R_e and, GEP during the previous year and the study year. As measurements started on July 9th 2014 there is a small overlap between the two years.

Study year	R_e	GEP	NEE	Previous year	R_e	GEP	NEE
	g C m^{-2} month^{-1}				g C m^{-2} month^{-1}		
Jan	6.17	7.50	-1.33	Jan	3.88	4.03	-0.16
Feb	6.94	12.46	-5.52	Feb	5.85	6.69	-0.81
Mar	17.33	25.89	-8.59	Mar	8.62	15.53	-7.22
Apr	23.52	59.73	-36.21	Apr	17.34	27.18	-9.84
May	36.46	92.63	-56.20	May	27.03	68.63	-41.60
Jun*	26.13	71.10	-44.97	Jun	34.11	87.72	-53.61
Jul	38.53	61.47	-22.94	Jul+	31.81	77.87	-46.04
Aug	36.15	42.97	-6.82	Aug	37.60	57.26	-19.65
Sep	24.84	25.08	-0.21	Sep	32.52	38.40	-5.88
Oct	10.76	9.58	1.18	Oct	24.06	23.62	0.43
Nov	5.16	3.39	1.77	Nov	8.22	6.09	2.13
Dec	3.63	2.79	0.87	Dec	4.59	3.72	0.87
Annual	g C m^{-2} year^{-1}			**Annual**	g C m^{-2} month^{-1}		
	235.61	**414.58**	**-178.97**		**235.62**	**416.75**	**-181.38**

* Jun 1st – 15th is from 2016; Jun 16th – 30th is from 2015.
+ Jul 1st – 9th is from 2015; Jul 10th – 31st is from 2014.

3.3.9 Comparison to CO_2 fluxes in other ecosystems

Table 3.11 compares annual NEE, R_e and GEP at the study site to measurements over other land cover in the same region (hence experiencing the same climate forcing). NEE at an unmanaged grassland site 15 km to the west of the study area in the Fraser River Delta (Westham Island, Delta, BC) was 1.3 times stronger than this study. Notably, at that grassland site, R_e and GEP values were higher than the study site by a factor of 5.2 and 3.5. A mature 55-year-old Douglas-fir forest on Vancouver Island (200 km NW of the study area; Krishnan et al., 2009) showed a NEE value which was 1.8 times stronger than this study. The R_e and GEP were even higher by factors of 7.8 and 5.2, respectively. The last site for which measurements in the same region exist, is a young forest plantation (Buckley Bay, 150 km W of the study area; Krishnan et al., 2009), which was a weak C source, but R_e was six and GEP was three times larger than the study site. The mature 55-year-old forest became a strong source of C in the first year following harvesting. GEP at this harvested forest was lower than this study site and almost nonexistent due to the slow recovery of vegetation, but R_e was five times larger than the study site.

To conclude, compared to other sites receiving similar climate, the study area was not an ecosystem of high productivity but one with considerably limited R_e that permits CO_2 sequestration to occur more efficiently (-NEE is 43 % of GEP, as opposed to 15% for the unmanaged grassland site and mature forest).

Table 3.11 Comparison of annual NEE, R_e and GEP, over different ecosystems (vegetation covers) in the Vancouver region using EC measurements. Sorted by magnitude of -NEE/GEP ratio.

Site	Land cover	NEE	R_e	GEP	-NEE/GEP
		g C m^{-2} $year^{-1}$			
Burns Bog (this study) Delta, BC	Rewetted raised bog ecosystem	-179	236	415	43%
Westham Island (CA-Wes)* Delta, BC	Unmanaged grassland	-222	1215	1438	15%
Campbell River (CA-Ca1)* Vancouver Island	Douglas-fir forest (~55 yrs)	-328+	1830+	2158+	15%
Buckley Bay (CA-Ca3)* Vancouver Island	Douglas-fir forest (~15 yrs)	64+	1487+	1423+	-4%
Campbell River (CA-Ca1)* Vancouver Island	Douglas-fir forest (~55 yrs)	1000#	1130#	130#	-769%

* Site identifier in global FLUXNET database (http://fluxnet.ornl.gov).
+ Data from Krishnan et al., 2009 before fertilisation.
# Data from Paul-Limoges, 2013 one year after harvest (clear cut).

3.4 CH_4 exchange at the BBECA

3.4.1 Data availability

The EC-2 had a much lower data availability compared to EC-1 (36.2% Table 3.12). The biggest issue was power from solar panels that was limited for this power-consuming system, especially in winter (November to April). In winter, even when it was managed to operate LI-7700, the signal strength was also far from satisfactory due to the long optical path and the unfavorable weather. The valid CH_4 fluxes were generally of good quality, only 5% of data were with lowest quality flag "2" (discarded). The CH_4 fluxes with the best quality were 40% of the valid CH_4 fluxes. The u_* filter and wind direction filter generally removed 10% of valid data.

Table 3.12 Data availabilities of valid data (filtered by signal strength), data with acceptable quality, data with best quality, and the filtered data in EC-2 for each of months in the study year.

Month	Valid CH_4 fluxes measured	CH_4 fluxes with quality flag "0" and "1"	CH_4 fluxes with quality flag "0"	CH_4 fluxes after u_* and wind direction filter applied
Jan	0.07%	0.07%	0.07%	0.07%
Feb	0.07%	0.07%	0.07%	0.07%
Mar	0.07%	0.07%	0.07%	0.07%
Apr	19.6%	17.5%	6.3 %	6.0%
May	75.1%	65.4%	44.6%	32.2%
Jun*	60.3%	54.5%	33.0%	22.7%
Jul	95.2%	90.0%	46.8%	45.4%
Aug	86.7%	77.8%	27.0%	25.5%
Sep	53.3%	43.3%	4.8%	4.3%
Oct	36.2%	31.9%	13.9%	11.5%
Nov	15.3%	10.9%	0.8%	0.4%
Dec	0.07%	0.07%	0.07%	0.07%
Study year	**36.2%**	**31.9 %**	**13.9 %**	**11.5 %**

* Jun 1 – 15 is from 2016, Jun 16 to 30 is from 2015.

3.4.2 Controls on CH_4 fluxes

As mentioned in 'Methods' (Section 2), the model to fill data gaps was determined by plotting all possible environmental controls against measured CH_4 fluxes by using flux data with the best quality (quality control flag "0" in EddyPro). The influences of T_a and $T_{s,5cm}$ on CH_4 fluxes were positively correlated (Figure 3.16a and 3.16b). $T_{s,5cm}$ even controlled CH_4 fluxes more strongly because CH_4 emissions highly depend on the activity of soil microbes regulated by T_s. Normally, water status is an important driver because the atmospheric oxygen can barely get into the water by diffusion, thereby restricting aerobic respiration production and boosting CH_4 emissions (Liblik et al., 1997; Silvola, 1986). However, two variables (WTH and θ_w) related to water status being measured at site showed opposite relationships vs. measured CH_4 fluxes due to the lack of CH_4 data in winter and spring (Figure 3.16c, 3.16d and 3.16e). Therefore, I chose the $T_{s,5cm}$ to build the empirical model.

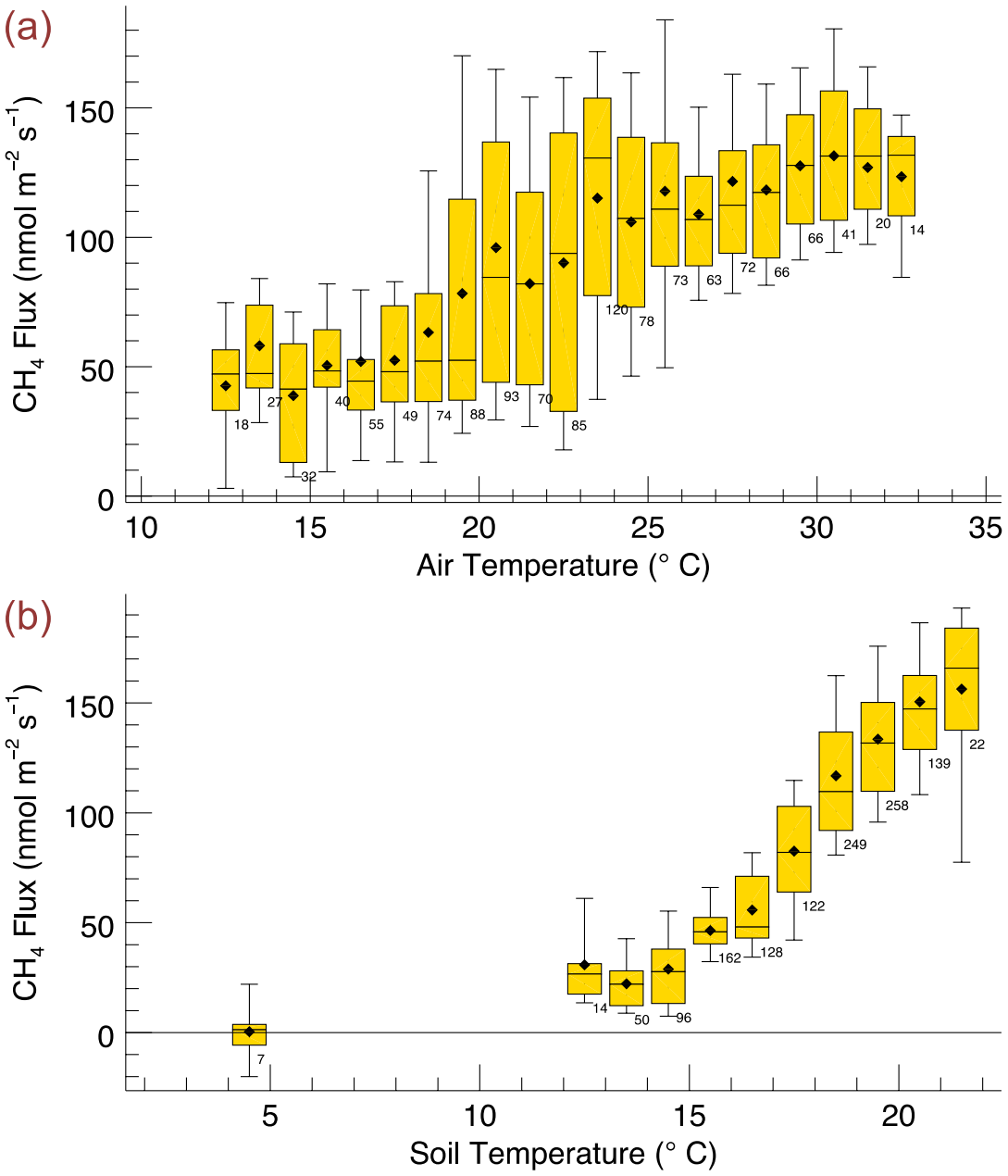
(a)
CH4 Flux (nmol m-2 s-1)
0
50
100
150
10
15
20
25
30
35
Air Temperature (° C)
18
27
32
40
55
49
74
88
93
70
85
120
78
73
63
72
66
66
41
20
14
(b)
CH4 Flux (nmol m-2 s-1)
0
50
100
150
5
10
15
20
Soil Temperature (° C)
7
14
50
96
162
128
122
249
258
139
22

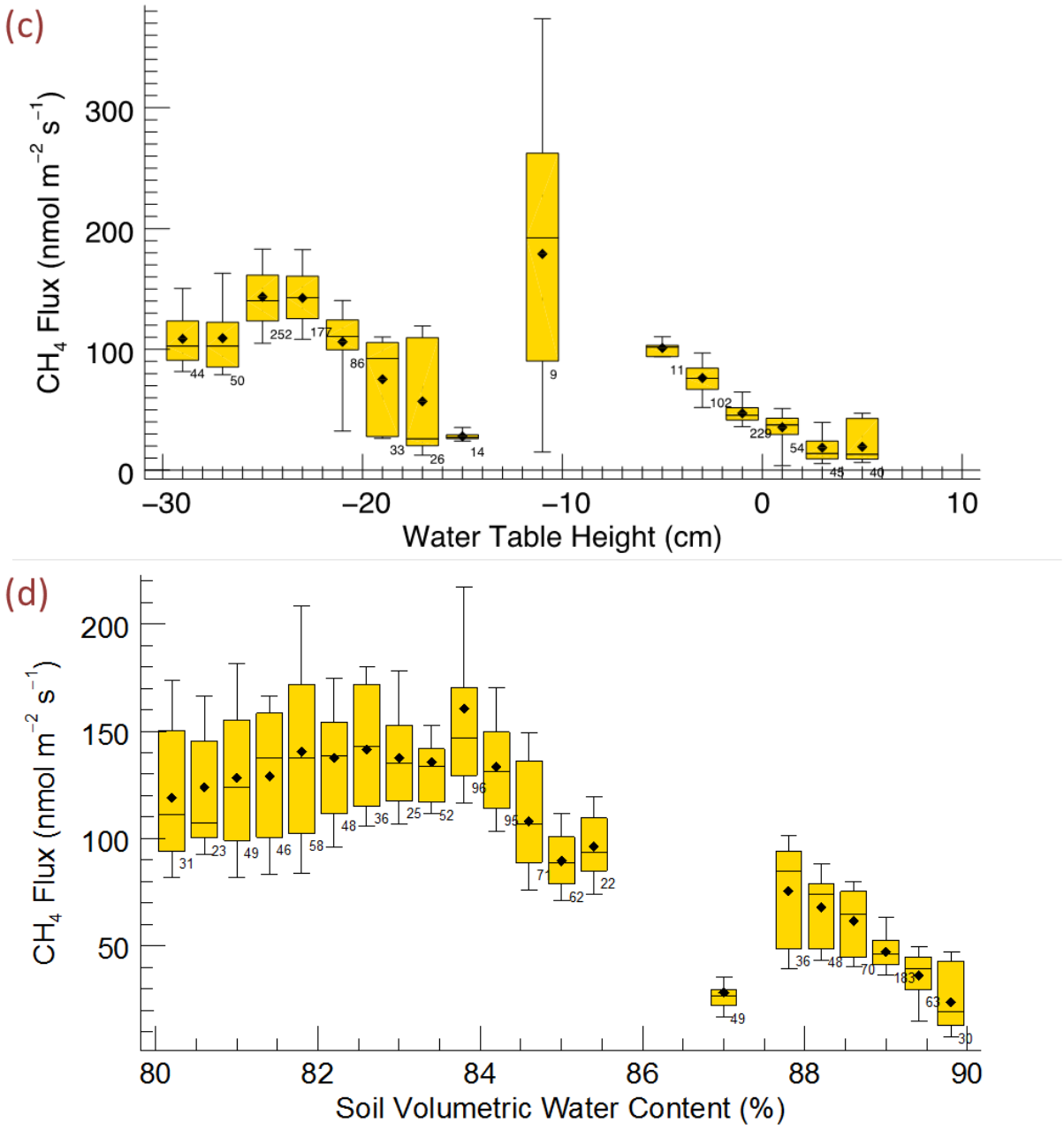

Figure 3.16 The relationships between CH_4 fluxes and all measured environmental factors.

3.4.3 CH_4 fluxes gap filling

The limited data availability in low-light situations means gaps in CH_4 fluxes were not random, and methods such as the mean diurnal course (MDC) cannot be used to fill CH_4 time traces. Up to 70% of data were measured in summer, so using an annual MDC, the total would be biased and lead to overestimated value. Therefore, it is critical to have a robust empirical model to fill the gaps. At the study site, CH_4 emissions were strongly related to $T_{s,5cm}$ (Figure 3.17), so an empirical fit was created between all measured and quality controlled CH_4 fluxes and $T_{s,5cm}$. The best relation with an $R^2 = 0.66$ yielded was an exponential relationship following Equation 14 (Section 2.4.2.2). The R^2 was 0.52 if the linear relationship was used, R^2 was 0.46 if the logarithmic relationship was used, and R^2 was 0.54 if the polynomial relationship was used.

Although the regression is not able to capture some extreme CH_4 emissions when $T_{s,5cm}$ was higher than 20℃, the mean of measured CH_4 fluxes (184.75 nmol m^{-2} s^{-1}) was still close to the mean of modelled CH_4 fluxes (161.44 nmol m^{-2} s^{-1}). Those extreme CH_4 emissions might be caused by the interaction between NEE and CH_4 fluxes. The greater quantity of C for CH_4 is made available when the ecosystem has higher plant productivity (Joabsson et al., 1999; Waddington et al., 1996; Whiting and Chanton, 1993).

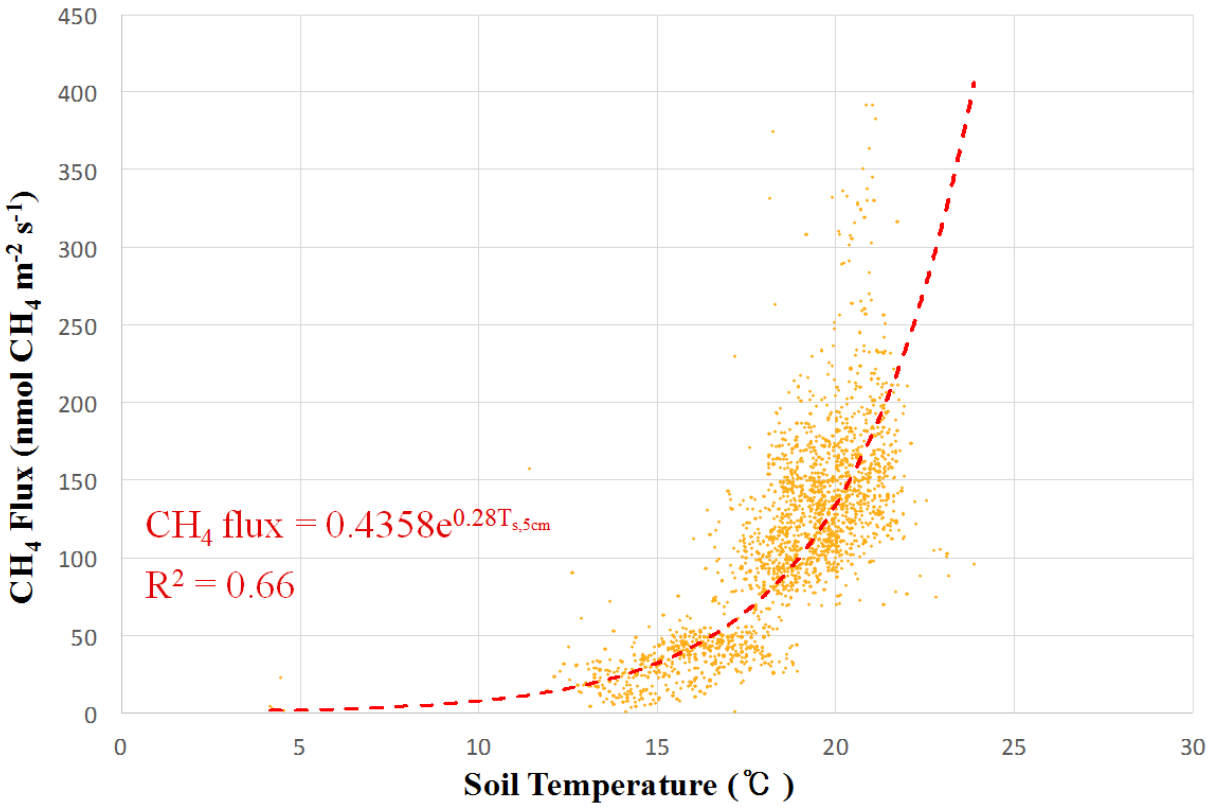

Figure 3.17 The relationships between CH_4 fluxes and $T_{s,5cm}$. The u* threshold was 0.08 m^{-2} s^{-1}. The fitted curve is the best result of the exponential equation.

3.4.4 Fingerprint of CH_4 fluxes

The ensemble diurnal courses of the gap-filled CH_4 fluxes (measured CH_4 emissions filled by modelled CH_4 fluxes) by the EC-2 system are shown in Figure 3.18 from June 16th 2015 to June 15th 2016. Surprisingly, there is not much of a diurnal course observed for CH_4 fluxes. CH_4 was continuously emitted through day and night. From January to March and October to December, the study site had constant CH_4 emissions of less than 50 nmol m^{-2} s^{-1}, and almost no changes happened through out the day (Figure 3.19). July has the greatest CH_4 emissions, and the highest magnitude (>150 nmol m^{-2} s^{-1}) appeared in the evening (3 pm to 9 pm). This

corresponded to the lag in soil to the change of temperature (Figure 3.20). The magnitude of CH_4 emissions increased/dropped at the rate of 50 nmol m^{-2} s^{-1} per month before summer and towards to winter.

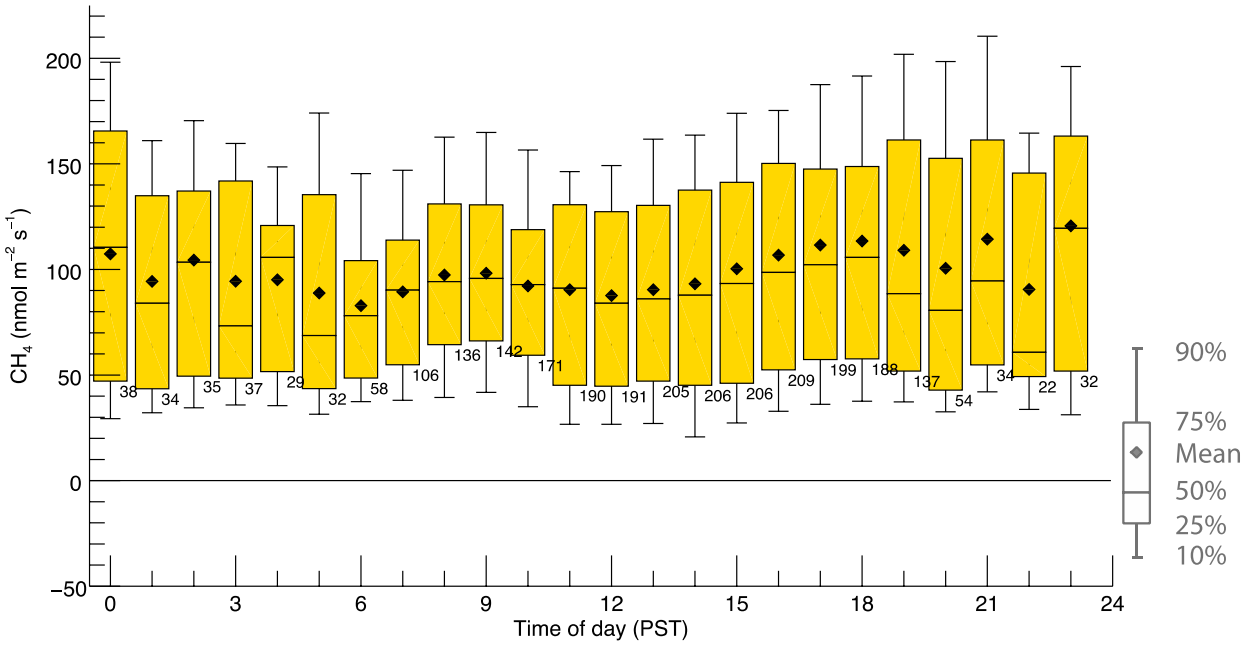

Figure 3.18 Diurnal course of filled CH_4 fluxes from the EC-2 system in the entire study period

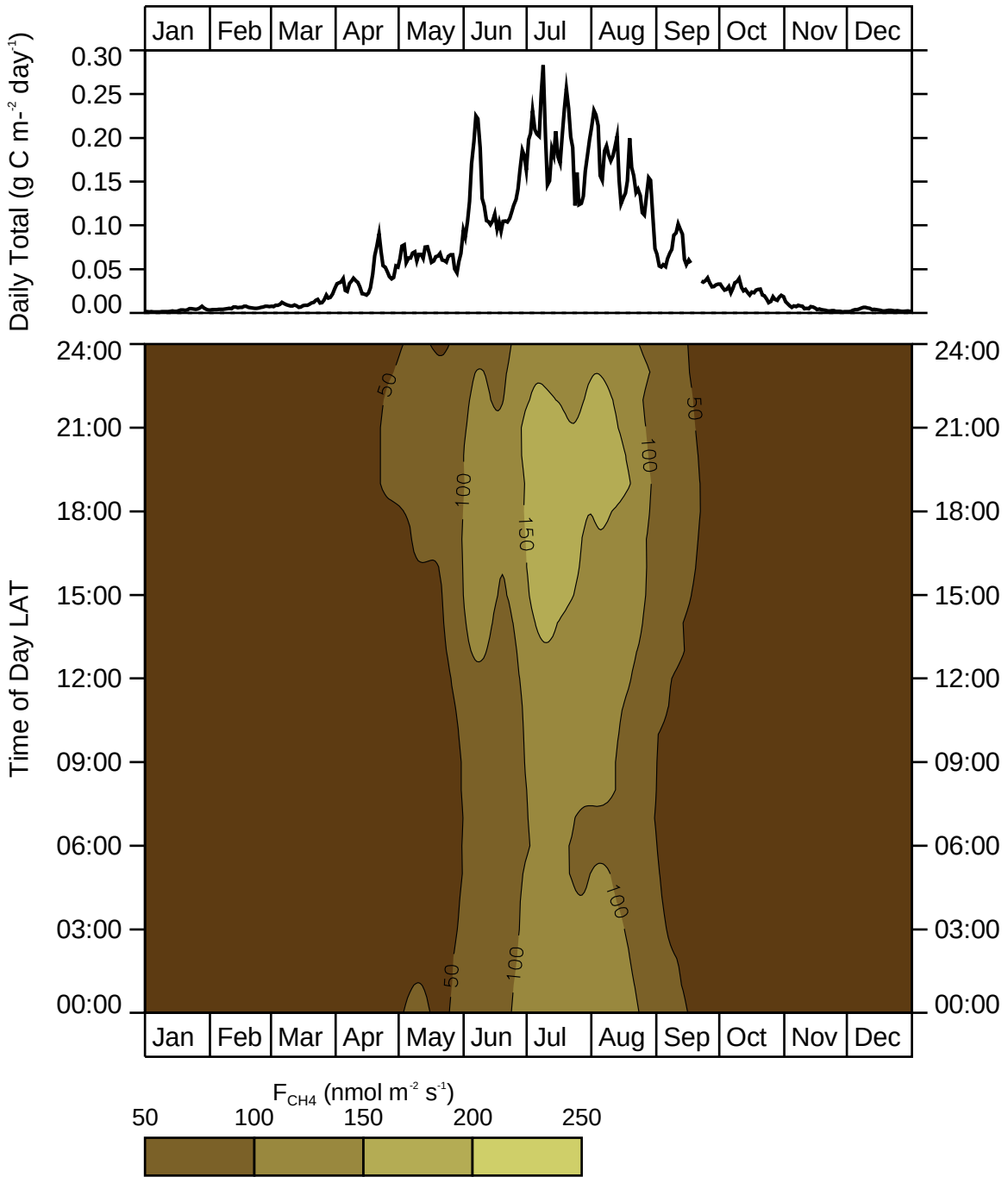

Figure 3.19 Isopleths of filled CH_4 fluxes from the EC-2 system plotted as a composite in year.

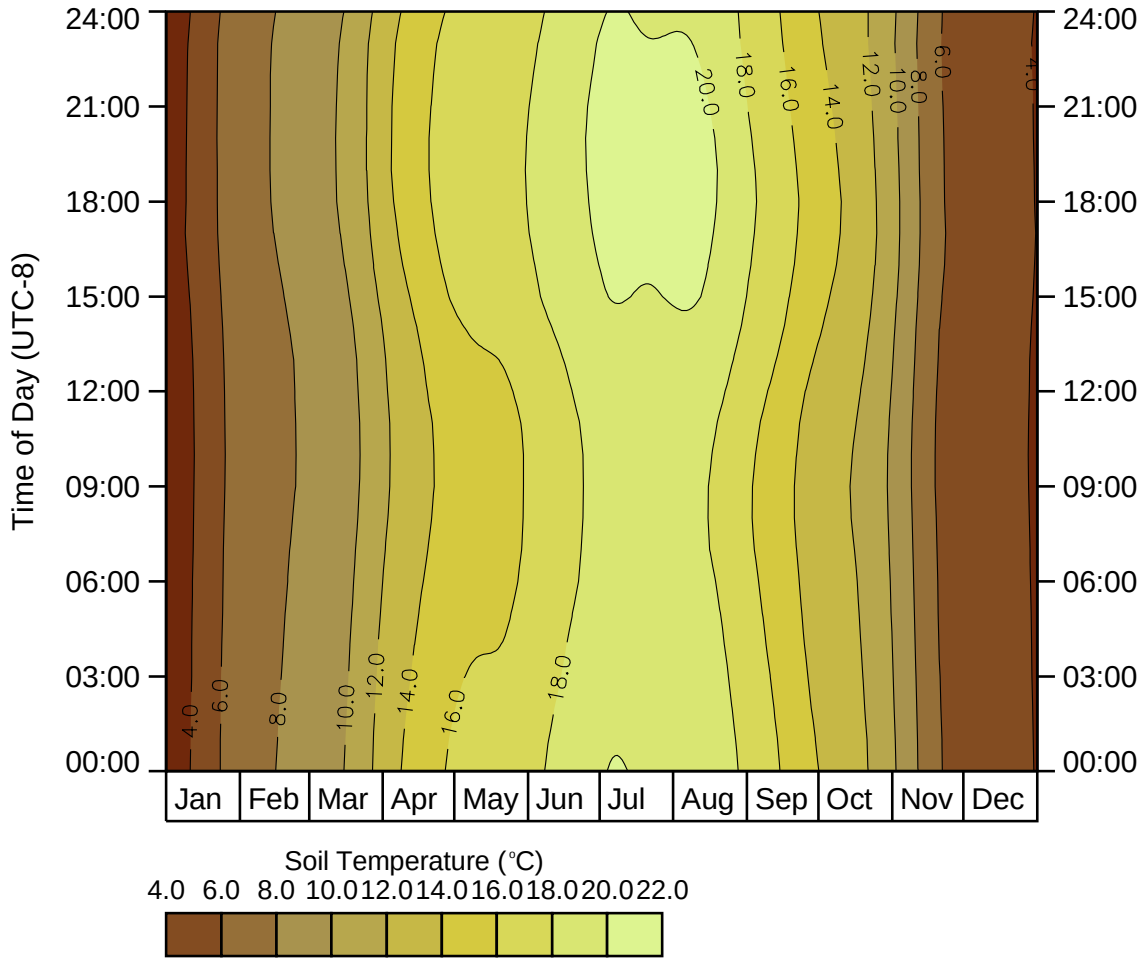

Figure 3.20 Isopleths of $T_{s,5cm}$ plotted as a composite in year.

3.4.5 Annual CH_4 budget

Overall, the study area was an annual CH_4 source, and it was a source in each of the twelve months (Figure 3.21). CH_4 emissions were close to zero in winter (8.72 mg CH_4-C m^{-2} day^{-1} for DJF). It was a slight CH_4 source in fall (21.51 mg CH_4-C m^{-2} day^{-1}) and spring (29.44 mg CH_4-C m^{-2} day^{-1}) , and then became a significant source in summer (120.95 mg CH_4-C m^{-2} day^{-1}). Over the entire year, the annual CH_4-C budget was 16 g CH_4-C m^{-2} yr^{-1}. Emissions of CH_4 ranged from 66 (November 2015) to 4436 (July 2016) mg CH_4-C m^{-2} $month^{-1}$. The cumulative CH_4 fluxes were presented as a composite in year (June 16th – December are from 2015, January – June 15th are from 2016) in Figure 3.21. The cumulative curves show an annual pattern, which is closely linked to the plant phenology and temperature. The rising T_a did not trigger CH_4 production immediately. CH_4 fluxes remained low in April and May. But once soil became warm enough, CH_4 emissions jumped from to 15 to 30 g CH_4-C m^{-2} $month^{-1}$ in June (Table 3.13). Then CH_4 emissions reached the peak in July (44 g CH_4-C m^{-2} $month^{-1}$) and held similar magnitude (37 g CH_4-C m^{-2} $month^{-1}$) in August even though the T_a had dropped.

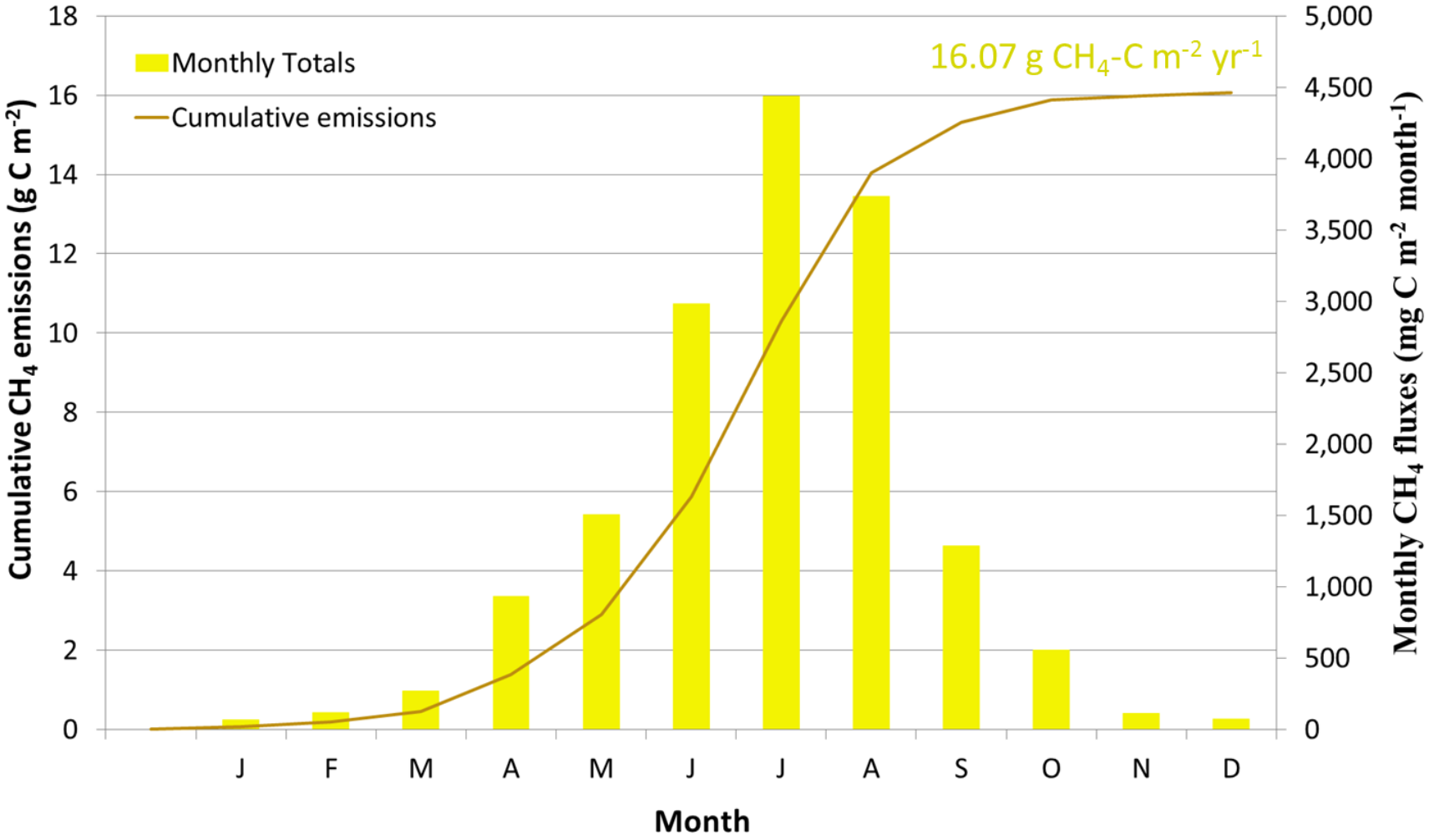

Figure 3.21 Monthly EC-measured and gap-filled CH_4 fluxes (right axis), and the cumulative CH_4 emissions at a monthly resolution (left axis).

Table 3.13 Monthly EC-measured and gap-filled CH_4 fluxes at the study site during the study period.

Month	Monthly CH_4 fluxes (mg CH_4-C m^{-2} $month^{-1}$)
Jan	66
Feb	118
Mar	269
Apr	933
May	1506
Jun	2980
Jul	4436
Aug	3734
Sep	1286
Oct	557
Nov	111
Dec	74

3.5 CO_2e exchange at the BBECA

Figure 3.22 and 3.23 shows CO_2 and CH_4 fluxes as CO_2e by using 100-year and 20-year GWPs, respectively. Considering fluxes of both trace gases together over the full year, this rewetted area was a slight net sink of GHGs at 100-year scale – net uptake by CO_2 (-656.23 g CO_2e m^{-2} $year^{-1}$) was slightly higher than year-round CH_4 emissions (632.76 g CO_2e m^{-2} $year^{-1}$). But looking at shorter time horizon (i.e., 20 years), the impact of CH_4 on warming became much greater, the study area became a significant net source of GHGs – net uptake by CO_2 (-656.23 g CO_2e m^{-2} $year^{-1}$) was exceeded by annual CH_4 emissions (1898.27 g CO_2e m^{-2} $year^{-1}$). The early onset of CO_2 sequestration in May, and the time lag in CH_4 fluxes meant that in late spring and early summer, the site acted as a GHG sink no matter what the GWP time horizon was considered. The peak CH_4 emissions in June and July were balanced out by CO_2 absorption at 100-year scale, but drew the site to a significant GHG source at 20-year scale. The quick drop in CO_2 sequestration in August and September allowed the highest net GHG fluxes to be observed at both time horizons in late summer. In short, the critical time period for both, CO_2 and CH_4 fluxes, was the growing season, and magnitude of fluxes changed differently across the growing season. Measurements made during a part of the growing season (such as in Christen et al., 2016 who measured in July and August) are not necessarily representative for the entire growing season nor the year. Christen et al., 2016 found CH_4 emission exceeded CO_2 uptake by a factor of 50 at 100-year time horizon in July and August in other areas of the BBECA. During spring and early summer (April and May), however, we expect that CO_2 uptake can exceed CH_4 emissions following the current measurements. There was not much activity in fall and winter when both CO_2 and CH_4 fluxes were small.

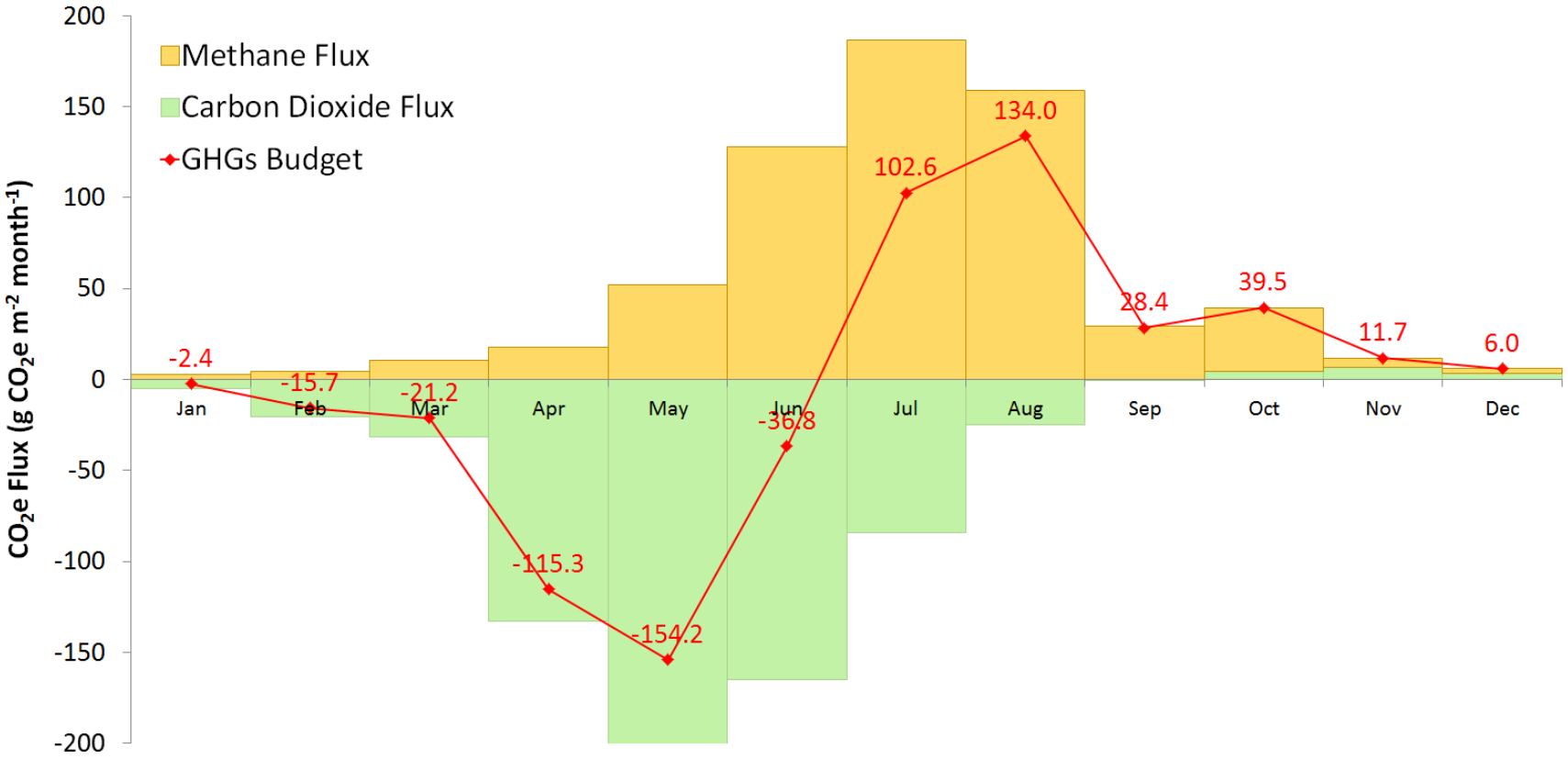

Figure 3.22 EC-measured monthly CO_2, CH_4 and net GHGs fluxes shown as CO_2e totals by using 100-year GWPs. Missing data were gap-filled.

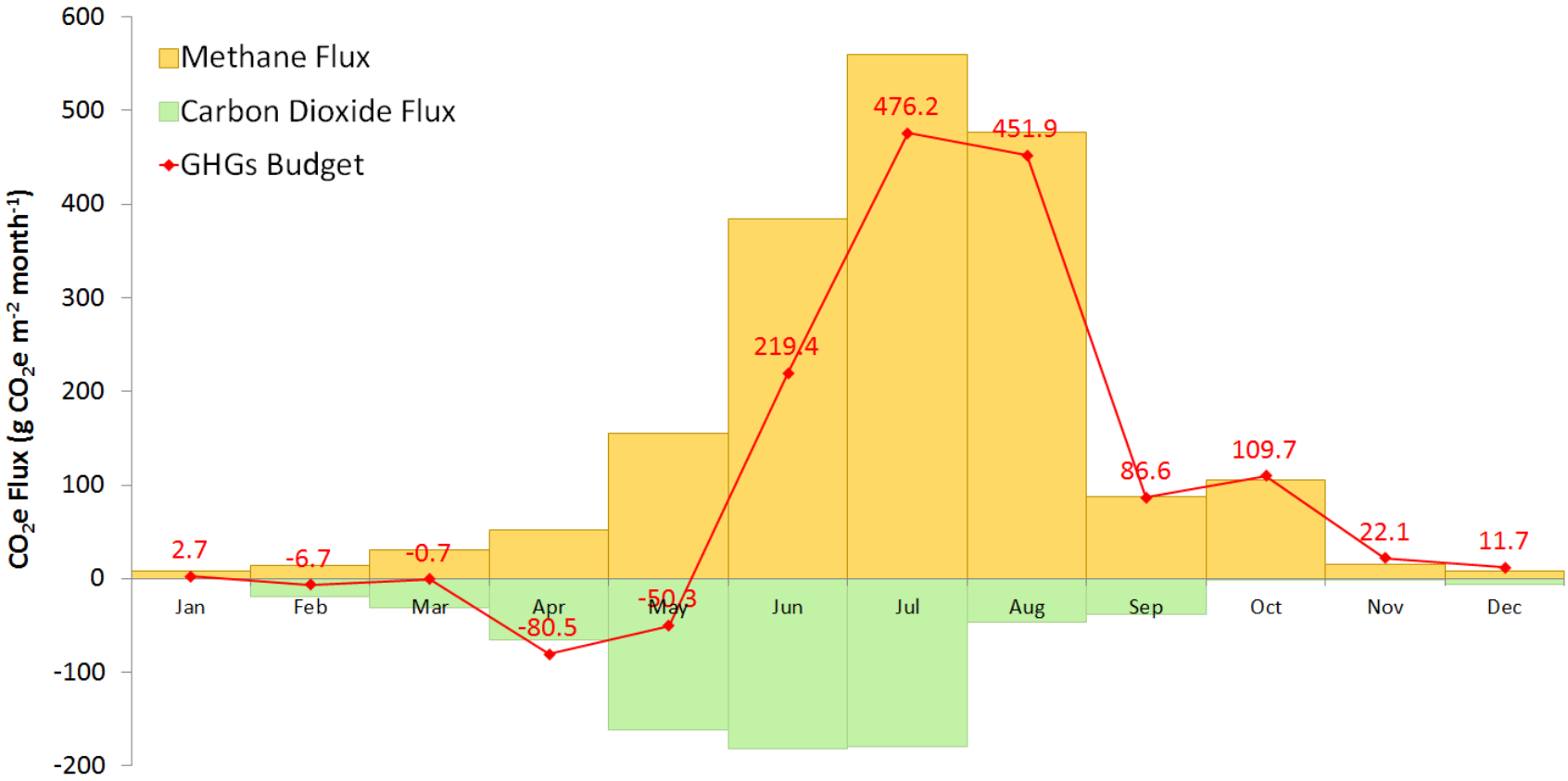

Figure 3.23 EC-measured monthly CO_2, CH_4 and net GHGs fluxes shown as CO_2e totals by using 20-year GWPs. Missing data were gap-filled.

Chapter 4: Summary and Conclusions

4.1 Summary of key findings

1. The study area, a rewetted plot in the BBECA undergoing ecological restoration, was a net CO_2 sink over a year (-179 g CO_2-C m^{-2} $year^{-1}$). The study area was not a highly productive ecosystem (annual GEP = 415 g CO_2-C m^{-2} $year^{-1}$); yet the proportionally very low R_e (annual R_e = 236 g CO_2-C m^{-2} $year^{-1}$) due to oxygen limitation permitted the study area to stay as a C neutral during the winter. The annual CO_2 fluxes were comparable with pristine temperate peatlands (Table 1.1). Compared to the few other restored wetlands reported in the literature, the study area sequestered less CO_2 (Table 1.3).

2. The major controls on CO_2 fluxes were PAR irradiance and $T_{s,5cm}$. The magnitude of PAR strongly controlled GEP, and the $T_{s,5cm}$ clearly regulated R_e. WTH also had some influence on R_e especially when the study ecosystem was flooded and it limited R_e in the topmost part of the peat.

3. Annual CH_4 emissions were 16.07 g CH_4-C m^{-2} $year^{-1}$; compared to other restored wetlands in the literature, the study area emitted less CH_4 (Table 1.3). CH_4 emissions in summer were 60 times stronger than in winter.

4. The ditch blocking permitted aerobic conditions with the water table within 30 cm of the surface throughout the year. Thus, any effects of WTH on CH_4 fluxes at the study area were not apparent. $T_{s,5cm}$ explained CH_4 fluxes best (R^2 = 0.66).

5. After a 7-year restoration, the study area was overall a slight GHG sink at the 100-year GWP timescale, where CO_2 uptake was stronger than CH_4 emissions. But the rewetted area was a substantial source of GHG if one considers only a 20-year time horizon.

4.2 Implications

Restoration efforts applied in disturbed peatlands aim at returning characteristic plant species, create habitats, and hydrological conditions to a state when peatlands can form peat and accumulate C in the long term (Rochefort et al., 2003). Some peatlands have been found to be turning into C sinks were found turning to be C sinks after a short period (< 10 years) of restoration in the growing season (Tuittila et al., 1999; Waddington et al., 2010). Waddington et al., 2010 expected their site would become a net annual C sink having 6 to 10 years of restoration. But it would take much longer to turn a degraded peatlands into a net annual C sink. Samaratani et al., 2011 even suggested that it may require up to 50 years before C accumulation function is regained at their study area . Data suggest that the study area was a net C sink during the study year, which overlapped with the 7^{th} year following rewetting For the site's future, having more mosses covering the surface, it could more efficiently store C and be expected to be a stronger C sink (Hugron et al., 2013; Keddy, 2010).

4.3 Future work

4.3.1 Following measurement

The EC-1 system was taken down in June 2016, yet the EC-2 system and all other sensors for weather measurement are still on the tower. These sensors will be running for another year. Having a second year of fluxes of both CO_2 and CH_4 will be useful to get a better data coverage, especially during wintertime. To enable this, the currently separate power systems for EC-1 (now obsolete) and EC-2 will be combined allowing more power for EC-2.

4.3.2 Gap-filling of CO_2 fluxes

Few studies showed how water availability restricts CO_2 fluxes (Barr et al., 2007; Krishnan et al., 2006; Reichstein et al., 2002). The effects of soil moisture conditions must be considered when modelling R_e and GEP to get better estimation of annual budget and simulate the responses of C exchanges of this ecosystem to climate change. Having several years of CO_2 flux data will allow us to compare wet and dry summers.

4.3.3 Gap-filling of CH_4 fluxes

Numerous studies have found a strong relationship between NEE (plant activity) and CH_4 flux. When plant production increases, a greater quantity of C substrate for methanogenic metabolism is made available and allows more CH_4 be released through plants themselves (Chanton et al., 1993; Hatala et al., 2012; Whalen, 2005; Whiting and Chanton, 1993). This could be further explored.

4.3.4 Identifying the C sources

The surface is quite homogenous in the footprint areas, but still has small fraction of bare soil and water ponds. The open water pools are net sources of CO_2 and the path for CH_4 (ebullition) to the atmosphere (Pelletier et al., 2015; Waddington and Roulet, 2000). C fluxes are

related to a water pond's morphology (size and depth) (McEnroe et al., 2009). Therefore, to better understand the C sources in the study area, the effects of water ponds are needed to be considered.

4.3.5 Effect of special events on GHG fluxes

Wildfire can reduce the temperature and affected shortwave and longwave irradiance. A wildfire which started inside the BBECA in July 2016 burned more than 100 hectares. Fortunately, it did not spread to the study area, but it was only 1 km away. When modelling the bog, fires are an essential part of the C-cycle, and suppressing fires, and the associated C-loss, is an important motivation of the restoration activities strategy using the ditch-blocking program (Hogg et al., 1992; Joosten, 2009).

Bibliography

Alkhatib, M., Jennerjahn, T.C., Samiaji, J., 2007. Biogeochemistry of the Dumai River estuary, Sumatra, Indonesia, a tropical black-water river. Limnology and Oceanography 52(6), 2410-2417.

Alm, J., Talanov, A., Saarnio, S., Silvola, J., Ikkonen, E., Aaltonen, H., Nykänen, H., Martikainen, P.J., 1997. Reconstruction of the carbon balance for microsites in a boreal oligotrophic pine fen, Finland. Oecologia 110(3), 423-431.

Anderson, F.E., Bergamaschi, B., Sturtevant, C., Knox, S., Hastings, L., Windham-Myers, L., Detto, M., Hestir, E.L., Drexler, J., Miller, R.L., Matthes, J.H., Verfaillie, J., Baldocchi, D., Snyder, R.L., Fujii, R., 2016. Variation of energy and carbon fluxes from a restored temperate freshwater wetland and implications for carbon market verification protocols. Journal of Geophysical Research: Biogeosciences 121(3), 777-795.

Augustin, J., Merbach, W., Rogasik, J., 1998. Factors influencing nitrous oxide and methane emissions from minerotrophic fens in northeast Germany. Biol Fertil Soils 28(1), 1-4.

Aurela, M., Laurila, T., Tuovinen, J.-P., 2001. Seasonal CO2 balances of a subarctic mire. Journal of Geophysical Research: Atmospheres 106(D2), 1623-1637.

Barr, A.G., Griffis, T.J., Black, T.A., Lee, X., Staebler, R.M., Fuentes, J.D., Chen, Z., Morgenstern, K., 2002. Comparing the carbon budgets of boreal and temperate deciduous forest stands. Canadian Journal of Forest Research 32(5), 813-822.

Baum, A., Rixen, T., Samiaji, J., 2007. Relevance of peat draining rivers in central Sumatra for the riverine input of dissolved organic carbon into the ocean. Estuarine, Coastal and Shelf Science 73(3–4), 563-570.

Bellisario, L.M., Bubier, J.L., Moore, T.R., Chanton, J.P., 1999. Controls on CH4 emissions from a northern peatland. Global Biogeochemical Cycles 13(1), 81-91.

Biggs, W., 1976. An Ecological And Land Use Study Of Burns Bog, Delta, B.C., University of British Columbia, Vancouver.

Bridgham, S., Megonigal, J.P., Keller, J., Bliss, N., Trettin, C., 2006. The carbon balance of North American wetlands. Wetlands 26(4), 889-916.

Brovkin, V., Bendtsen, J., Claussen, M., Ganopolski, A., Kubatzki, C., Petoukhov, V., Andreev, A., 2002. Carbon cycle, vegetation, and climate dynamics in the Holocene: Experiments with the CLIMBER-2 model. Global Biogeochemical Cycles 16(4), 1139.

Bubier, J.L., Crill, P.M., Moore, T.R., Savage, K., Varner, R.K., 1998. Seasonal patterns and controls on net ecosystem CO2 exchange in a boreal peatland complex. Global Biogeochemical Cycles 12(4), 703-714.

Burch, D. E., Singleton, E. B., and Williams, D.: Absorption Line Broadening in the Infrared, Appl. Optics, 1, 359–363, 1962

Burns, B., 1977. Discover Burns Bog. Vancouver, B.C. Hurricane Press.

Calvin, M., 1962. The Path of Carbon in Photosynthesis. Angewandte Chemie International Edition in English 1(2), 65-75.

Cao, M., Gregson, K., Marshall, S., 1998. Global methane emission from wetlands and its sensitivity to climate change. Atmospheric Environment 32(19), 3293-3299.

Chanton, J.P., Whiting, G.J., Happell, J.D., Gerard, G., 1993. Contrasting rates and diurnal patterns of methane emission from emergent aquatic macrophytes. Aquatic Botany 46(2), 111-128.

Chasar, L.S., Chanton, J.P., Glaser, P.H., Siegel, D.I., 2000. Methane Concentration and Stable Isotope Distribution as Evidence of Rhizospheric Processes: Comparison of a Fen and Bog in the Glacial Lake Agassiz Peatland Complex. Annals of Botany 86(3), 655-663.

Chestnutt, C., 2015. For peak's sake: A water balance study and comparison of the eddy covariance technique and semi-empirical calculation to determine summer evapotranspiration in Burns Bog, British Columbia., The University of Edinburgh, The University of British Columbia.

Chojnicki, B.H., Michalak, M., Acosta, M., Juszczak, R., Augustin, J., Drösler, M., Olejnik, J., 2010. Measurements of carbon dioxide fluxes by chamber method at the Rzecin wetland ecosystem, Poland. Polish Journal of Environmental Studies 19(2), 283-291.

Christen, A., Coops, N.C., Crawford, B.R., Kellett, R., Liss, K.N., Olchovski, I., Tooke, T.R., van der Laan, M., Voogt, J.A., 2011. Validation of modeled carbon-dioxide emissions from an urban neighborhood with direct eddy-covariance measurements. Atmospheric Environment 45(33), 6057-6069.

Christen, A., Jassal, R., Black, A.T., Grant, N., Hawthorne, I., Johnson, M., Ketler, R., Lee, S.-C., Merkens, M., Moore, R.D., Nesic, Z., Schmid, K., Stevenson, A., Wang, Y., 2014. Quantifying summertime greenhouse gases fluxes from soils in various stages of restoration in the Burns Bog Ecological Conservancy Area. In: P.a.E. Metro Vancouver Department of Planning (Ed.). Metro Vancouver Department of Planning, Policy and Environment.

Christen, A., Jassal, R.S., Black, T.A., Grant, N.J., Hawthorne, I., Johnson, M.S., Lee, S.C., M., M., 2016. Summertime greenhouse gas fluxes from an urban bog undergoing restoration through rewetting. Mires and Peat 18(3), 1-24.

Clement, R.J., Verma, S.B., Verry, E.S., 1995. Relating chamber measurements to eddy correlation measurements of methane flux. Journal of Geophysical Research: Atmospheres 100(D10), 21047-21056.

Cowen, G.J., 2015. Social and environmental interaction in urban wetlands, Burns Bog Conservation Society.

Crawford, B., Christen, A., Ketler, R., 2013. Processing and quality control procedures of turbulent flux measurements during the Vancouver EPiCC experiment, The University of British Columbia.

Crill, P., Bartlett, K., Roulet, N., 1992. Methane flux from boreal peatlands, International workshop on carbon cycling in boreal peatlands and climatic change, Hyytiaelae, Finland, pp. 10.

Czobel, S., Foti, S., Balogh, J., Nagy, Z., Bartha, S., Tuba, Z., 2005. Chamber series and space-scale analysis of CO2 gas-exchange in grassland vegetation: A novel approach. Photosynthetica 43(2), 267-272.

Davidson, E.A., Savage, K., Verchot, L.V., Navarro, R., 2002. Minimizing artifacts and biases in chamber-based measurements of soil respiration. Agricultural and Forest Meteorology 113(1–4), 21-37.

den Hartog, G., Neumann, H.H., King, K.M., Chipanshi, A.C., 1994. Energy budget measurements using eddy correlation and Bowen ratio techniques at the Kinosheo Lake tower site during the Northern Wetlands Study. Journal of Geophysical Research: Atmospheres 99(D1), 1539-1549.

Dijk, A.v., Moene, A.F., Debruin, H.A.R., 2004. The principles of surface flux physics: theory, practice and description of the ECPACK library, Meteorology and Air Quality (MAQ), Wageningen.

Dise, N.B., Gorham, E., Verry, E.S., 1993. Environmental factors controlling methane emissions from peatlands in northern Minnesota. Journal of Geophysical Research: Atmospheres 98(D6), 10583-10594.

Edwards, N.T., 1975. Effects of Temperature and Moisture on Carbon Dioxide Evolution in a Mixed Deciduous Forest Floor1. Soil Science Society of America Journal 39(2), 361-365.

Ellis, T., Hill, P.W., Fenner, N., Williams, G.G., Godbold, D., Freeman, C., 2009. The interactive effects of elevated carbon dioxide and water table draw-down on carbon cycling in a Welsh ombrotrophic bog. Ecological Engineering 35(6), 978-986.

Evans, M., Allott, T., Holden, J., Flitcroft, C., Bonn, A., 2005. Understanding gully blocking in deep peat. Moors for the Future, Castleton, pp. 105.

Falge, E., Baldocchi, D., Tenhunen, J., Aubinet, M., Bakwin, P., Berbigier, P., Bernhofer, C., Burba, G., Clement, R., Davis, K.J., Elbers, J.A., Goldstein, A.H., Grelle, A., Granier, A., Guðmundsson, J., Hollinger, D., Kowalski, A.S., Katul, G., Law, B.E., Malhi, Y., Meyers, T., Monson, R.K., Munger, J.W., Oechel, W., Paw U, K.T., Pilegaard, K., Rannik, Ü., Rebmann, C., Suyker, A., Valentini, R., Wilson, K., Wofsy, S., 2002. Seasonality of ecosystem respiration and gross primary production as derived from FLUXNET measurements. Agricultural and Forest Meteorology 113(1–4), 53-74.

Fechner-Levy, E.J., Hemond, H.F., 1996. Trapped methane volume and potential effects on methane ebullition in a northern peatland. Limnology and Oceanography 41(7), 1375-1383.

Finér, L., Laine, J., 1998. Root dynamics at drained peatland sites of different fertility in southern Finland. Plant and Soil 201(1), 27-36.

Foken, T., Gockede, M., Mauder, M., Mahrt, L., Amiro, B.D., Munger, J.W., 2004. Post-field data quality control. In: X. Lee (Ed.), Handbook of Micrometeorology: A Guide for Surface Flux Measurements. Kluwer Academic Publishers, Dordrecht, pp. 81-108.

Fraser, C.J.D., Roulet, N.T., Moore, T.R., 2001. Hydrology and dissolved organic carbon biogeochemistry in an ombrotrophic bog. Hydrological Processes 15(16), 3151-3166.

Frolking, S.E., Bubier, J.L., Moore, T.R., Ball, T., Bellisario, L.M., Bhardwaj, A., Carroll, P., Crill, P.M., Lafleur, P.M., McCaughey, J.H., Roulet, N.T., Suyker, A.E., Verma, S.B., Waddington, J.M., Whiting, G.J., 1998. Relationship between ecosystem productivity and photosynthetically active radiation for northern peatlands. Global Biogeochemical Cycles 12(1), 115-126.

Gaveau, D.L.A., Salim, M.A., Hergoualc'h, K., Locatelli, B., Sloan, S., Wooster, M., Marlier, M.E., Molidena, E., Yaen, H., DeFries, R., Verchot, L., Murdiyarso, D., Nasi, R., Holmgren, P., Sheil, D., 2014. Major atmospheric emissions from peat fires in Southeast Asia during non-drought years: evidence from the 2013 Sumatran fires. Scientific Reports 4, 6112.

Glenn, A.J., Flanagan, L.B., Syed, K.H., Carlson, P.J., 2006. Comparison of net ecosystem CO2 exchange in two peatlands in western Canada with contrasting dominant vegetation, Sphagnum and Carex. Agricultural and Forest Meteorology 140(1–4), 115-135.

Gorham, E., 1991. Northern Peatlands: Role in the Carbon Cycle and Probable Responses to Climatic Warming. Ecological Applications 1(2), 182-195.

Griffis, T.J., Rouse, W.R., Waddington, J.M., 2000. Interannual variability of net ecosystem CO2 exchange at a subarctic fen. Global Biogeochemical Cycles 14(4), 1109-1121.

Hatala, J.A., Detto, M., Baldocchi, D.D., 2012. Gross ecosystem photosynthesis causes a diurnal pattern in methane emission from rice. Geophysical Research Letters 39(6), n/a-n/a.

Heathwaite, A.L., Göttlich, K., 1993. Mires: process, exploitation, and conservation. Wiley.

Hebda, R.J., Gustavson, K., Golinski, K., Calder, A.M., 2000. Burns Bog Ecosystem Review Synthesis for Burns Bog, Fraser River Delta, South-western British Columbia, Canada, Environmental Assessment Office, Victoria, B.C.

Herbst, M., Friborg, T., Ringgaard, R., Soegaard, H., 2011. Interpreting the variations in atmospheric methane fluxes observed above a restored wetland. Agricultural and Forest Meteorology 151(7), 841-853.

Hogg, E.H., Lieffers, V.J., Wein, R.W., 1992. Potential Carbon Losses From Peat Profiles: Effects of Temperature, Drought Cycles, and Fire. Ecological Applications 2(3), 298-306.

Howie, S.A., Whitfield, P.H., Hebda, R.J., Munson, T.G., Dakin, R.A., Jeglum, J.K., 2009. Water Table and Vegetation Response to Ditch Blocking: Restoration of a Raised Bog in Southwestern British Columbia. Canadian Water Resources Journal / Revue canadienne des ressources hydriques 34(4), 381-392.

Hugron, S., Bussières, J., Rochefort, L., 2013. Tree plantations within the context of ecological restoration of peatlands: a practical guide., Peatland Ecology Research Group, Université Laval, Québec.

IPCC, 2007. Climate Change 2007 - The Physical Science Basis: Working Group I Contribution to the Fourth Assessment Report of the IPCC. Cambridge University Press.

IPCC, 2013. Summary for Policymakers. In: T.F. Stocker, D. Qin, G.-K. Plattner, M. Tignor, S.K. Allen, J. Boschung, A. Nauels, Y. Xia, V. Bex, P.M. Midgley (Eds.), Climate Change 2013: The Physical Science Basis. Contribution of Working Group I to the Fifth Assessment Report of the Intergovernmental Panel on Climate Change. Cambridge University Press, Cambridge, United Kingdom and New York, NY, USA, pp. 1–30.

IPCC, 2014. Climate Change 2014: Impacts, Adaptation, and Vulnerability. Part A: Global and Sectoral Aspects. Contribution of Working Group II to the Fifth Assessment Report of the Intergovernmental Panel on Climate Change [Field, C.B., V.R. Barros, D.J. Dokken, K.J. Mach, M.D. Mastrandrea, T.E. Bilir, M. Chatterjee, K.L. Ebi, Y.O. Estrada, R.C. Genova, B. Girma, E.S. Kissel, A.N. Levy, S. MacCracken, P.R. Mastrandrea, and L.L. White (eds.)]. Cambridge University Press, Cambridge, United Kingdom and New York, NY, USA.

Järveoja, J., Peichl, M., Maddison, M., Soosaar, K., Vellak, K., Karofeld, E., Teemusk, A., Mander, Ü., 2016. Impact of water table level on annual carbon and greenhouse gas balances of a restored peat extraction area. Biogeosciences 13(9), 2637-2651.

Joabsson, A., Christensen, T.R., Wallén, B., 1999. Vascular plant controls on methane emissions from northern peatforming wetlands. Trends in Ecology & Evolution 14(10), 385-388.

Joiner, D.W., Lafleur, P.M., McCaughey, J.H., Bartlett, P.A., 1999. Interannual variability in carbon dioxide exchanges at a boreal wetland in the BOREAS northern study area. Journal of Geophysical Research: Atmospheres 104(D22), 27663-27672.

Joosten, H., 2009. The Global Peatland CO2 Picture: peatland status and drainage related emissions in all countries of the world. Wetlands International, Wageningen, pp. 35 pp.

Juszczak, R., Humphreys, E., Acosta, M., Michalak-Galczewska, M., Kayzer, D., Olejnik, J., 2013. Ecosystem respiration in a heterogeneous temperate peatland and its sensitivity to peat temperature and water table depth. Plant and Soil 366(1), 505-520.

Keddy, P.A., 2010. Wetland Ecology: Principles and Conservation. Cambridge University Press.

Kleinen, T., Brovkin, V., von Bloh, W., Archer, D., Munhoven, G., 2010. Holocene carbon cycle dynamics. Geophysical Research Letters 37(2), L02705.

Kljun, N., Black, T.A., Griffis, T.J., Barr, A.G., Gaumont-Guay, D., Morgenstern, K., McCaughey, J.H., Nesic, Z., 2006. Response of Net Ecosystem Productivity of Three Boreal Forest Stands to Drought. Ecosystems 9(7), 1128-1144.

Knox, S.H., Sturtevant, C., Matthes, J.H., Koteen, L., Verfaillie, J., Baldocchi, D., 2015. Agricultural peatland restoration: effects of land-use change on greenhouse gas (CO2 and CH4) fluxes in the Sacramento-San Joaquin Delta. Global Change Biology 21(2), 750-765.

Komulainen, V.-M., Tuittila, E.-S., Vasander, H., Laine, J., 1999. Restoration of Drained Peatlands in Southern Finland: Initial Effects on Vegetation Change and CO2 Balance. Journal of Applied Ecology 36(5), 634-648.

Kormann, R., Meixner, F.X., 2001. An analytical footprint model for non-neutral stratification. Boundary-Layer Meteorology 99(2), 207-224.

Krishnan, P., Black, T.A., Barr, A.G., Grant, N.J., Gaumont-Guay, D., Nesic, Z., 2008. Factors controlling the interannual variability in the carbon balance of a southern boreal black spruce forest. Journal of Geophysical Research: Atmospheres 113(D9), n/a-n/a.

Krishnan, P., Black, T.A., Jassal, R.S., Chen, B., Nesic, Z., 2009. Interannual variability of the carbon balance of three different-aged Douglas-fir stands in the Pacific Northwest. Journal of Geophysical Research: Biogeosciences 114(G4), n/a-n/a.

Lafleur, P.M., McCaughey, J.H., Joiner, D.W., Bartlett, P.A., Jelinski, D.E., 1997. Seasonal trends in energy, water, and carbon dioxide fluxes at a northern boreal wetland. Journal of Geophysical Research: Atmospheres 102(D24), 29009-29020.

Lafleur, P.M., Roulet, N.T., Admiral, S.W., 2001. Annual cycle of CO2 exchange at a bog peatland. Journal of Geophysical Research: Atmospheres 106(D3), 3071-3081.

Langeveld, C.A., Segers, R., Dirks, B.O.M., van den Pol-van Dasselaar, A., Velthof, G.L., Hensen, A., 1997. Emissions of CO2, CH4 and N2O from pasture on drained peat soils in the Netherlands. In: M.K.v. Ittersum, S.C.v.d. Geijn (Eds.), Developments in Crop Science. Elsevier, pp. 57-64.

Lashof, D.A., Ahuja, D.R., 1990. Relative contributions of greenhouse gas emissions to global warming. Nature 344(6266), 529-531.

Lasslop, G., Reichstein, M., Papale, D., Richardson, A.D., Arneth, A., Barr, A., Stoy, P., Wohlfahrt, G., 2010. Separation of net ecosystem exchange into assimilation and respiration using a light response curve approach: critical issues and global evaluation. Global Change Biology 16(1), 187-208.

Le Mer, J., Roger, P., 2001. Production, oxidation, emission and consumption of methane by soils: A review. European Journal of Soil Biology 37(1), 25-50.

Lee, S.-C., Christen, A., Black, A., Grant, N., Jerreat-Poole, H., Ketler, R., Merkens, M., Nesic, Z., 2015. Net ecosystem exchange of a disturbed and rewetted raised bog ecosystem measured by eddy covariance, CMOS 2015, Whistler, BC, Canada.

Lehner, B., Döll, P., 2004. Development and validation of a global database of lakes, reservoirs and wetlands. Journal of Hydrology 296(1–4), 1-22.

Levy, P.E., Burden, A., Cooper, M.D.A., Dinsmore, K.J., Drewer, J., Evans, C., Fowler, D., Gaiawyn, J., Gray, A., Jones, S.K., Jones, T., McNamara, N.P., Mills, R., Ostle, N., Sheppard, L.J., Skiba, U., Sowerby, A., Ward, S.E., Zieliński, P., 2012. Methane emissions from soils: synthesis and analysis of a large UK data set. Global Change Biology 18(5), 1657-1669.

Liblik, L.K., Moore, T.R., Bubier, J.L., Robinson, S.D., 1997. Methane emissions from wetlands in the zone of discontinuous permafrost: Fort Simpson, Northwest Territories, Canada. Global Biogeochemical Cycles 11(4), 485-494.

Limpens, J., Berendse, F., Blodau, C., Canadell, J.G., Freeman, C., Holden, J., Roulet, N., Rydin, H., Schaepman-Strub, G., 2008. Peatlands and the carbon cycle: from local processes to global implications – a synthesis. Biogeosciences 5(5), 1475-1491.

Lindroth, A., Lund, M., Nilsson, M., Aurela, M., Christensen, T.R., Laurila, T., Rinne, J., Riutta, T., Sagerfors, J., Ström, L., Tuovinen, J.-P., Vesala, T., 2011. Environmental controls on the CO 2 exchange in north European mires. Tellus B 59(5).

Lloyd, C.R., Lisa-Maria, R., Finlayson, C.M., 2013. Providing low-budget estimations of carbon sequestration and greenhouse gas emissions in agricultural wetlands. Environmental Research Letters 8(1), 015010.

Lloyd, J., Taylor, J.A., 1994. On the Temperature Dependence of Soil Respiration. Functional Ecology 8(3), 315-323.

Lund, M., Lindroth, A., Christensen, T.R., Strö M, L., 2007. Annual CO2 balance of a temperate bog. Tellus B 59(5), 804-811.

Müller, D., Warneke, T., Rixen, T., Müller, M., Jamahari, S., Denis, N., Mujahid, A., Notholt, J., 2015. Lateral carbon fluxes and CO₂ outgassing from a tropical peat-draining river. Biogeosciences 12(20), 5967-5979.

Madrone Consultants Ltd., 1999. Burns Bog Ecosystem Review. Plants and Plant Communities.

Maljanen, M., Hytönen, J., Mäkiranta, P., Laine, J., Minkkinen, K., Martikainen, P.J., 2013. Atmospheric impact of abandoned boreal organic agricultural soils depends on hydrological conditions. Boreal Environment Research 3, 250-268.

Maltby, E., Immirzi, P., 1993. Carbon dynamics in peatlands and other wetland soils regional and global perspectives. Chemosphere 27(6), 999-1023.

McDermitt, D., Burba, G., Xu, L., Anderson, T., Komissarov, A., Riensche, B., Schedlbauer, J., Starr, G., Zona, D., Oechel, W., Oberbauer, S., Hastings, S., 2011. A new low-power, open-path instrument for measuring methane flux by eddy covariance. Applied Physics B 102(2), 391-405.

McEnroe, N.A., Roulet, N.T., Moore, T.R., Garneau, M., 2009. Do pool surface area and depth control CO2 and CH4 fluxes from an ombrotrophic raised bog, James Bay, Canada? Journal of Geophysical Research: Biogeosciences 114(G1), n/a-n/a.

Menviel, L., Joos, F., 2012. Toward explaining the Holocene carbon dioxide and carbon isotope records: Results from transient ocean carbon cycle-climate simulations. Paleoceanography 27(1), PA1207.

MetroVancouver, 2007. Burns Bog Ecological Conservancy Area Management Plan.

Metzger, C., Jansson, P.E., Lohila, A., Aurela, M., Eickenscheidt, T., Belelli-Marchesini, L., Dinsmore, K.J., Drewer, J., van Huissteden, J., Drösler, M., 2015. CO₂

fluxes and ecosystem dynamics at five European treeless peatlands – merging data and process oriented modeling. Biogeosciences 12(1), 125-146.

Mikkelä, C., Sundh, I., Svensson, B., Nilsson, M., 1995. Diurnal variation in methane emission in relation to the water table, soil temperature, climate and vegetation cover in a Swedish acid mire. Biogeochemistry 28(2), 93-114.

Minkkinen, K., Laine, J., 1998. Long-term effect of forest drainage on the peat carbon stores of pine mires in Finland. Canadian Journal of Forest Research 28(9), 1267-1275.

Moncrieff, J.B., Massheder, J.M., de Bruin, H., Elbers, J., Friborg, T., Heusinkveld, B., Kabat, P., Scott, S., Soegaard, H., Verhoef, A., 1997. HAPEX-SahelA system to measure surface fluxes of momentum, sensible heat, water vapour and carbon dioxide. Journal of Hydrology 188, 589-611.

Moore, C.J., 1986. Frequency response corrections for eddy correlation systems. Boundary-Layer Meteorology 37(1), 17-35.

Moore, P.D., 2002. The future of cool temperate bogs. Environmental Conservation 29(01), 3-20.

Moore, T.R., Dalva, M., 1993. The influence of temperature and water table position on carbon dioxide and methane emissions from laboratory columns of peatland soils. Journal of Soil Science 44(4), 651-664.

Moore, T.R., Lafleur, P.M., Poon, D.M.I., Heumann, B.W., Seaquist, J.W., Roulet, N.T., 2006. Spring photosynthesis in a cool temperate bog. Global Change Biology 12(12), 2323-2335.

Moore, T.R., Roulet, N.T., 1995. Methane emissions from Canadian peatlands. In: J.M. Kimble, E.R. Levine, B.A. Stewart (Eds.), Soils and Global Change. CRC Press.

Mundava, C., 2011. Mapping vegetation in reconstructed peatlands using spectroscopy for the Haaksbergerveen. Thesis report GIRS;2011-05. s.n.], [S.l.

Nieveen, J.P., Jacobs, C.M.J., Jacobs, A.F.G., 1998. Diurnal and seasonal variation of carbon dioxide exchange from a former true raised bog. Global Change Biology 4(8), 823-833.

Oechel, W.C., Vourlitis, G., Hastings, S.J., 1997. Cold season CO2 emission from Arctic soils. Global Biogeochemical Cycles 11(2), 163-172.

Ö gren, E., Evans, J.R., 1993. Photosynthetic light-response curves. Planta 189(2), 182-190.

Oke, T.R., Hay, J.E., 1998. The Climate of Vancouver. BC Geographical Series. University of British Columbia.

Page, S.E., Siegert, F., Rieley, J.O., Boehm, H.-D.V., Jaya, A., Limin, S., 2002. The amount of carbon released from peat and forest fires in Indonesia during 1997. Nature 420(6911), 61-65.

Paul-Limoges, E., 2010. Radiometer Calibration, University of British Columbia.

Pelletier, L., Strachan, I.B., Roulet, N.T., Garneau, M., Wischnewski, K., 2015. Effect of open water pools on ecosystem scale surface-atmosphere carbon dioxide exchange in a boreal peatland. Biogeochemistry 124(1), 291-304.

Petrone, R.M., Price, J.S., Waddington, J.M., von Waldow, H., 2004. Surface moisture and energy exchange from a restored peatland, Québec, Canada. Journal of Hydrology 295(1–4), 198-210.

Pihlatie, M.K., Kiese, R., Brüggemann, N., Butterbach-Bahl, K., Kieloaho, A.J., Laurila, T., Lohila, A., Mammarella, I., Minkkinen, K., Penttilä, T., Schönborn, J., Vesala, T., 2010. Greenhouse gas fluxes in a drained peatland forest during spring frost-thaw event. Biogeosciences 7(5), 1715-1727.

Price, J.S., Waddington, J.M., 2000. Advances in Canadian wetland hydrology an biogeochemistry. Hydrological Processes 14(9), 1579-1589.

Quinty, F., Rochefort, L., 2003. Peatland Restoration Guide: Second Edition, Canadian Sphagnum Peat Moss Association and New Brunswick Department of Natural Resources and Energy.

Randerson, J.T., Field, C.B., Fung, I.Y., Tans, P.P., 1999. Increases in early season ecosystem uptake explain recent changes in the seasonal cycle of atmospheric CO2 at high northern latitudes. Geophysical Research Letters 26(17), 2765-2768.

Reichstein, M., Falge, E., Baldocchi, D., Papale, D., Aubinet, M., Berbigier, P., Bernhofer, C., Buchmann, N., Gilmanov, T., Granier, A., Grünwald, T., Havránková, K., Ilvesniemi, H., Janous, D., Knohl, A., Laurila, T., Lohila, A., Loustau, D., Matteucci, G., Meyers, T., Miglietta, F., Ourcival, J.-M., Pumpanen, J., Rambal, S., Rotenberg, E., Sanz, M., Tenhunen, J., Seufert, G., Vaccari, F., Vesala, T., Yakir, D., Valentini, R., 2005. On the separation of net ecosystem exchange into assimilation and ecosystem respiration: review and improved algorithm. Global Change Biology 11(9), 1424-1439.

Revelle, R., Suess, H.E., 1957. Carbon Dioxide Exchange Between Atmosphere and Ocean and the Question of an Increase of Atmospheric CO2 during the Past Decades. Tellus 9(1), 18-27.

Reynolds, O., 1895. On the Dynamical Theory of Incompressible Viscous Fluids and the Determination of the Criterion. Proceedings: Mathematical and Physical Sciences 451(1941), 5-47.

Rhoades, J.D., Manteghi, N.A., Shouse, P.J., Alves, W.J., 1989. Soil Electrical Conductivity and Soil Salinity: New Formulations and Calibrations. Soil Science Society of America Journal 53(2), 433-439.

Richards, B., Craft, C.B., 2015. Greenhouse Gas Fluxes from Restored Agricultural Wetlands and Natural Wetlands, Northwestern Indiana. In: J. Vymazal (Ed.), The Role of Natural and Constructed Wetlands in Nutrient Cycling and Retention on the Landscape. Springer International Publishing, Cham, pp. 17-32.

Rinne, J., Riutta, T., Pihlatie, M., Aurela, M., Haapanala, S., Tuovinen, J.-P., Tuittila, E.-S., Vesala, T., 2007. Annual cycle of methane emission from a boreal fen measured by the eddy covariance technique. Tellus B 59(3), 449-457.

Rochefort, L., Quinty, F., Campeau, S., Johnson, K., Malterer, T., 2003. North American approach to the restoration of Sphagnum dominated peatlands. Wetlands Ecol Manage 11(1), 3-20.

Roehm, C.L., Roulet, N.T., 2003. Seasonal contribution of CO2 fluxes in the annual C budget of a northern bog. Global Biogeochemical Cycles 17(1), 1029.

Rothman, L.S., Gordon, I.E., Barbe, A., Benner, D.C., Bernath, P.F., Birk, M., Boudon, V., Brown, L.R., Campargue, A., Champion, J.P., Chance, K., Coudert, L.H., Dana, V., Devi, V.M., Fally, S., Flaud, J.M., Gamache, R.R., Goldman, A., Jacquemart, D., Kleiner, I., Lacome, N., Lafferty, W.J., Mandin, J.Y., Massie, S.T., Mikhailenko, S.N., Miller, C.E., Moazzen-Ahmadi, N., Naumenko, O.V., Nikitin, A.V., Orphal, J., Perevalov, V.I., Perrin, A., Predoi-Cross, A., Rinsland, C.P., Rotger, M., Šimečková, M., Smith, M.A.H., Sung, K., Tashkun, S.A., Tennyson, J., Toth, R.A., Vandaele, A.C., Vander Auwera, J., 2009.

The HITRAN 2008 molecular spectroscopic database. Journal of Quantitative Spectroscopy and Radiative Transfer 110(9–10), 533-572.

Salm, J.-O., Maddison, M., Tammik, S., Soosaar, K., Truu, J., Mander, Ü ., 2012. Emissions of CO2, CH4 and N2O from undisturbed, drained and mined peatlands in Estonia. Hydrobiologia 692(1), 41-55.

Samaritani, E., Siegenthaler, A., Yli-Petäys, M., Buttler, A., Christin, P.-A., Mitchell, E.A.D., 2011. Seasonal Net Ecosystem Carbon Exchange of a Regenerating Cutaway Bog: How Long Does it Take to Restore the C-Sequestration Function? Restoration Ecology 19(4), 480-489.

Schipper, L.A., Reddy, K.R., 1994. Methane Production and Emissions from Four Reclaimed and Pristine Wetlands of Southeastern United States. Soil Sci. Soc. Am. J. 58(4), 1270-1275.

Schotanus, P., Nieuwstadt, F.T.M., Bruin, H.A.R.D., 1983. Temperature measurement with a sonic anemometer and its application to heat and moisture fluxes. Boundary-Layer Meteorology 26, 13.

Schreader, C.P., Rouse, W.R., Griffis, T.J., Boudreau, L.D., Blanken, P.D., 1998. Carbon dioxide fluxes in a northern fen during a hot, dry summer. Global Biogeochemical Cycles 12(4), 729-740.

Schulze, E.D., Lloyd, J., Kelliher, F.M., Wirth, C., Rebmann, C., Lühker, B., Mund, M., Knohl, A., Milyukova, I.M., Schulze, W., Ziegler, W., Varlagin, A.β., Sogachev, A.F., Valentini, R., Dore, S., Grigoriev, S., Kolle, O., Panfyorov, M.I., Tchebakova, N., Vygodskaya, N.N., 1999. Productivity of forests in the Eurosiberian boreal region and their potential to act as a carbon sink –- a synthesis. Global Change Biology 5(6), 703-722.

Segers, R., 1998. Methane production and methane consumption: a review of processes underlying wetland methane fluxes. Biogeochemistry 41(1), 23-51.

Shannon, R., White, J., 1994. A three-year study of controls on methane emissions from two Michigan peatlands. Biogeochemistry 27(1), 35-60.

Shurpali, N.J., HyvÖ Nen, N.P., Huttunen, J.T., Biasi, C., NykÄ Nen, H., Pekkarinen, N., Martikainen, P.J., 2008. Bare soil and reed canary grass ecosystem respiration in peat extraction sites in Eastern Finland. Tellus B 60(2), 200-209.

Shurpali, N.J., Verma, S.B., Kim, J., Arkebauer, T.J., 1995. Carbon dioxide exchange in a peatland ecosystem. Journal of Geophysical Research: Atmospheres 100(D7), 14319-14326.

Silvola, J., 1986. Carbon dioxide dynamics in mires reclaimed for forestry in eastern Finland. Annales Botanici Fennici 23(1), 59-67.

Strack, M., Waddington, J.M., Rochefort, L., Tuittila, E.S., 2006. Response of vegetation and net ecosystem carbon dioxide exchange at different peatland microforms following water table drawdown. Journal of Geophysical Research: Biogeosciences 111(G2), n/a-n/a.

Strack, M., Zuback, Y.C.A., 2013. Annual carbon balance of a peatland 10 yr following restoration. Biogeosciences, 12.

Suyker, A.E., Verma, S.B., Arkebauer, T.J., 1997. Season-long measurement of carbon dioxide exchange in a boreal fen. Journal of Geophysical Research: Atmospheres 102(D24), 29021-29028.

Tapio-Biström, M.L., Joosten, H., Tol, S., Food, Project, A.O.o.t.U.N.M.o.C.C.i.A., International, W., 2012. Peatlands: Guidance for Climate Change Mitigation Through Conservation,

Rehabilitation and Sustainable Use. Food and Agriculture Organization of the United Nations.

Treat, C.C., Bubier, J.L., Varner, R.K., Crill, P.M., 2007. Timescale dependence of environmental and plant-mediated controls on CH4 flux in a temperate fen. Journal of Geophysical Research: Biogeosciences 112(G1), G01014.

Tuittila, E.-S., Komulainen, V.-M., Vasander, H., Laine, J., 1999. Restored cut-away peatland as a sink for atmospheric CO2. Oecologia 120(4), 563-574.

Tuittila, E.-S., Komulainen, V.-M., Vasander, H., Nykänen, H., Martikainen, P.J., Laine, J., 2000. Methane dynamics of a restored cut-away peatland. Global Change Biology 6(5), 569-581.

Turetsky, M., Wieder, K., Halsey, L., Vitt, D., 2002. Current disturbance and the diminishing peatland carbon sink. Geophysical Research Letters 29(11), 21-21-21-24.

van der Werf, G.R., Randerson, J.T., Collatz, G.J., Giglio, L., Kasibhatla, P.S., Arellano, A.F., Olsen, S.C., Kasischke, E.S., 2004. Continental-Scale Partitioning of Fire Emissions During the 1997 to 2001 El Niño/La Niña Period. Science 303(5654), 73-76.

Vasander, H., Kettunen, A., 2006. Carbon in Boreal Peatlands. In: R.K. Wieder, D.H. Vitt (Eds.), Boreal Peatland Ecosystems. Springer Berlin Heidelberg, Berlin, Heidelberg, pp. 165-194.

Waddington, J.M., Roulet, N.T., 2000. Carbon balance of a boreal patterned peatland. Global Change Biology 6(1), 87-97.

Waddington, J.M., Roulet, N.T., Swanson, R.V., 1996. Water table control of CH4 emission enhancement by vascular plants in boreal peatlands. Journal of Geophysical Research: Atmospheres 101(D17), 22775-22785.

Waddington, J.M., Strack, M., Greenwood, M.J., 2010. Toward restoring the net carbon sink function of degraded peatlands: Short-term response in CO2 exchange to ecosystem-scale restoration. Journal of Geophysical Research: Biogeosciences 115(G1), n/a-n/a.

Webb, E.K., Pearman, G.I., Leuning, R., 1980. Correction of flux measurements for density effects due to heat and water vapour transfer. Quarterly Journal of the Royal Meteorological Society 106(447), 85-100.

Whalen, S.C., 2005. Biogeochemistry of Methane Exchange between Natural Wetlands and the Atmosphere. Environmental Engineering Science 22(1), 73-94.

Whiting, G.J., Chanton, J.P., 1993. Primary production control of methane emission from wetlands. Nature 364(6440), 794-795.

Yu, Z., 2011. Holocene carbon flux histories of the world's peatlands: Global carbon-cycle implications. The Holocene.

Appendices

Appendix A Calculation of aerodynamic roughness length

The roughness length (z_0) was needed for the turbulent source area model (Section 3.2.1) and required as an input to SMARTFlux (for on-site calculations) to Eddy Pro (in post-processing). The z_0 was calculated using half-hourly mean wind speed and friction velocity measurements from EC-1 during the year preceding the current study year (July 10th 2014 to May 31st 2015). It was calculated by rearranging the logarithmic wind profile in neutral conditions. The equation for the calculation was:

$$z_0 = (z - d)e^{\frac{-k\bar{u}}{u_*}} \quad \text{(A1)}$$

where z is measurement height, d is 0.1 m (zero-plane displacement height is 2/3 of average vegetation height), k is 0.41 (von Karman constant), $\bar{u}$ is the mean wind velocity, and u_* is the friction velocity. For each time series, when dynamic stability was neutral (i.e. $-10 < z/L < 1$, L is Obukhov length), z_0 was calculated. The mean z_0 (0.055 m) from n = 3360 measurements that fulfilled the criteria, was entered into SMARTFlux in EC-2 when the system was set up and used to calculate the turbulent source area (Section 3.2.1). z_0 did not change much over in different seasons, it was 0.052 m in spring, 0.061 m in summer, 0.056 m in fall and 0.049 m in winter.

Appendix B Calibration of PAR sensors

Eight PAR sensors were placed on the circular plate mounted on a tripod and the horizontal balance was checked by a level at Totem Field on UBC Campus (49°15'19.5"N, 123°14'56.5"W) from April 8th 12:00 to April 10th 8:30, 2015. The tripod was located to the south of the climate station tower and the logger was placed in sealed box with silica gel (Figure B.1).

Figure B.1 Temporary station for quantum sensor calibration.

Six uncalibrated sensors were labeled from No.3 to No.8. In order to get the conversion coefficients of these six sensors, the measured mV from uncalibrated sensors was plotted against

measured PAR by Biomet laboratory standard (Q34488) (Figure B.2). The coefficients were found by applying linear regression with intercept forced to be zero (Table B.1). Two sensors (No. 4 and No. 7) were used at the study tower to measure incoming PAR (No.4) and outgoing PAR (No.7), because they showed best linearity.

Table B.1 Conversion coefficients for six previously uncalibrated sensors.

Quantum sensors	**Conversion coefficient (μmol m^{-2} s^{-1} mV^{-1})**
No.3 (Apogee 3)	4.82
No.4 (Q21634)	287.59
No.5 (Q2085?)	281.22
No.6 (Q02718)	310.25
No.7 (Q20855)	290.93
No.8 (Apogee 8)	5.78

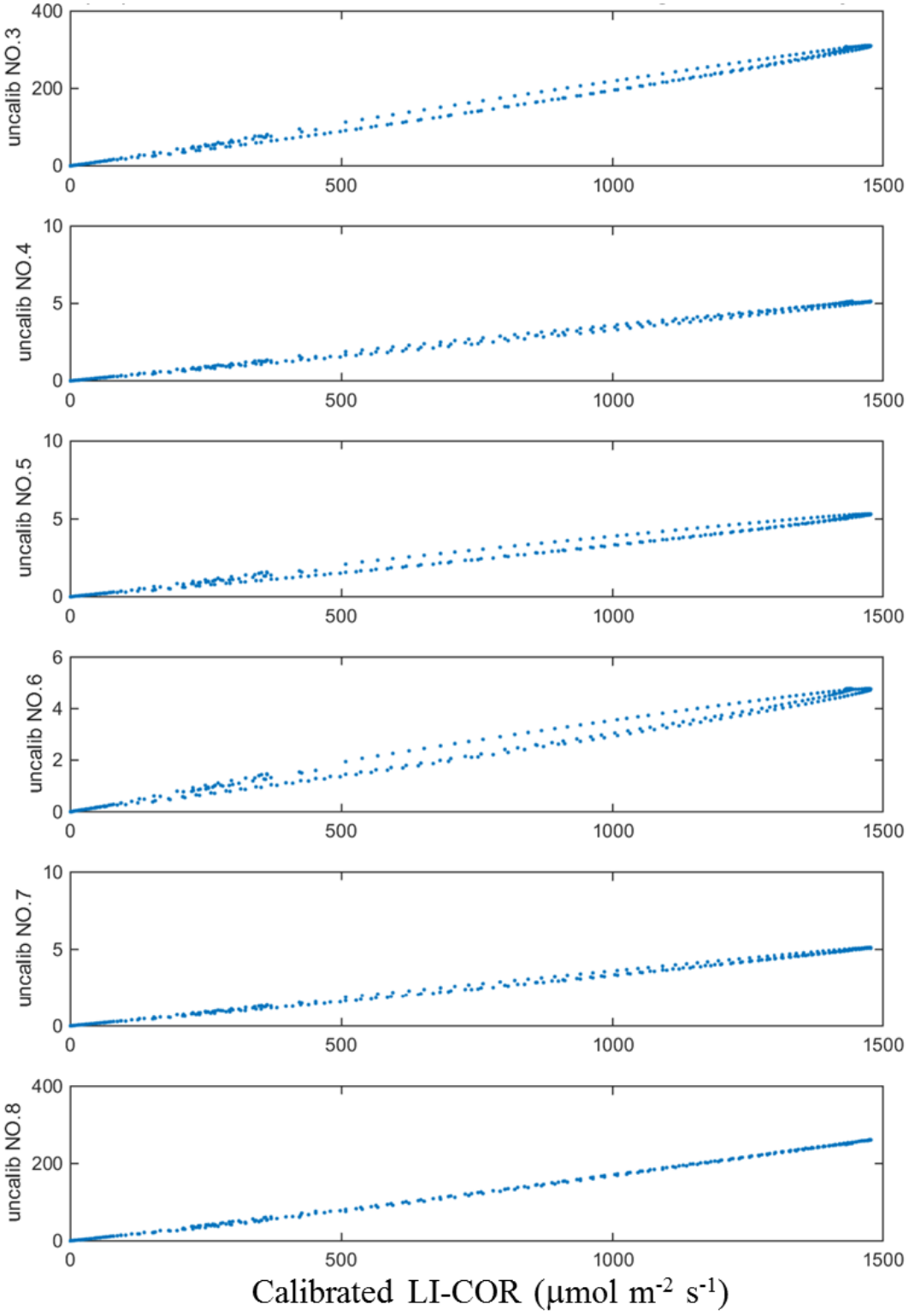

Figure B.2 Measured mV from previously uncalibrated sensors plotted against measured PAR from standard (LI-COR quantum sensor).

Appendix C Corrections of ultrasonic anemometer signals from EC-2

C.1 Methods

In spring 2016 it was found that one of the pins in the cable connecting sonic anemometer (CSAT-3) to LI-7550 was bent (Figure C.1a) and hence might not have allowed a proper connection of a differential analog output signal (floating channel). Hence any data transferred data via analog output signal to the LI-7550 before the time was only single ended and the mean of the signal floated (Figure C.1b). That affected the high channel of the vertical wind signal which led to unrealistic mean vertical wind signals. However, mean wind is not used (other than for rotation), and when calculating fluxes it is important to properly resolve fluctuations on shorter time scales. Unfortunately, it was found that also vertical wind fluctuations had about a 10% weaker magnitude at EC-2 compared to EC-1 of from June 15th 2015 to April 30th 2016. After this problem was discovered and isolated, the cable was replaced on April 30, 2016 and vertical wind fluctuations EC-2 and EC-1 were within 3%.

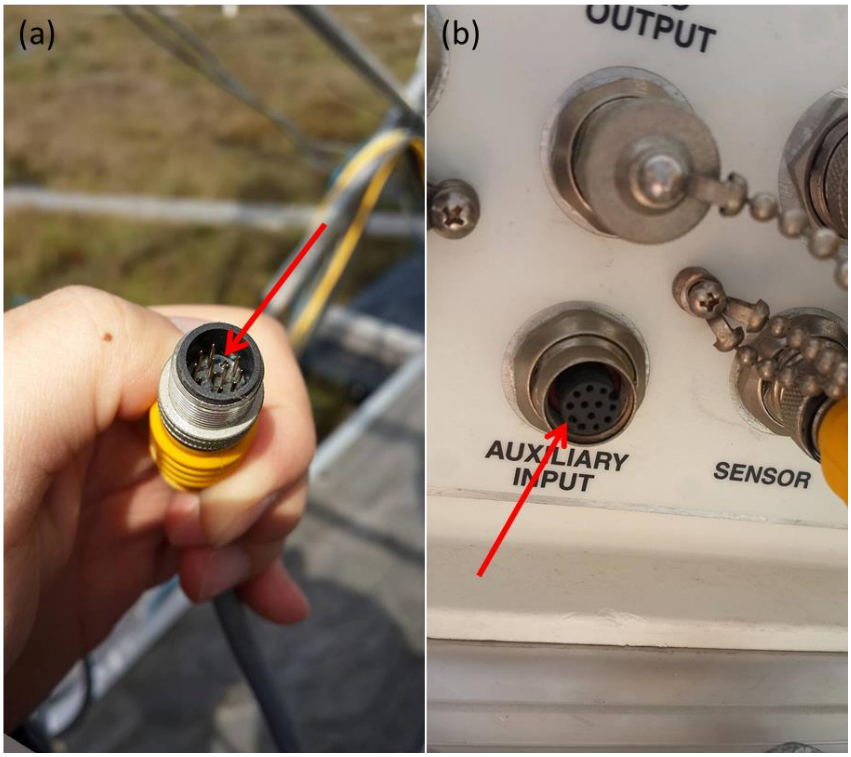

Figure C.1 (a) The bent pin. (b) The incorrect connection of one of the pins (photos taken by Sung-Ching Lee on April 29th 2016).

To explore the problem and possibly correct it, we plotted the standard deviations of vertical wind in EC-1 ($\sigma_{w,\mathrm{EC1}}$) against the standard deviations of vertical wind in EC-2 ($\sigma_{w,\mathrm{EC2}}$). Fortunately, the ratio ($\sigma_{w,\mathrm{EC2}}/\sigma_{w,\mathrm{EC1}}$) was very consistent and close to linear over time (Figure C.2) with a value of $\frac{\sigma_{w,\mathrm{EC2}}}{\sigma_{w,\mathrm{EC1}}} = 0.8985$ and an $R^2 = 0.92$. Therefore, we subtracted the mean wind of the floating vertical wind signal (i.e. force mean vertical wind of EC-2 in any half hour to zero). Afterward, the faulty raw vertical wind signal in EC-2 was multiplied by the factor 1 / 0.8985. The equation to correct the faulty raw vertical wind signal is:

$$w_{corrected} = \left(w_{original} - \overline{w_{original}}\right) * \frac{1}{0.8985} \qquad \text{(C1)}$$

where $w_{original}$ is the faulty raw vertical wind signal, $\overline{w_{original}}$ is the mean of faulty raw vertical wind signal and $w_{corrected}$ is the corrected vertical wind signal.

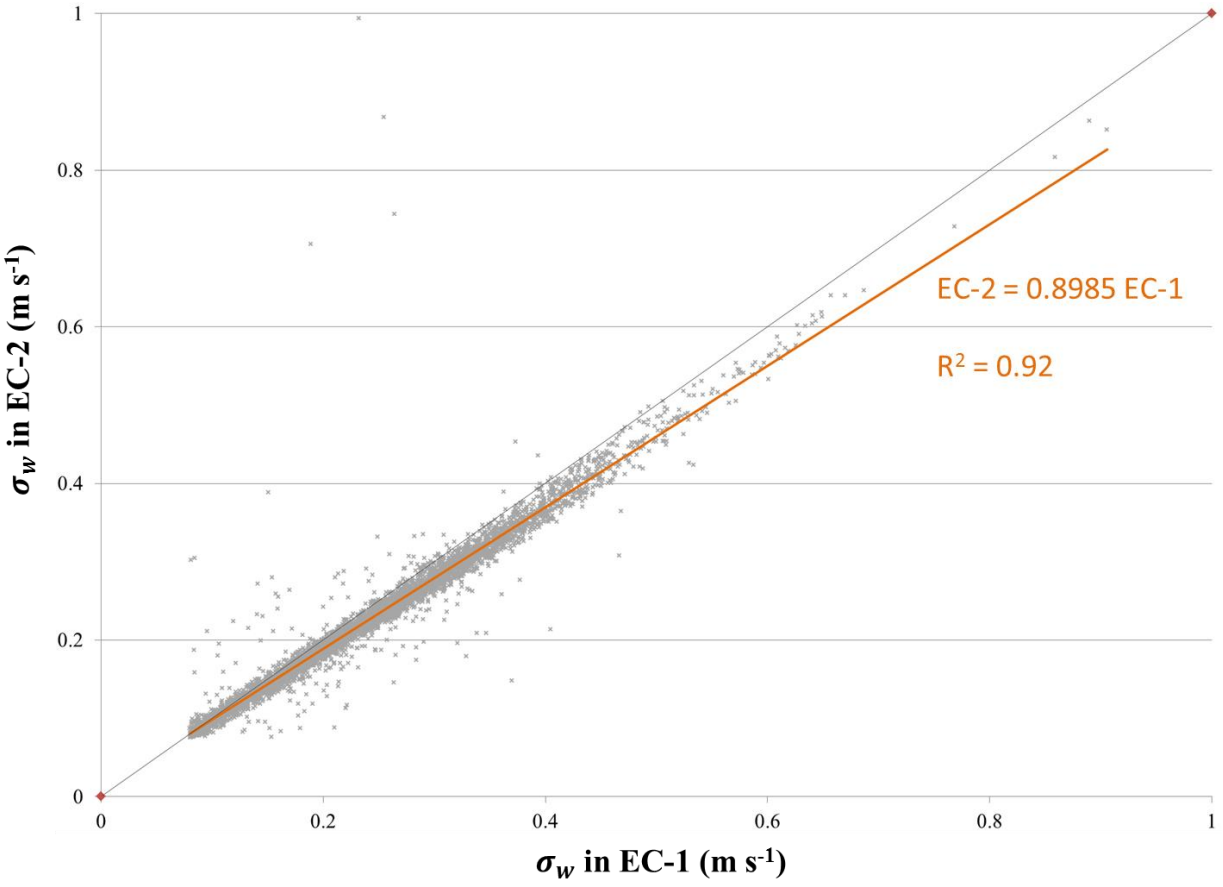

Figure C.2 The comparison between the standard deviations of vertical wind (σ_w) in EC-1 and in EC-2. Data were from June 16th 2015 to April 29th 2016.

C.2 Validation

Fortunately, both systems were running side by side over the study year. Note, however, that the two systems use different calculation and processing and correction steps (see Section 2.3.2) and they are operated 1.8 m apart. EC-1 runs at 10 Hz. EC-2 runs at 20 Hz. After the correction was applied (Equation C1), all corrected mean components, TKE and variances measured by the sonic anemometer at EC-2 were compared to the one at EC-1 to ensure proper fluxes were measured. Data from June 16th 2015 to April 29th 2016 were used, and the wind direction filter (the wind directions from 290° to 70° were discarded) and u_* filter were applied. Based on Figure C.3, the measurements from EC-2 were confirmed to be restored.

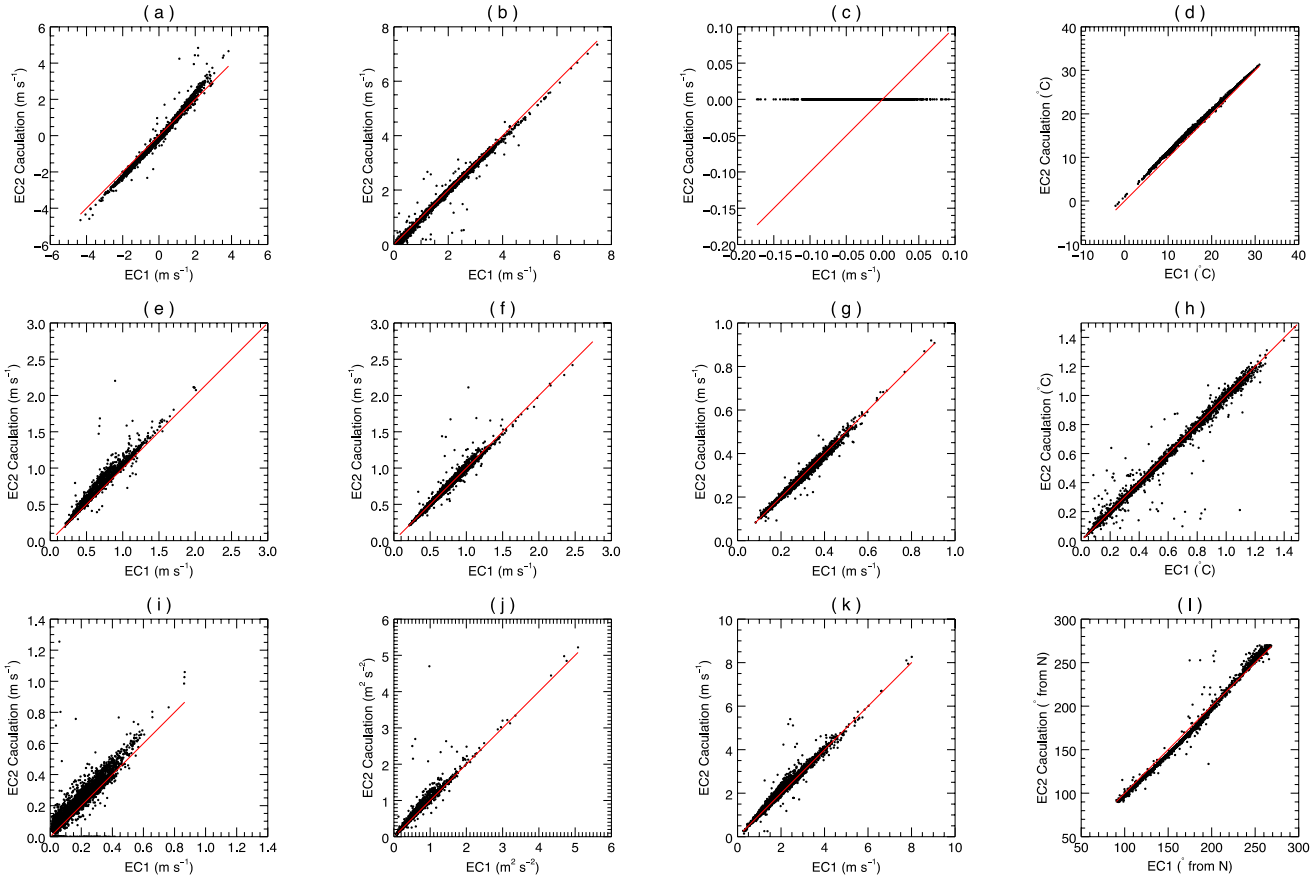

Figure C.3 The comparison between all variables (a) average of easting wind, (b) average of northing wind, (c) average of vertical wind, (d) average of acoustic temperature, (e) standard deviation of easting wind, (f) standard deviation of northing wind, (g) standard deviation of vertical wind, (h) standard deviation of acoustic temperature, (i) friction velocity, (j) turbulence kinetic energy, (k) wind velocity, and (l) wind direction calculated by each half-hourly high-frequency data from the sonic anemometer in EC-2 with corrections and the same variables from EC-1.

C.3 Re-calculated energy and CO_2 fluxes in EC-2

With corrected components, fluxes (*H*, *LE* and CO_2 fluxes) were re-calculated and compared to EC-1 (Figure C.4). Also, to explore how well the two systems compare without the cable issue, the two EC systems were compared when the new cable was in place from May 1st – May 25th, 2016 (Figure C.5). Re-calculated *H*, *LE* and CO_2 fluxes in EC-2 during the time with the faulty cable became pretty close to EC-1 system. Also, these three fluxes measured by EC-2 and by EC-1 were identical.

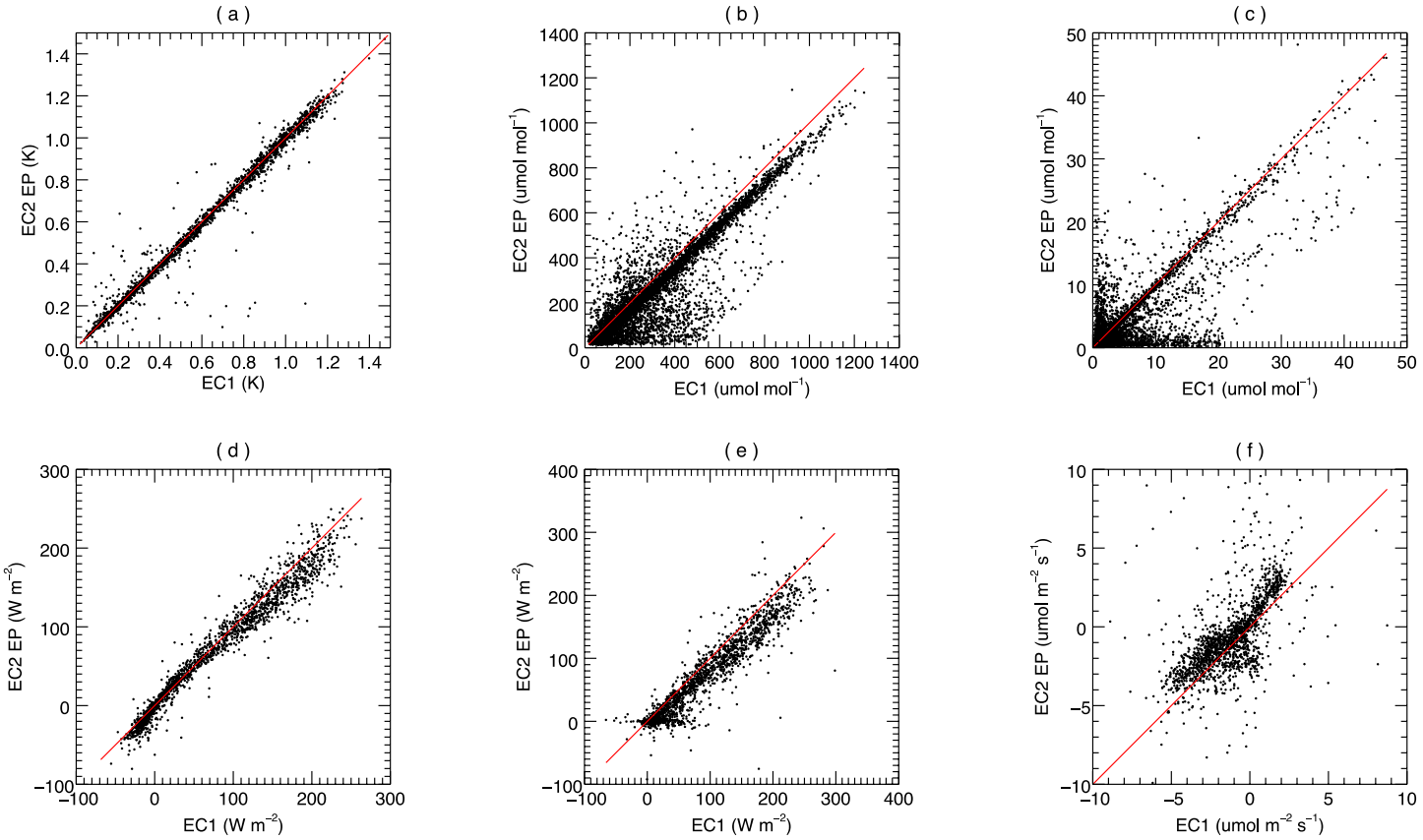

Figure C.4 The comparison between (a) standard deviation of acoustic temperature, (b) standard deviation of H_2O mixing ratio, (c) standard deviation of CO_2 mixing ratio, (d) sensible heat fluxes, (e) latent heat fluxes, (f) CO_2 fluxes calculated by EddyPro in EC-2 with corrections from June 15th 2015 to April 30th 2016 and the same variables from EC-1.

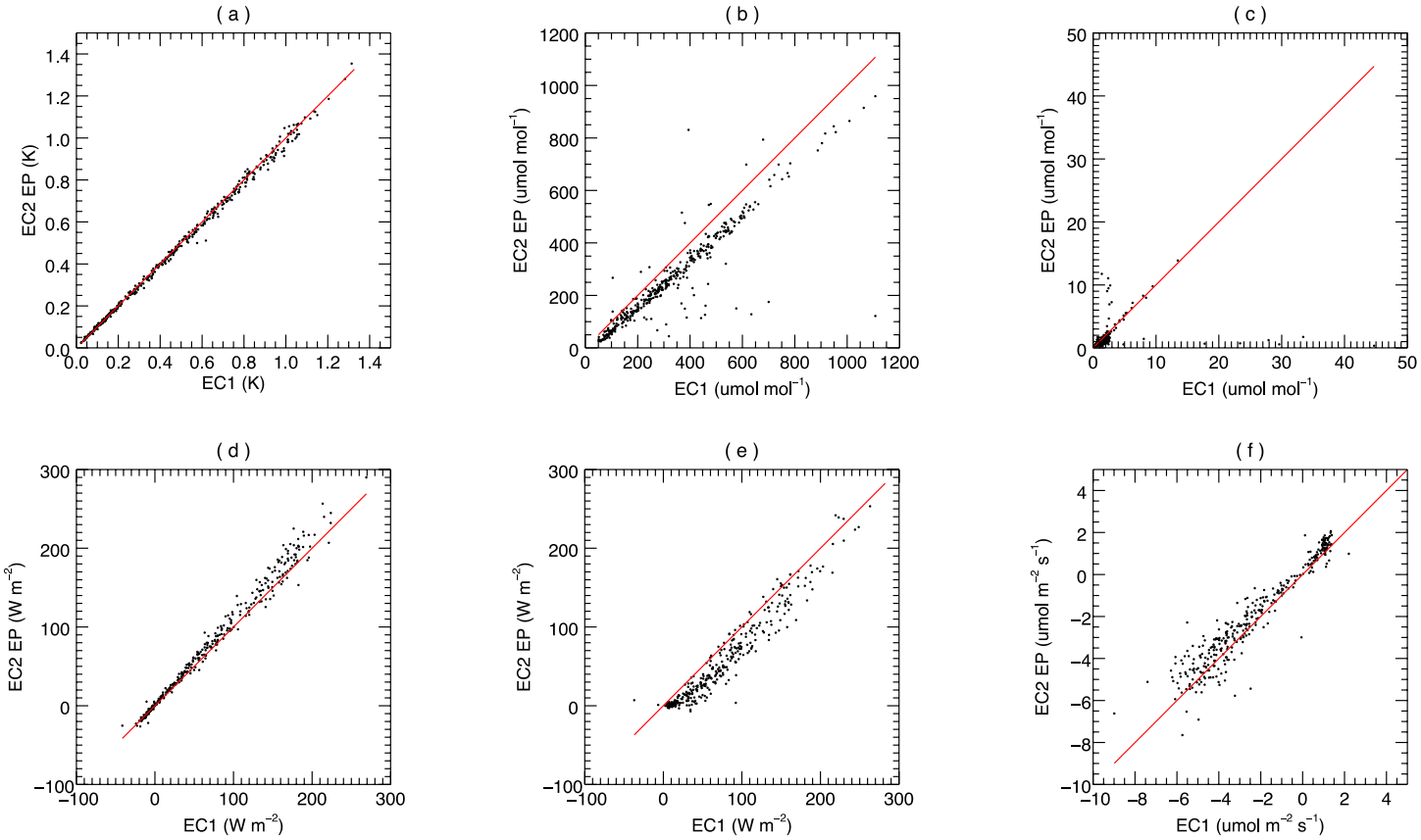

Figure C.5 The comparison between (a) standard deviation of acoustic temperature, (b) standard deviation of H_2O mixing ratio, (c) standard deviation of CO_2 mixing ratio, (d) sensible heat fluxes, (e) latent heat fluxes, (f) CO_2 fluxes calculated by SMARTFlux in EC-2 with the good cable from May 1st 2016 to June 15th 2016 and the same variables from EC-1.

C.4 Data processing in EC-2

After replacing the faulty cable with a new one, the outputs from SMARTFlux and the post-processed fluxes using Eddy Pro were compared. We compared the fluxes calculated by EddyPro with same settings with the fluxes calculated on-site using SMARTFlux. The two outputs are in perfect agreement (Figure C.6), thus it does not matter whether fluxes are post-processed using EddyPro or calculated on-site by SMARTFlux.

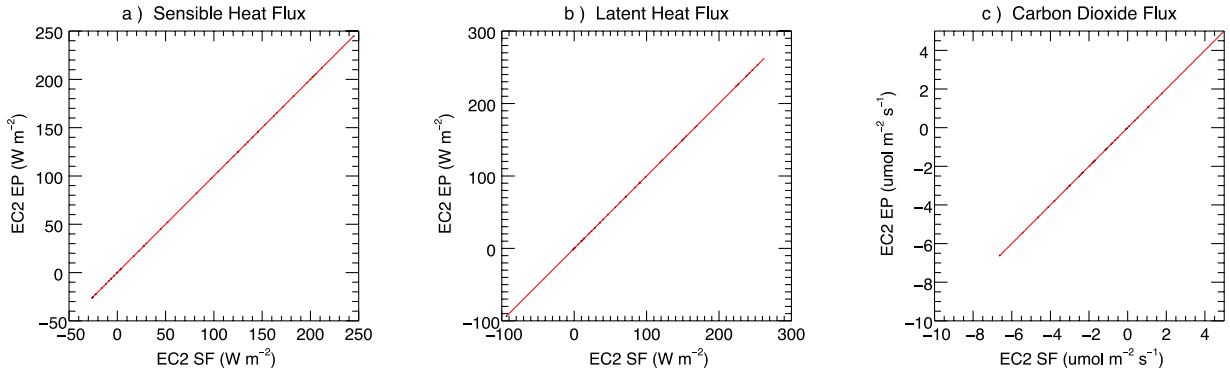

Figure C.6 The comparison between *H*, *LE* and CO_2 fluxes calculated by EddyPro (EP) and SMARTFlux (SF). Data from May 1st to May 25th 2016 were used, and the wind direction filter (the wind directions from 330° to 30° were discarded) was applied.

C.5 CH_4 fluxes in EC-2

EC-2 was only used for CH_4 fluxes in this thesis. CH_4 fluxes from June 16th 2015 to April 30th 2016 were calculated using EddyPro with the vertical wind corrected. This was practically achieved by reading and correcting (applying Equation C1, and re-creating all raw GHG-files and re-running Eddy pro with the corrected files). Figure C.7 compares CH_4 fluxes before and after applying the correction, hence identifies the effect of the corrected vertical wind on CH_4 fluxes, which was substantial (on average) 60% in CH_4 fluxes.

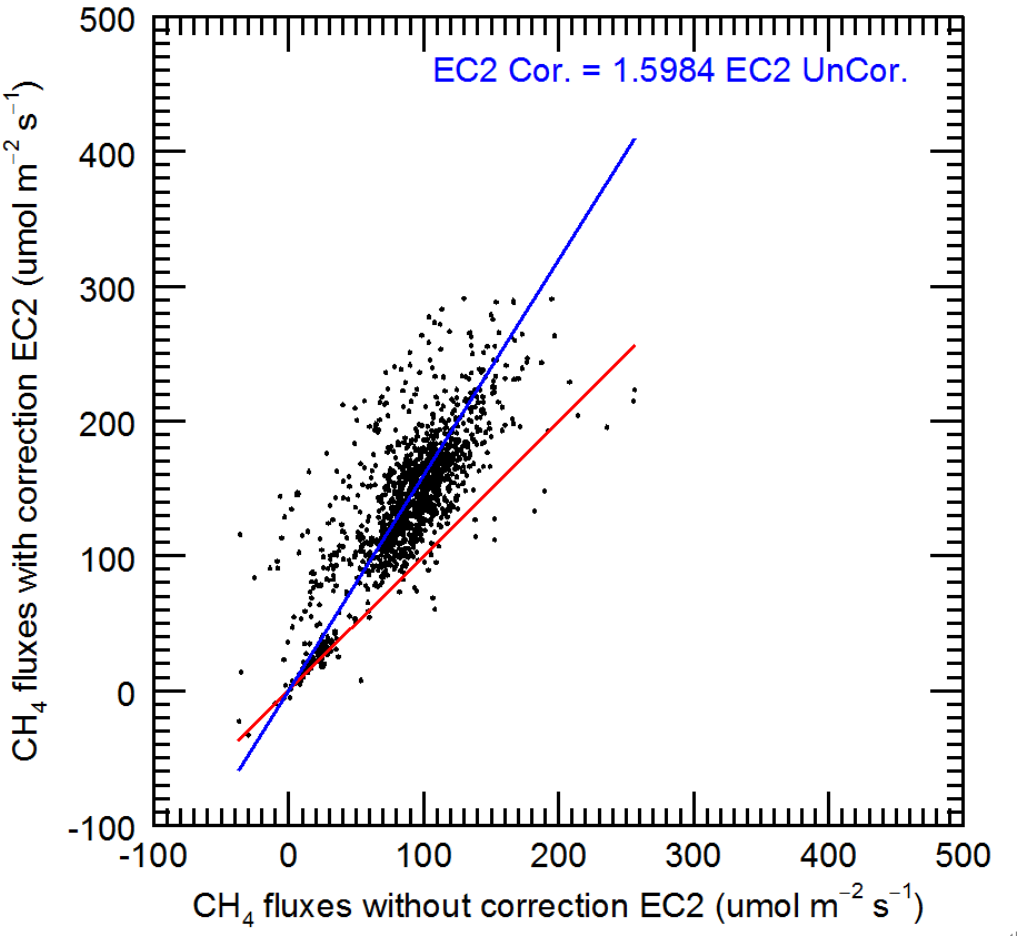

Figure C.7 The difference between CH_4 fluxes with (EC2 Cor.) and without (EC2 Uncor.) corrections applied. Data from June 16th 2015 to April 29th 2016 were used, and the wind direction filter (the wind directions from 330° to 30° were discarded) was applied.

Appendix D Tests for CO_2 gap-filling models

D.1 Dataset

The gap-filling depends on the dataset used to train the model (derive parameters) and the dataset selected to be gap-filled. Usually, at most FLUXNET sites, there is only one dataset. But in this study, CO_2 fluxes were measured by two EC systems (EC-1 and EC-2). Therefore, the dataset could be EC-1, EC-2 or a combination of the two systems to train the gap-filling. And these datasets could be selected to be gap-filled. Table D.1 concludes the results of modelled NEE, R_e, and GEP fitted by different datasets, and the results of filled NEE, model R_e, and calculated GEP (GEP = R_e – NEE) from filling the gaps in different datasets. Window sizes used to model R_e and GEP are both 365 days in Table D.1. The first year was from July 10th 2014 to July 9th 2015 (previous year), and the second year was from June 16th 2015 to June 15th 2016 (study year). Dataset A includes all data from EC-1. Dataset B includes all data from EC-2 (so data in the first year were all NaN). Dataset C includes data from EC-1 in the first year, and data from EC-1 filled by EC-2 if there is a gap in the second year. Dataset D includes data from EC-1 in the first year, and data from EC-2 filled by EC-1 if there is a gap in the second year. Dataset E includes data from EC-1 in the first year, and data from the combination of EC-1 and EC-2; it uses average when both are available. The modelled NEE, R_e, and GEP trained by Dataset A showed higher stability between two years. The filled NEE, modelled R_e and calculated GEP from filling the Dataset A are also more stable no matter what model was used.

Table D.1 T results of modelled NEE, R_e, and GEP fitted by different datasets, and the results of filled NEE, modelled R_e, and calculated GEP (GEP = R_e – NEE) from filling the gaps in different datasets.

	Model A			**Model B**			**Model C**			**Model D**			**Model E**		
Dataset used	Dataset A			Dataset B			Dataset C			Dataset D			Dataset E		
Modelled	NEE	R_e	GEP	NEE	R_e	GEP	NEE	R_e	GEP	NEE	R_e	GEP	NEE	R_e	GEP
First Year	-62.3	245.7	308.0	-11.3	357.0	368.3	-60.4	246.9	307.3	-4.2	275.5	279.8	-14.3	270.8	285.0

Input / Fill	Model A			Model B			Model C			Model D			Model E			Gaps (%)
	Filled NEE	Model R_e	Cal. *GEP*	Filled NEE	Model R_e	Cal. GEP	Filled NEE	Model R_e	Cal. *GEP*	Filled NEE	Model R_e	Cal. GEP	Filled NEE	Model R_e	Cal. GEP	
Dataset A – 1st	-172.4	245.7	418.1	-158.4	357.0	515.4	-172.3	246.9	419.2	-161.3	275.5	436.9	-163.3	270.8	434.1	41.37
Dataset B – 1st	-45.9	245.7	291.6	-5.5	357.0	362.5	-44.4	246.9	291.3	5.9	275.5	269.6	-3.1	270.8	273.8	91.75
Dataset C – 1st	-164.5	245.7	410.2	-151.7	357.0	508.7	-164.5	246.9	411.4	-154.0	275.5	429.6	-155.9	270.8	426.7	41.37
Dataset D – 1st	-133.8	245.7	379.5	-121.1	357.0	478.0	-133.8	246.9	300.7	-123.3	275.5	398.9	-125.2	270.8	396.0	41.37
Dataset E – 1st	-149.2	245.7	394.8	-136.4	357.0	493.4	-149.1	246.9	396.0	-138.7	275.5	414.2	-140.6	270.8	411.3	41.37

Modelled	NEE	R_e	GEP	NEE	R_e	GEP	NEE	R_e	GEP	NEE	R_e	GEP	NEE	R_e	GEP
Second Year	-70.1	226.3	296.5	-37.2	322.5	359.7	-68.3	227.5	295.8	-17.5	252.0	269.4	-27.8	246.7	274.5

Input / Fill	Model A			Model B			Model C			Model D			Model E			Gaps (%)
	Filled NEE	Model R_e	Cal. *GEP*	Filled NEE	Model R_e	Cal. GEP	Filled NEE	Model R_e	Cal. *GEP*	Filled NEE	Model R_e	Cal. GEP	Filled NEE	Model R_e	Cal. GEP	
Dataset A – 2nd	-169.9	226.3	396.2	-167.7	322.5	490.1	-170.1	227.5	397.6	-159.6	252.0	411.5	-161.7	246.7	408.4	37.76
Dataset B – 2nd	144.9	226.3	81.4	120.6	322.5	201.9	143.5	227.5	84.0	153.9	252.0	98.0	152.4	246.7	94.3	76.13
Dataset C – 2nd	-58.6	226.3	285.0	-70.0	322.5	392.5	-59.7	227.5	287.1	-59	252.0	310.9	-58.7	246.7	305.5	28.69
Dataset D – 2nd	134.3	226.3	92.0	123.0	322.5	199.5	133.3	227.5	94.2	134.0	252.0	118.0	134.2	246.7	112.5	28.69
Dataset E – 2nd	37.8	226.3	188.5	26.5	322.5	296.0	36.8	227.5	190.7	37.5	252.0	214.5	37.7	246.7	209.0	28.69

D.2 Window size

Table D.2 determines the effect of using different window sizes (60 days, 90 days, 120 days and full year) on the annual filled NEE, modelled R_e and calculated GEP. Data were not enough for modelling determining stable fitting parameters for GEP when a window size of < 90-day was chosen (shown as NaN in Table D.2), thus 90-day was the lowest window size determined. Modelled R_e can be obtained no matter what window size was applied, but the monthly R_e curves were not retrieving realistic fitting parameters using window size of 60-day and 90-day. Therefore, a window size of 120 days was selected for modelling R_e.

Table D.2 The results of filled NEE, modelled R_e, and calculated GEP (GEP = R_e – NEE) by using different window sizes.

First year												
R_e windows / GEP Windows	60 Days			90 Days			120 Days			365 Days		
	Filled NEE	Modelled R_e	Cal. GEP	Filled NEE	Modelled R_e	Cal. GEP	Filled NEE	Modelled R_e	Cal. GEP	Filled NEE	Modelled R_e	Cal. GEP
60 Days	NaN	NaN	NaN	NaN	NaN	NaN	NaN	NaN	NaN	NaN	NaN	NaN
90 Days	-183.3	235.4	418.6	-181.9	238.1	420.1	-181.1	235.7	416.8	-182.9	245.7	428.6
120 Days	-179.2	235.4	414.6	-177.9	238.1	416.0	-177.0	235.7	412.7	-178.9	245.7	424.5
365 Days	-172.8	235.4	408.1	-171.5	238.1	409.6	-170.6	235.7	406.3	-172.4	245.7	418.1

Second year												
R_e windows / GEP Windows	**60 Days**			**90 Days**			**120 Days**			**365 Days**		
	Filled NEE	Modelled R_e	Cal. GEP	Filled NEE	Modelled R_e	Cal. GEP	Filled NEE	Modelled R_e	Cal. GEP	Filled NEE	Modelled R_e	Cal. GEP
60 Days	NaN	NaN	NaN	NaN	NaN	NaN	NaN	NaN	NaN	NaN	NaN	NaN
90 Days	-183.2	228.6	411.7	-182.5	228.2	410.7	-182.4	220.9	403.3	-188.2	226.3	414.5
120 Days	-176.8	228.6	405.4	-176.1	228.2	404.3	-176.1	220.9	396.9	-181.8	226.3	408.2
365 Days	-164.9	228.6	393.4	-164.1	228.2	392.4	-164.1	220.9	385.0	-169.9	226.3	396.2

D.3 Gap-filling methods

Gap filling method for this study followed the FLUXNET Canada protocol (Lasslop et al., 2010) described in Section 2.4.2. It is of interest how sensitive the current results are if a different gap filling strategy is used. Another gap filling and partitioning approach tested was an online tool based on Reichstein et al., 2005. It is provided by the Department of Biogeochemical Integration at the Max Planck Institute for Biogeochemistry in Jena, Germany[2] and it was built in R language (REddyProc). This tool fills the gaps in NEE first based on the co-variation of fluxes with environmental variables. Secondly, it fits the ecosystem respiration model (Lloyd and Taylor, 1994). Figure D.1 shows the different procedures between the method used by the online tool and the method used in this study. Differences between the online tool and the current approach on annual NEE, R_e and GEP are small (Table D.3).

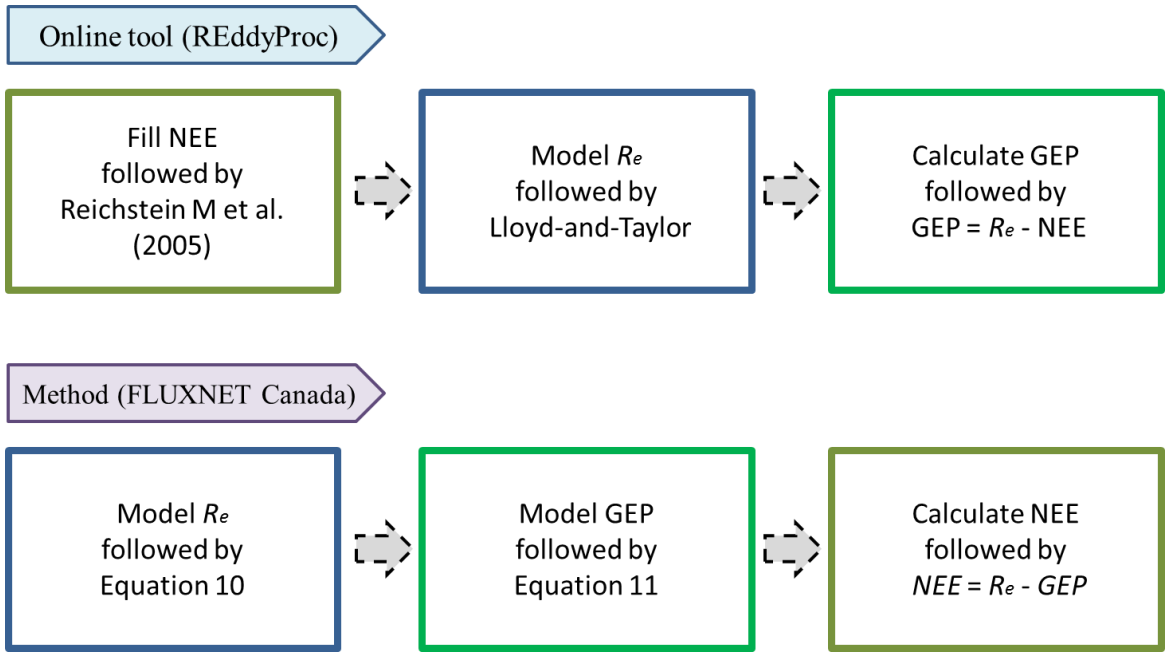

Figure D.1 The flow chart of procedures in two gap-filling methods of CO_2 fluxes.

[2] https://www.bgc-jena.mpg.de/bgi/index.php/Services/REddyProcWeb

Table D.3 The comparisons of outputs (CO_2 fluxes) from the online tool and this study's calculation. And the comparisons of outputs (energy fluxes) from using the online tool three times.

CO_2 fluxes			
Annual Budget (June 16th 2015 to June 15th 2016)	NEE (g C m^{-2} yr^{-1})	R_e (g C m^{-2} yr^{-1})	GEP (g C m^{-2} yr^{-1})
1st run with input having two-year data	-163.43	216.95	380.38
2nd run with input having two-year data	-154.85	253.42	408.27
This study (FLUXNET Canada)	-178.97	235.61	414.58
Standard deviation of three results	12.23	18.23	18.20

Energy fluxes		
	H (GJ m^{-2} yr^{-1})	*LE* (GJ m^{-2} yr^{-1})
1st run with input having two-year data through online tool	656.54	1022.36
2nd run with input having two-year data through online tool	631.84	1000.86
3rd run with input having two-year data through online tool	674.36	1053.06
Standard deviation of three results	20.58	30.35